ACHIEVING WIDE BANDWIDTH ELECTRICALLY SMALL ANTENNAS USING INTERNAL NON-FOSTER ELEMENTS

by

Ryan T. Cutshall

A Thesis Submitted to the Faculty of the

DEPARTMENT OF ELECTRICAL AND COMPUTER ENGINEERING

In Partial Fulfillment of the Requirements

For the Degree of

MASTER OF SCIENCE

In the Graduate College

THE UNIVERSITY OF ARIZONA

2013

STATEMENT BY AUTHOR

This thesis has been submitted in partial fulfillment of requirements for an advanced degree at the University of Arizona and is deposited in the University Library to be made available to borrowers under rules of the Library.

Brief quotations from this thesis are allowable without special permission, provided that an accurate acknowledgement of the source is made. Requests for permission for extended quotation from or reproduction of this manuscript in whole or in part may be granted by the head of the major department or the Dean of the Graduate College when in his or her judgment the proposed use of the material is in the interests of scholarship. In all other instances, however, permission must be obtained from the author.

SIGNED: Ryan T. Cutshall

APPROVAL BY THESIS DIRECTOR

This thesis has been approved on the date shown below:

Richard W. Ziolkowski
Professor of Electrical Engineering

August 15, 2013 .
Date

ACKNOWLEDGEMENTS

In writing these acknowledgments, I found it difficult to know where to begin, since I have so many wonderful people to thank. Well, as they say, let's begin at the beginning.

First, I would like to thank Dr. Ziolkowski. He has been my graduate advisor since before I began my graduate-level classes, and his help has been invaluable every step of the way. I am so grateful that he accepted me as one of his graduate students, and that he took the time to explain the ins and outs of electromagnetics and antennas to a lowly mechanical engineer. His background and vast knowledgebase has always amazed me, and I am so grateful that he was willing to impart some of that knowledge on all of his graduate students, myself included.

Next, I would like to thank my section heads and department managers at Raytheon (they know who they are). They have been very supportive throughout all of my graduate studies, and I am very thankful that they allowed me to pursue my graduate degree while attending work part-time. I also very much appreciate that they encouraged one of their mechanical engineers to pursue a degree in electrical engineering.

Last (but definitely not least), I would like to give a ton of my thanks and love to my supportive wife. She actually became my wife quite recently (on May 25, 2013), and throughout this process, I couldn't have asked for a more supportive girlfriend, fiancée, and wife. She has been willing to drive while I work on homework (and this thesis) while in the car, and she has brought me many cups of coffee while I work on homework (and this thesis) while at home.

DEDICATION

This work is dedicated to my supportive wife and partner in life, Sarah.

TABLE OF CONTENTS

LIST OF FIGURES 7
LIST OF TABLES 11
ABSTRACT 12
CHAPTER 1 | INTRODUCTION 13
1-1 Maxwell's Equations 16
1-2 Dipole and Monopole Antennas 19
1-2-1 Electrically Small Dipole (Linear Wire) Antennas 19
1-2-2 Electrically Small Monopole Antennas over Finite Circular Ground Planes . 24
1-3 Impedance Matching with Near-Field Resonant Parasitic Elements 27
CHAPTER 2 | INTRODUCTION TO PLANAR AND 3D EGYPTIAN AXE DIPOLE ANTENNAS 29
2-1 Planar (2D) Egyptian Axe Dipole 29
2-2 Three-Dimensional (3D) Egyptian Axe Dipole 37
CHAPTER 3 | ANALYSIS OF THE INSTANTANEOUS PERFORMANCE OF THE EAD ANTENNAS 43
3-1 Analysis of the Bandwidth Values 43
3-2 Analysis of the Directivity and Radiation Efficiency Values 49
CHAPTER 4 | FREQUENCY AGILE PERFORMANCE OF THE EAD ANTENNAS 53
4-1 Comparisons between the 2D and 3D EAD Frequency Agile Results 53
4-2 Frequency Agile Simulations in HFSS 57
4-2-1 Obtaining the Frequency Agile Data in HFSS 58
4-2-2 Exporting the Frequency Agile Data from HFSS 60
4-3 Frequency Agile Simulations in ADS 66
CHAPTER 5 | PERFORMANCE OF THE NON-FOSTER AUGMENTED EAD ANTENNAS 73
5-1 Comparisons between the 2D and 3D EAD Non-Foster Results 73
5-2 Radiation Efficiencies of the Non-Foster Augmented EAD Antennas 85
5-3 Details on How to Calculate the Exponential Regression Coefficients 87
5-4 Non-Foster Simulations in HFSS 90
5-4-1 Obtaining the Necessary Data from HFSS for the Non-Foster Plot 90
5-4-2 Creating the Non-Foster $|S_{11}|$ Curve 92

TABLE OF CONTENTS (CONTINUED)

5-4-3 Creating the Non-Foster Radiation Efficiency Curve 94
5-5 Non-Foster Simulations in ADS 96
CHAPTER 6 | CONCLUSIONS AND FUTURE WORK 102
6-1 Conclusions 102
6-2 Future Work 103
APPENDIX A | ABBREVIATIONS, ACRONYMS, AND SYMBOLS LIST 104
APPENDIX B | MATLAB CODE FOR GENERATING THE REGRESSION-BASED INDUCTOR VALUES 108
APPENDIX C | MATLAB CODE FOR PLOTTING THE NON-FOSTER $|S_{11}|$ CURVE 111
APPENDIX D | HFSS MACROS FOR GENERATING A NON-FOSTER RADIATION EFFICIENCY CURVE 113
REFERENCES 115

LIST OF FIGURES

Figure 1-1: A dipole antenna driven by an ideal current source. 20
Figure 1-2: Total directivity patterns of the small dipole antenna oriented along the z-axis. Solid blue curve is the E-plane pattern plotted versus θ. Dashed red curve is the H-plane pattern plotted versus ϕ. 22
Figure 1-3: Analytical results for the resistance and reactance of the input impedance of a small dipole antenna ($a = l/2 = \lambda_0/18$ when f_0 = 300 MHz, ka = 0.35, $b = a/20$). 23
Figure 1-4: Illustration of a monopole antenna with length h over a finite circular ground plane of radius a driven with an ideal current source. 25
Figure 1-5: Diagram of the underlying physic of a NFRP element. Figure originally presented in [7], reused here with the lead author's permission. 28
Figure 2-1: The planar (2D) Egyptian axe dipole (EAD) design. The substrate and NFRP element are shown as semi-transparent for ease of viewing. 30
Figure 2-2: Directivity patterns of the 2D EAD antenna at f_0 = 300 MHz. The solid blue curve is the E-plane pattern plotted versus θ; the dashed red curve is the H-plane pattern plotted versus ϕ. 31
Figure 2-3: Vector plot of the magnitude and direction of the surface current on the NFRP element of the 2D EAD at 300 MHz when ka = 0.35 and the input phase is set at 0°. 32
Figure 2-4: Resistance and reactance of the 2D EAD antenna when ka = 0.35. 33
Figure 2-5: $|S_{11}|$ versus frequency for the 2D EAD antenna for several values of ka. 35
Figure 2-6: Equivalent circuit model for the 2D and 3D EAD antenna designs (note that $\eta 0$ in this diagram represents the impedance of free space, not the radiation efficiency). 36
Figure 2-7: Resistance and reactance curves for the 2D EAD antenna with ka = 0.35, calculated with the full wave simulation (HFSS), and with the equivalent circuit shown in Figure 2-6 with C_{sub} = 0.92 pF, L_{eff} = 257.5 nH, C_{eff} = 1.1 pF, C_{higher} = 2.0 pF, R_{sub} = 9.8 kΩ, and l_{eff} = 70.0 mm. 36
Figure 2-8: Isometric view of the three-dimensional Egyptian axe dipole (3D EAD) antenna. The substrate and the ground plane are semi-transparent for ease of viewing. 38
Figure 2-9: Resistance and reactance for the 3D EAD antenna when ka = 0.35. 39
Figure 2-10: Directivity patterns of the 3D EAD antenna at f_0 = 300 MHz. The solid blue curve is the E-plane pattern plotted versus θ; the dashed red curve is the H-plane pattern plotted versus ϕ. 39
Figure 2-11: Plot showing the magnitude and direction of the surface current on the 3D EAD antenna's NFRP element at 300 MHz when ka = 0.35 and the phase is set at 0°. 40
Figure 2-12: $|S_{11}|$ of the 3D EAD for varying values of ka. 40

LIST OF FIGURES (CONTINUED)

Figure 2-13: Resistance and reactance of the 3D EAD antenna, calculated with full wave simulations (HFSS), and the equivalent circuit in Figure 2-6 with C_{sub} = 0.4 pF, L_{eff} = 153 nH, C_{eff} = 1.2 pF, C_{higher} = 2.0 pF, R_{sub} = 39.1 kΩ, and l_{eff} = 50.0 mm..... 42
Figure 3-1: The 3dB fractional bandwidth values of the 2D and 3D EAD designs. Three theoretical limits for the 3dB fractional bandwidth are also shown..... 45
Figure 3-2: Real (resistance) and imaginary (reactance) parts of the input impedance for the 2D and 3D EAD designs when *ka* = 0.35..... 47
Figure 3-3: Electric fields within the substrate for the 2D EAD antenna when *ka* = 0.35. 48
Figure 3-4: Electric fields within the substrate for the 3D EAD antenna when *ka* = 0.35. 49
Figure 3-5: Maximum directivity of the 2D and 3D EAD antennas versus *ka*..... 50
Figure 3-6: Radiation efficiency of the 2D and 3D EAD designs versus *ka*. 50
Figure 3-7: Radiation efficiency of the 3D EAD at *ka* = 0.35 for varying trace widths. The width of the NFRP element was increased at the same rate as the width of the monopole element. 52
Figure 4-1: $|S_{11}|$ plots for the 2D EAD antenna with *ka* = 0.35 when its inductor value is varied (obtained using HFSS). 54
Figure 4-2: Inductor values and the corresponding $|S_{11}|_{min}$ values plotted against the resulting resonance frequencies for the 2D EAD antenna with *ka* = 0.35 (obtained using HFSS). 54
Figure 4-3: Inductor values and the corresponding $|S_{11}|_{min}$ values plotted against the resulting resonance frequencies for the 3D EAD antenna with *ka* = 0.35 (obtained using HFSS). 55
Figure 4-4: The real (resistive) and imaginary (reactive) parts of the input impedance for the frequency agile 2D and 3D EAD designs when *ka* = 0.35. 57
Figure 4-5: Creating a "Parametric" run within HFSS. 58
Figure 4-6: "Add/Edit Sweep" window after finalizing the sweep values. 59
Figure 4-7: Selecting only one simulation set-up from the "General" tab of the "Setup Sweep Analysis" window. 59
Figure 4-8: Running the frequency agile parametric setup within HFSS. 60
Figure 4-9: First step in creating the frequency agile data table in HFSS. 61
Figure 4-10: The "Report" window after selecting the applicable set-up and sweep..... 61
Figure 4-11: The "Set Range Function" window after selecting the "min" function. 62
Figure 4-12: The "Report" window after setting the range function. 62
Figure 4-13: First two columns of the frequency agile data table. 63
Figure 4-14: "Set Range Function" window after selecting the "XAtYVal" function. 63

LIST OF FIGURES (CONTINUED)

Figure 4-15: "Report" window before adding the third column to the frequency agile data table. 64
Figure 4-16: Frequency agile data table with all three columns. 65
Figure 4-17: Demonstration on how to export the Data Table from HFSS. 65
Figure 4-18: Model tree after deleting the lumped RLC boundary, and adding the second lumped port excitation. 66
Figure 4-19: The "Solutions" window prior to exporting the S2P file. 67
Figure 4-20: Settings used when exporting the S2P files. 68
Figure 4-21: ADS circuit model and parameter sweep settings for the 2D EAD frequency agile simulation. 68
Figure 4-22: Individual $|S_{11}|$ curves from the ADS frequency agile simulation for the 2D EAD (ka = 0.35) as the inductor value was swept. 69
Figure 4-23: Equations used to generate the frequency agile curve within ADS. 70
Figure 4-24: Frequency agile curve generated directly within ADS for the 2D EAD antenna (ka = 0.35). 71
Figure 4-25: Exporting ADS data to a tab-delimited ASCII file. 71
Figure 4-26: Comparison between the frequency agile curves obtained using HFSS and ADS for the 2D EAD antenna (ka = 0.35). 72
Figure 4-27: Comparison between the frequency agile curves obtained using HFSS and ADS for the 3D EAD antenna (ka = 0.35). 72
Figure 5-1: The inductor values of the frequency agile 2D EAD design (ka = 0.35) obtained with HFSS are compared to those calculated using (5-1). 76
Figure 5-2: The inductor values of the frequency agile 3D EAD design (ka = 0.35) obtained with HFSS are compared to those calculated using (5-1). 76
Figure 5-3: The percent error, calculated with (5-2), for the inductor values found using the regression equation for the 2D EAD when ka = 0.35. 77
Figure 5-4: The percent error, calculated with (5-2), for the inductor values found using the regression equation for the 3D EAD when ka = 0.35. 77
Figure 5-5: Illustration of the procedure for calculating the performance of the non-Foster 2D EAD antenna (ka=0.35) at a single frequency. 79
Figure 5-6: Comparison of the non-Foster 2D EAD antenna $|S_{11}|$ (dB) values with the original frequency agile values when ka = 0.35. 80
Figure 5-7: Comparison of the non-Foster 3D EAD antenna $|S_{11}|$ (dB) values with the original frequency agile values when ka = 0.35. 80
Figure 5-8: The relatively wide instantaneous bandwidth of the original 2D EAD antenna leads to a good non-Foster performance. 82
Figure 5-9: The relatively narrow instantaneous bandwidth of the original 3D EAD leads to a poor non-Foster performance. 83
Figure 5-10: Non-Foster performance of the 2D EAD (ka = 0.35), calculated using an adaptive mesh frequency of 500 MHz. 84
Figure 5-11: Non-Foster performance of the 3D EAD (ka = 0.35), calculated using an adaptive mesh frequency of 500 MHz. 85

LIST OF FIGURES (CONTINUED)

Figure 5-12: Radiation efficiencies of the 2D and 3D non-Foster designs when *ka* = 0.35. 86
Figure 5-13: Screenshot of creating a parametric sweep from a CSV file. 91
Figure 5-14: First step in creating the plot of the $L_{regression}$ simulation results. 92
Figure 5-15: Selecting only the $L_{regression}$ inductor values. 93
Figure 5-16: Snippet of an example CSV file used for the non-Foster simulations in ADS. 97
Figure 5-17: Screen shot of the ADS schematic for the non-Foster simulations. 97
Figure 5-18: $|S_{11}|$ curves generated using the $Lregression$ values in ADS for the 2D EAD when *ka* = 0.35. 98
Figure 5-19: Non-Foster curves obtained using HFSS and ADS for the 2D EAD antenna (*ka* = 0.35). 99
Figure 5-20: Non-Foster curves obtained using HFSS and ADS for the 3D EAD antenna (*ka* = 0.35). 100

LIST OF TABLES

Table 2-1: Inductor and BW_{3dB} values for 2D EAD antennas with different *ka* values 35
Table 2-2: Inductor and BW_{3dB} values for 3D EAD antennas with different *ka* values 41
Table 3-1: Comparison of Element Values of the Circuit Model for the 2D and 3D EAD Antennas 48
Table 4-1: -20 dB bandwidths for the 2D and 3D EAD frequency agile designs with *ka* = 0.35 (obtaining using HFSS). 56
Table 5-1. Regression parameter values for the 2D and 3D EAD with *ka* = 0.35 75
Table 5-2: Largest continuous -20 dB bandwidths for the non-Foster 2D and 3D EAD designs with *ka* = 0.35 80

ABSTRACT

Electromagnetic equations pertaining to electrically small dipole antennas and electrically small monopole antennas with small circular ground planes are reviewed. Two electrically small antenna designs are analyzed numerically and the results are compared. The first is a frequency agile version of the two-dimensional (2D) planar Egyptian axe dipole (EAD) antenna. The second is its three-dimensional (3D) counterpart. The frequency agile performance characteristics of both the 2D and 3D EAD designs are studied and compared. The potential for non-Foster augmentation to achieve large instantaneous fractional impedance bandwidths is detailed for each antenna. In addition, details are given on how to run frequency agile simulations in both ANSYS HFSS and Agilent's ADS. Details are also provided on how to generate an antenna's non-Foster $|S_{11}|$ and radiation efficiency curves using HFSS, and how to generate an antenna's non-Foster $|S_{11}|$ curve using ADS.

CHAPTER 1 | INTRODUCTION

As modern electronic devices continue to shrink in size, researchers have become increasingly focused on electrically small antenna (ESA) designs to reduce the footprint of the antenna within the overall electronics system. Engineers in many fields, including wireless communications, biomedical technology, and national defense, can benefit from electrically small antennas as long as the performance of their designs meets the necessary system specifications.

One accepted definition of an electrically small antenna is $ka \leq 1$ [1], where k is the free-space wave number and a is the radius of the smallest sphere which encloses the entire antenna structure. This is the definition for an ESA that will be used herein, and corresponds to an antenna that fits within a sphere whose radius equals one radianlength. A sphere of this size is often referred to as a radiansphere, and is sometimes viewed as the boundary that separates the near-field region from the far-field region.

Electrically small antennas are promising, but designs of this nature that have both large bandwidths and high radiation efficiencies may be difficult to obtain. In fact, as noted, for instance, in the works by Chu [2], McLean [3], Thal [4], and Gustafsson *et. al.* [5], the impedance bandwidth of a passive antenna is theoretically limited by the electrical size of the antenna. A well known method of increasing the bandwidth of any resonant object, such as an antenna, is to increase its losses. However, this method reduces the radiation efficiency of the antenna. Another approach is to accept the fact that the antenna may have a high radiation efficiency while being matched to its source over a narrow bandwidth, but then design it to be frequency agile, i.e., introduce

equivalent elements or circuits that maintain those desirable performance characteristics when their impedance values are adjusted with frequency in some prescribed manner, either manually or electronically. For example, an antenna system is described in [6] that includes multiple inductors which can be turned on or off using diodes, thereby changing the overall reactance of the antenna system.

Electrically small antennas based on the near-field resonant parasitic (NFRP) paradigm have achieved high radiation efficiencies and multi-functionalities while being nearly completely impedance matched to their source over narrow bandwidths [7]. Several classes of these ESAs have reactive elements, inductors or capacitors, built into their NFRP element(s) for tuning purposes. Thus, they too can be made frequency agile by introducing passive elements whose impedance values can be adjusted with frequency in some prescribed manner. Unfortunately, a large instantaneous bandwidth cannot be achieved with such passive element-based antennas because it is found that the requisite component values decrease fast enough with increasing frequency that the element would violate Foster's reactance theorem [8], i.e., the frequency derivative of their reactance is less than zero. Thus they require the introduction of active, non-Foster elements to overcome this passive constraint.

Non-Foster circuit elements are devices whose reactances decrease with increasing frequency. Active elements of this type have been constructed with *negative impedance converters* (NICs) to achieve broad bandwidth matching with external networks [9], [10]; internal elements connected to the driven radiator [11], [12]; and internal elements integrated into the NFRP elements [13], [14], [15], [16], [17]. These

NIC devices were originally introduced using lumped elements [18] and have recently been realized with integrated circuits [19].

For our NFRP antenna applications, the reactance curve of a NIC can be designed to follow a given mathematical function over a large frequency band. This function is specified by the simulated or measured frequency agile behavior of the antenna. Thus, while the design and implementation of the NIC circuit is itself challenging, the realization of the frequency agile response curve sets the goals for those efforts. These will be the major concerns of the following two-dimensional (2D) versus three-dimensional (3D) design comparisons.

To begin the discussion, Maxwell's equations are reviewed in Section 1-1. Then, a brief study on electrically small dipole and monopole antennas is completed in Section 1-2. Finally, Section 1-3 shall introduce the reader to a matching technique that employs an element referred to as a near-field resonant parasitic.

Two related electrically small antenna designs are then introduced in Chapter 2. The first antenna is a planar, or 2D, design and the second is a 3D design. The bandwidths and radiation efficiencies of each design were simulated numerically and are compared in Chapter 3. Circuit models of both antennas are also introduced to help explore their designs and performance characteristics. The corresponding frequency agile behaviors of the 2D and 3D designs are analyzed and compared in Chapter 4. Additionally, notes on how to construct and run frequency agile simulations in both HFSS and ADS are given in Chapter 4. Next, in Chapter 5, the non-Foster behavior of the 2D and 3D designs are discussed, and instructions on how to run non-Foster simulations

in both HFSS and ADS are presented. Conclusions and recommendations for future work are given in Chapter 6. For the reader's convenience, a list of frequently used abbreviations, acronyms, and symbols is given in Appendix A.

As an important note, all of the numerical simulation data presented herein was obtained with either ANSYS/ANSOFT's High Frequency Structure Simulator (HFSS) v13.2, Agilent's Advanced Design System (ADS) v2011.10, or Mathworks' MATLAB v2011a. To simplify the discussion, the desired center frequency was selected to be 300 MHz, corresponding to a free space wavelength of 1000.0 mm, giving ka = 1.0 (0.5) when a = 159.15 (79.58) mm. Unless otherwise noted, the target frequency for the HFSS adaptive mesh generation was set as 400 MHz, and the convergence criteria was set as $\Delta S = 0.001$ with a minimum of two consecutive passes that meet the convergence criteria.

1-1 Maxwell's Equations

To begin any lengthy discourse on antennas, a review of the equations that govern the realm of electromagnetics is well served. These equations are commonly referred to as Maxwell's equations. These four coupled differential equations, originally developed by James Clerk Maxwell, and improved upon by Heinrich Hertz and Oliver Heaviside [20], are presented in time-harmonic form as [21, p. 25]

$$\nabla \times \vec{\mathbf{E}} = -\vec{\mathbf{M}}_i - j\omega\vec{\mathbf{B}} \tag{1-1}$$

$$\nabla \times \vec{\mathbf{H}} = \vec{\mathbf{J}}_i + \vec{\mathbf{J}}_c + j\omega\vec{\mathbf{D}} \tag{1-2}$$

$$\nabla \cdot \mathbf{D} = q_{ev} \tag{1-3}$$

$$\nabla \cdot \mathbf{B} = q_{mv} \tag{1-4}$$

where

- $\vec{\mathbf{E}}$ is the electric field intensity [V/m]
- $\vec{\mathbf{H}}$ is the magnetic field intensity [A/m]
- $\vec{\mathbf{D}}$ is the electric flux density [C/m^2]
- $\vec{\mathbf{B}}$ is the magnetic flux density [Wb/m^2]
- $\vec{\mathbf{J}}_i$ is the impressed electric current density [A/m^2]
- $\vec{\mathbf{J}}_c$ is the conduction electric current density [A/m^2]
- $\vec{\mathbf{M}}_i$ is the impressed magnetic current density [V/m^2]
- q_{ev} is the electric charge density [C/m^3]
- q_{mv} is the magnetic charge density [Wb/m^3]
- ω is the angular frequency [rad/s]
- and $j = \sqrt{-1}$.

By imposing appropriate boundary and/or initial conditions, these four coupled differential equations can (in theory) be solved to determine the electric and magnetic fields anywhere in a problem space. However, in practice, these solutions can become quite cumbersome, especially in inhomogeneous media or when the electric and/or equivalent magnetic current distributions are complicated. Therefore, engineers typically

rely on software programs such as Ansoft/ANSYS's HFSS or Computer Simulation Technology's (CST's) Electromagnetic (EM) Studio to perform full-wave simulations of their systems of interest.

However, when the problem is presented in a homogeneous medium, the magnetic vector potential $\vec{\mathbf{A}}$ and the electric vector potential $\vec{\mathbf{F}}$ can be employed to simplify the process of obtaining the electric and magnetic fields generated by an electric current density and/or an equivalent magnetic current density. A formal derivation of $\vec{\mathbf{A}}$ and $\vec{\mathbf{F}}$ is given in [21, pp. 256-261], and as such, shall not be repeated here. However, a condensed version of a convenient procedure for calculating the total electric and magnetic fields generated in a homogenous medium by electric currents and/or equivalent magnetic currents given in [22] is repeated here, since it will be used during our discussion of dipole and monopole antennas.

1. Specify $\vec{\mathbf{J}}$ and $\vec{\mathbf{M}}$ (electric and magnetic current density sources)
2. a. Find $\vec{\mathbf{A}}$ with

$$\vec{\mathbf{A}} = \frac{\mu}{4\pi} \iiint_V \vec{\mathbf{J}} \frac{e^{-jkR}}{R} dv' \tag{1-5}$$

b. Find $\vec{\mathbf{F}}$ with

$$\vec{\mathbf{F}} = \frac{\varepsilon}{4\pi} \iiint_V \vec{\mathbf{M}} \frac{e^{-jkR}}{R} dv' \tag{1-6}$$

In (1-5) and (1-6), ε is the permittivity of free space, μ is the permeability of free space, $k^2 = \omega^2 \varepsilon \mu$, and R is the distance from any point in the source to the

observation point. The integrations are taken over all of the source points (primed coordinates) and the values of the vector potentials are given at the observation point. It should be noted that if $\vec{\mathbf{J}}$ and $\vec{\mathbf{M}}$ represent linear densities with units of A/m, then (1-5) and (1-6) reduce to surface integrals; also, if $\vec{\mathbf{J}}$ and $\vec{\mathbf{M}}$ represent currents with units of A, then (1-5) and (1-6) reduce to line integrals.

3. The total fields are then given by

$$\vec{\mathbf{E}} = -j\omega\vec{\mathbf{A}} - j\frac{1}{\omega\mu\varepsilon}\nabla\left(\nabla\cdot\vec{\mathbf{A}}\right) - \frac{1}{\varepsilon}\nabla\times\vec{\mathbf{F}} \tag{1-7}$$

and

$$\vec{\mathbf{H}} = \frac{1}{\mu}\nabla\times\vec{\mathbf{A}} - j\omega\vec{\mathbf{F}} - j\frac{1}{\omega\mu\varepsilon}\nabla\left(\nabla\cdot\vec{\mathbf{F}}\right). \tag{1-8}$$

In a homogeneous medium, (1-7) and (1-8) are valid everywhere except at observation points on the sources themselves.

1-2 Dipole and Monopole Antennas

In the following chapters, the discussion will focus on electrically small planar and three-dimensional printed antennas. As we will demonstrate, these antennas behave quite similarly to small dipole and monopole antennas. Therefore, a brief review of small dipole and monopole antennas may be helpful for the reader.

1-2-1 Electrically Small Dipole (Linear Wire) Antennas

As explained previously, an electrically small antenna is defined herein as an antenna that meets the criteria of *ka* being less than one. With this in mind, if *l* is the total

length of a dipole element and $\lambda_0 = k/2\pi$ is the free-space wavelength of the frequency (f_0) of the source driving it, then this dipole antenna is electrically small if

$$l/2 < \lambda_0/2\pi \, . \tag{1-9}$$

Figure 1-1 depicts a simple dipole antenna driven with an ideal current source.

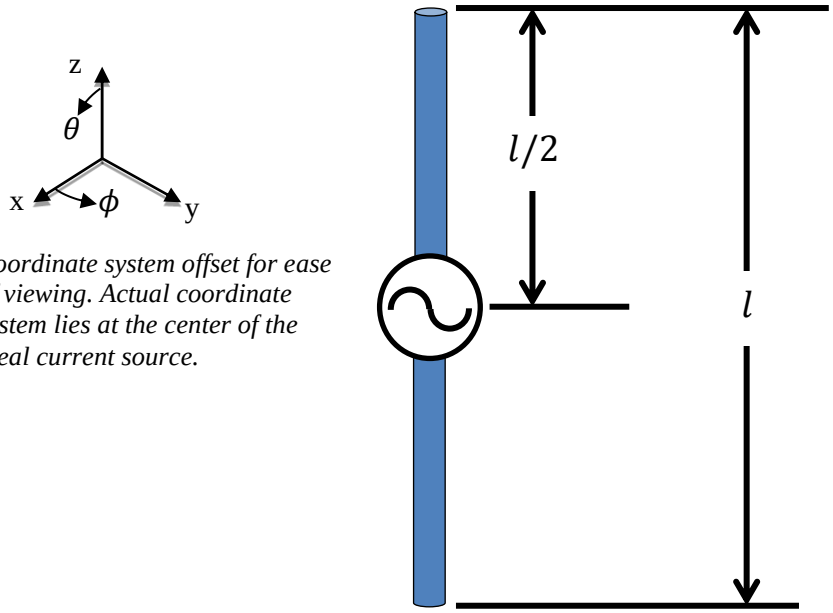

Coordinate system offset for ease of viewing. Actual coordinate system lies at the center of the ideal current source.

Figure 1-1: A dipole antenna driven by an ideal current source.

A good approximation for the current distribution on a small dipole antenna is a triangular distribution [22, pp. 162-165]. Thus, if the dipole is oriented along the z-axis, the current distribution of a small dipole is given as [22]

$$\vec{\mathbf{I}}_e(x', y', z') = \begin{cases} I_o\left(1 - \dfrac{2}{l}z'\right)\hat{\mathbf{z}} \, , & 0 < z' \leq l/2 \\ I_o\left(1 + \dfrac{2}{l}z'\right)\hat{\mathbf{z}} \, , & -l/2 \leq z' \leq 0 \end{cases} \tag{1-10}$$

As we learned in the previous section, once we have the expression for the electric and equivalent magnetic currents in a homogeneous region, we can calculate the electric and

magnetic fields in that region. Since there are no equivalent magnetic currents associated with the electric dipole, (1-10) can be substituted into (1-5) to calculate the magnetic vector potential. After doing so, we can make the approximation that $R \approx r$ over the integration region; and thus by calculating the integrals, we obtain [22]

$$\vec{\mathbf{A}} = \frac{1}{2}\left[\frac{\mu I_o l e^{-jkr}}{4\pi r}\right]\hat{\mathbf{z}}\,. \tag{1-11}$$

Due to the approximation, this magnetic vector potential is more accurate as kr goes to infinity, i.e., in the far-field region. For this discussion, we are interested in obtaining the total directivity pattern of the small dipole antenna, which can be calculated from the far-field electric fields of the dipole. Thus, substituting (1-11) into (1-7), and taking the limit as $kr \to \infty$, we obtain [22]

$$\vec{\mathbf{E}}_{ff}^{\,small\ dipole} \approx j\eta_0 \frac{kI_o l e^{-jkr}}{8\pi r}\sin(\theta)\,\hat{\boldsymbol{\theta}}\,, \tag{1-12}$$

which is the expression for the far-field electric fields of a small dipole oriented along the z-axis. In (1-12), η_0 represents the impedance of free space, where $\eta_0 = \sqrt{\mu/\varepsilon}$.

In order to calculate the total directivity pattern of the small dipole, we must first calculate the radiation intensity and the total radiated power. In the far-field, the radiation intensity $U(\theta,\phi)$ can be approximated as [22]

$$U(\theta,\phi) \approx \frac{r^2}{2\eta_0}\left[|E_\theta(r,\theta,\phi)|^2 + \left|E_\phi(r,\theta,\phi)\right|^2\right]. \tag{1-13}$$

The total radiated power P_{rad} is given as [22]

$$P_{rad} = \int_0^{2\pi}\int_0^{\pi} U(\theta,\phi)\sin(\theta)\,d\theta\,d\phi\,. \tag{1-14}$$

Finally, the total directivity can be calculated as

$$D(\theta,\phi) = 4\pi \frac{U(\theta,\phi)}{P_{rad}}. \tag{1-15}$$

Using a combination of (1-12), (1-13), (1-14), and (1-15), we find that the total directivity for the small dipole oriented along the z-axis is given as

$$D_{total}^{small\ dipole}(\theta,\phi) = \frac{3}{2}\sin^2(\theta)\,. \tag{1-16}$$

Figure 1-2 shows the total directivity patterns for the small dipole in the E-and H-planes.

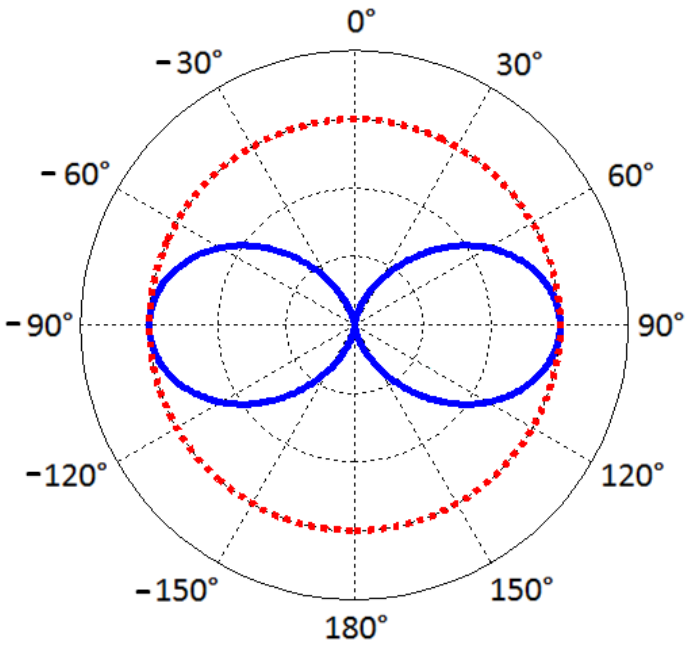

Figure 1-2: Total directivity patterns of the small dipole antenna oriented along the z-axis. Solid blue curve is the E-plane pattern plotted versus θ. Dashed red curve is the H-plane pattern plotted versus ϕ.

Now that we have determined the directivity of the small electric dipole antenna, we would also like to determine its input impedance. As is well known, the input impedance of a small electric dipole antenna can be derived analytically. For illustration,

we will use the equations given in [22] to determine the resistive and reactive parts of a dipole antenna whose half-length equals $\lambda_0/18$ when f_0 = 300 MHz, which corresponds to a *ka* value of approximately 0.35 at a frequency of 300 MHz. From [22], the resistive part of the input impedance (i.e., resistance) of a small dipole antenna (assumed to be dominated by its radiation resistance, R_r) is given by

$$Re\{Z_{in,small\ dipole}\} \approx R_r \approx 20\pi^2 \left(\frac{l}{\lambda}\right)^2 = 20(ka)^2\,, \tag{1-17}$$

and its corresponding reactive part (i.e., reactance) is given by

$$Im\{Z_{in,small\ dipole}\} \approx -120\frac{\ln\left(l/b\right)-1}{\tan(kl)}\,, \tag{1-18}$$

where *b* is the radius of the dipole. The resistance and reactance of the *ka* = 0.35 dipole antenna with $b = a/20$ were calculated as functions of frequency in a range of interest; they are shown in Figure 1-3.

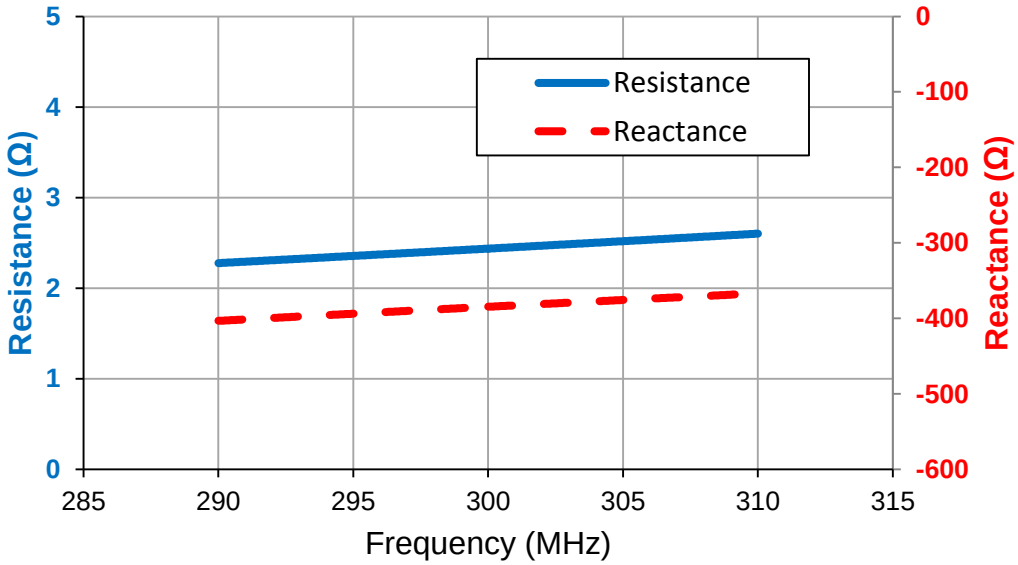

Figure 1-3: Analytical results for the resistance and reactance of the input impedance of a small dipole antenna ($a = l/2 = \lambda_0/18$ when f_0 = 300 MHz, *ka* = 0.35, $b = a/20$).

As observed, the small dipole antenna has a very small radiation resistance and is a highly capacitive element. If one were to attempt to match this antenna to a typical 50Ω source, one would normally use some sort of external matching network, e.g., a large inductor and a quarter-wavelength transformer, which generally increases the overall size of the antenna system to the point where it is no longer electrically small. Since the definition of the radiation efficiency η of an antenna is given as

$$\eta = \frac{R_r}{R_r + R_L}, \tag{1-19}$$

where R_L is the loss resistance of the antenna, any additional loss attributed to the matching network would increase R_L and thus further decrease the overall radiation efficiency of the system. For these reasons, the small dipole antenna by itself is not an ideal design for many electrically small antenna functions. Similarly, small loop antennas are highly inductive with very low radiation resistance; therefore, they also are not ideal for many electrically small antenna applications.

1-2-2 Electrically Small Monopole Antennas over Finite Circular Ground Planes

In the previous section, it was shown how electrically small dipole antennas, by themselves, are not well matched to common transmission line impedances. Another simple linear wire antenna is the monopole antenna. Typically, ideal monopole antennas are positioned over an infinite ground plane of electrically conductive material. However, since we are concerned with electrically small antennas, the ground plane in our case must be finite. An illustration of a simple monopole antenna of length h over a finite

circular ground plane of radius a driven with an ideal current source is shown in Figure 1-4.

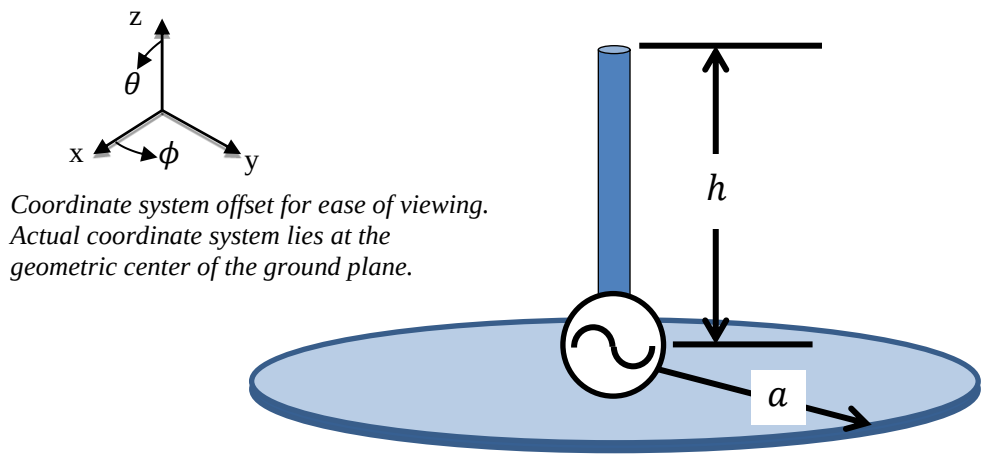

Figure 1-4: Illustration of a monopole antenna with length h over a finite circular ground plane of radius a driven with an ideal current source.

With the monopole antenna over a circular ground plane, the entire antenna structure must lie within the radiansphere for the antenna to be classified as electrically small. Therefore, both kh and ka must be less than or equal to unity for the monopole antenna with a finite ground plane to be classified as electrically small.

To determine the far-field pattern and the input impedance of the electrically small monopole antenna over a finite circular ground plane, the procedure introduced in Section 1-1 could be used, as long as we could derive the electrical currents induced on the ground plane by the monopole antenna. However, if we assume that the circular ground plane is infinitely thin, we must also account for the diffraction effects caused by the infinitely sharp edge of the ground plane. These additional pieces of information complicate the calculations significantly.

Therefore, instead of deriving the results herein, we shall rely on the results presented in [23] for monopole elements that are located at the center of a circular ground plane whose radius is small compared to a wavelength. We are interested in the case where ka and kh are less than unity, which is the same as the case where a/λ and h/λ are less than $(2\pi)^{-1} \approx 0.161$. By interpolating the results given in [23], we find that, due to the near-field diffraction from the edge of the circular ground plane, the directivity patterns of the electrically small monopole look identical to those of the electrically small dipole, shown in Figure 1-2. The highest directivity values occur where $\theta = 90°$, and at those locations, the total directivity is equal to 1.5 (1.76 dB).

Through an interpretation of the results in [23], we also find that the input resistance of an electrically small monopole (assumed to be dominated by its radiation resistance, R_r) over a circular ground plane with $ka = kh \leq 1$ can be approximated as

$$Re\{Z_{in,small\ monopole}\} \approx 20\pi^2 \left(\frac{h}{\lambda}\right)^2 = 5(ka)^2 \,. \tag{1-20}$$

By comparing (1-17) with (1-20), we find that the resistance of an electrically small monopole over a small circular ground plane is one-fourth the resistance of an electrically small dipole. Also, in both cases, the reactance of each antenna is largely negative, and hence both antenna types are largely capacitive. Consequently, like the dipole, the electrically small monopole by itself is not a good a candidate for electrically small antenna applications when using commonplace transmission line impedances.

1-3 Impedance Matching with Near-Field Resonant Parasitic Elements

As mentioned in the previous two sections, electrically small dipole and electrically small monopole antennas, by themselves, are not well suited for many small antenna applications. However, when a matching network of some kind is used to match these types of antennas to the characteristic impedance of the transmission line, then these antennas become more viable.

The problem of matching electrically small antennas to typical transmission line impedances (either 50Ω or 75Ω) is one that has been investigated quite thoroughly [22], [24]. One successful method that eliminates the need for an external matching circuit is to use a near-field resonant parasitic (NFRP) element based on metamaterial-inspired designs along with a simple driven element. The underlying physics behind this kind of internal impedance transformer arrangement was reviewed in [7], but shall also be summarized herein for the reader's convenience.

The NFRP configuration consists of a driven element (shown on the left in Figure 1-5) and the NFRP element (shown on the right in Figure 1-5). As we have seen previously, the electrically small dipole and the electrically small monopole are both highly capacitive antennas. Therefore, by adding the NFRP element, the goal is to achieve a total reactance equal to zero and a total resistance equal to the transmission line impedance at a desired resonant frequency, while also realizing a high radiation efficiency value. The driven element with the NFRP configuration is shown conceptually in Figure 1-5.

To obtain these conditions, the NFRP element must be a lossy RLC resonator. With this configuration, the size and material properties of the NFRP and the driven element may then be adjusted such that the NFRP provides conjugate matching to the driven element at a specified resonance frequency.

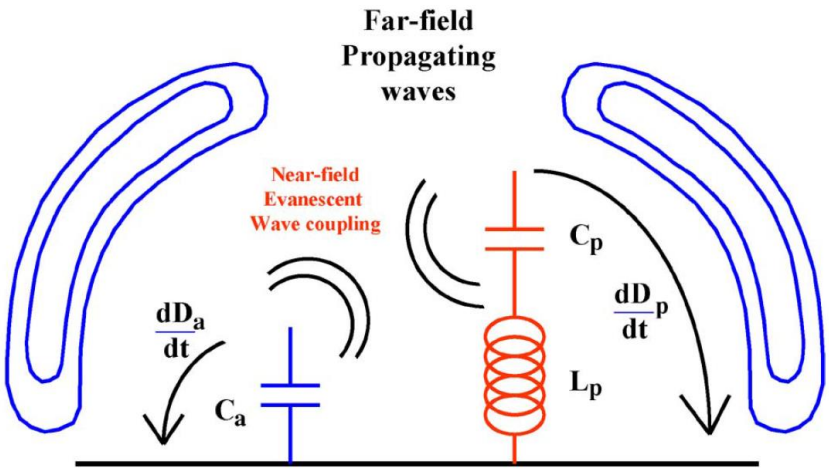

Figure 1-5: Diagram of the underlying physic of a NFRP element. Figure originally presented in [7], reused here with the lead author's permission.

NFRP elements can therefore be used along with electrically small dipole or small monopole antennas. Since the NFRP can be placed in the near field of the dipole/monopole, and since the NFRP itself can be constructed such that it is also electrically small, the overall electrical size of the antenna structure remains electrically small. Thus, by adding a NFRP, the resulting electrically small dipole and monopole antenna systems can become nearly completely impedance matched to the source without incorporating any matching network, and can have a high radiation efficiency, which makes both now viable candidates for many electrically small antenna applications.

CHAPTER 2 | INTRODUCTION TO PLANAR AND 3D EGYPTIAN AXE DIPOLE ANTENNAS

As was discussed in the previous chapter, printed dipole or monopole antennas can be used in conjunction with near-field resonant parasitic elements to efficiently match the antennas to the source impedance, while still maintaining a small *ka* value. One such configuration has been referred to as the Egyptian axe dipole (EAD) [7], [15], [17], [25]. In Section 2-1, the planar, or 2D, EAD antenna will be introduced and analyzed. In the following section, Section 2-2, the three-dimensional (3D) EAD antenna will be introduced an analyzed. From these sections, we shall see how the 2D and the 3D EAD designs perform similarly. In Chapter 3, the differences between the two designs will be highlighted and further analyzed.

2-1 Planar (2D) Egyptian Axe Dipole

The planar, or 2D, EAD design is shown in Figure 2-1. This antenna has a driven printed dipole element on the bottom side of the substrate, and a printed NRFP element on its top side. The substrate used was 0.7874 mm (31 mil) thick Rogers Duroid^{TM} 5880 with 2 oz. (70 μm thick) copper cladding. The NFRP element and the driven monopole were modeled as copper. A lumped element inductor is incorporated in the middle of the NFRP element outside of the substrate. To simplify the HFSS model, the driven dipole element is excited with a 50Ω lumped port, and the inductive element is placed in-line with the NFRP element. The trace widths of the dipole and NFRP elements are, respectively, 1.5 mm and 3 mm for the 2D EAD when $ka = 0.35$. The lumped port in the

dipole is located and centered directly below the inductive element in the NFRP element. When *ka* = 0.35, the gap in the dipole is 4.5 mm, and the gap in the NFRP is 2.0 mm.

The inductor element allows one to retune the resonance of the antenna to 300 MHz for different values of *ka*, i.e., for different substrate radii. The length of the driven element and the gap between the ends of the NFRP element are adjusted to fine tune the impedance matching. As will be illustrated, the presence of the inductive element is necessary when treating the antenna as either a frequency agile or a non-Foster design.

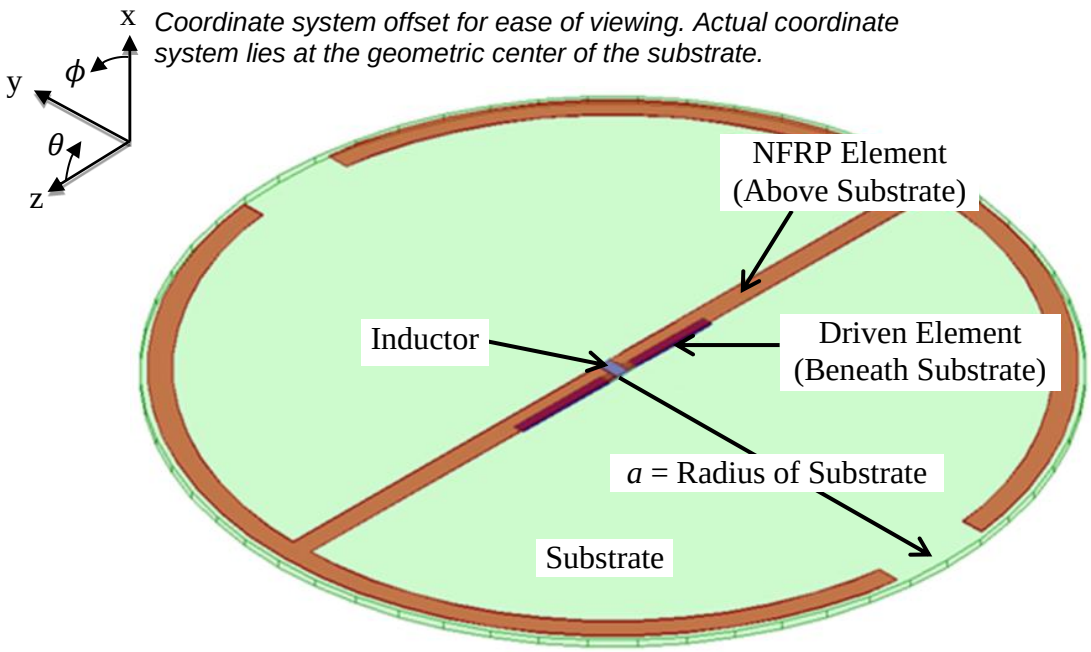

Figure 2-1: The planar (2D) Egyptian axe dipole (EAD) design. The substrate and NFRP element are shown as semi-transparent for ease of viewing.

As one might expect, the 2D EAD antenna acts like an electrically small dipole antenna. Typical E and H-plane directivity patterns for the 2D EAD antenna are shown in Figure 2-2. The maximum directivity is 1.65 (2.17 dB) when *ka* equals 0.35

(i.e., a = 56 mm ~ $\lambda_0/18$). For further understanding of the far-field radiation pattern, a vector plot showing the magnitude and direction of the surface current on the NFRP element of the 2D EAD antenna at resonance is shown in Figure 2-3. The observed currents correspond nicely to the dipole pattern shown in Figure 2-2 and confirm that the far-field of the 2D EAD antenna is linearly polarized. It is interesting to note that the 2D EAD has a higher maximum directivity than the electrically small dipole, which implies that the while the 2D EAD radiates primarily in the lowest order TM mode, a bit of the lowest order TE mode has begun to express itself. In contrast, the electrically small electric dipole only radiates a single (lowest order) TM mode.

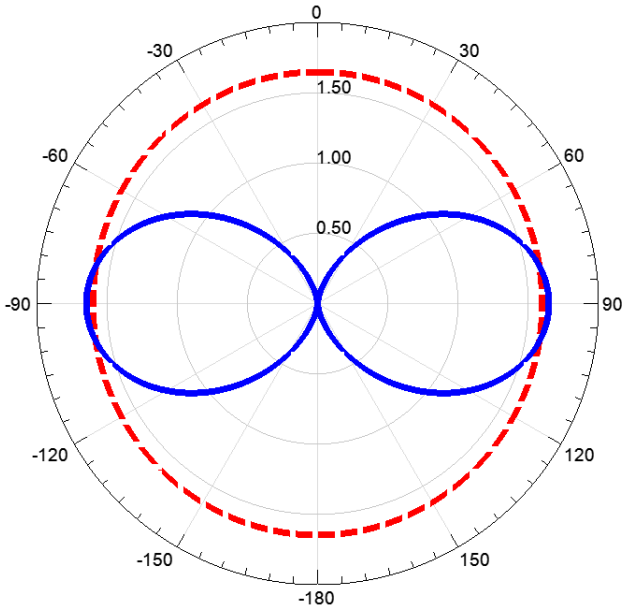

Figure 2-2: Directivity patterns of the 2D EAD antenna at f_0 = 300 MHz. The solid blue curve is the E-plane pattern plotted versus θ; the dashed red curve is the H-plane pattern plotted versus ϕ.

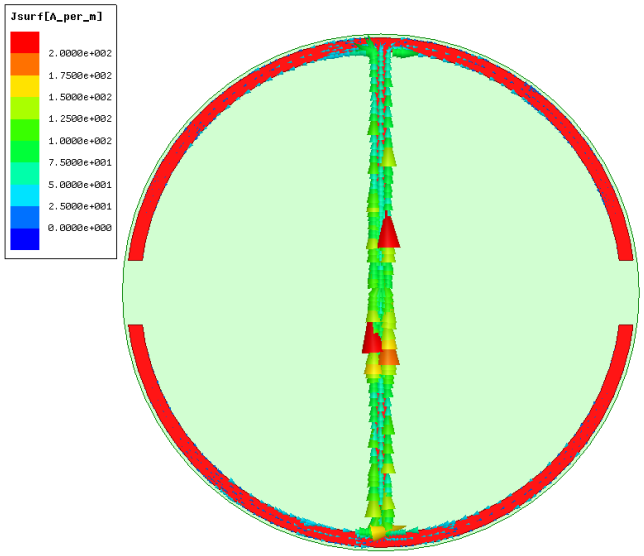

Figure 2-3: Vector plot of the magnitude and direction of the surface current on the NFRP element of the 2D EAD at 300 MHz when *ka* = 0.35 and the input phase is set at 0°.

The resistance and reactance of the 2D EAD antenna when *ka* = 0.35 are shown in Figure 2-4. Based on simulation data, the 2D EAD antenna has a complex input impedance of Z_{in} = 47.0 + *j*0.4 Ω at f_0 = 300 MHz, i.e., it is nearly completely matched to the source at its resonance frequency. To demonstrate how well this antenna is matched to its Z_0 = 50Ω source, the reflection coefficient Γ is calculated as

$$\Gamma = \frac{Z_{in} - Z_0}{Z_{in} + Z_0}, \tag{2-1}$$

and the magnitude of the scattering parameter S_{11} in dB is calculated as

$$|S_{11}|_{dB} = 20\log_{10}(|\Gamma|) \ . \tag{2-2}$$

By using (2-1) and (2-2), the $|S_{11}|$ value at resonance turns out to be equal to -30.1 dB. Therefore, at f_0, the 2D EAD antenna is very well matched to its 50Ω source.

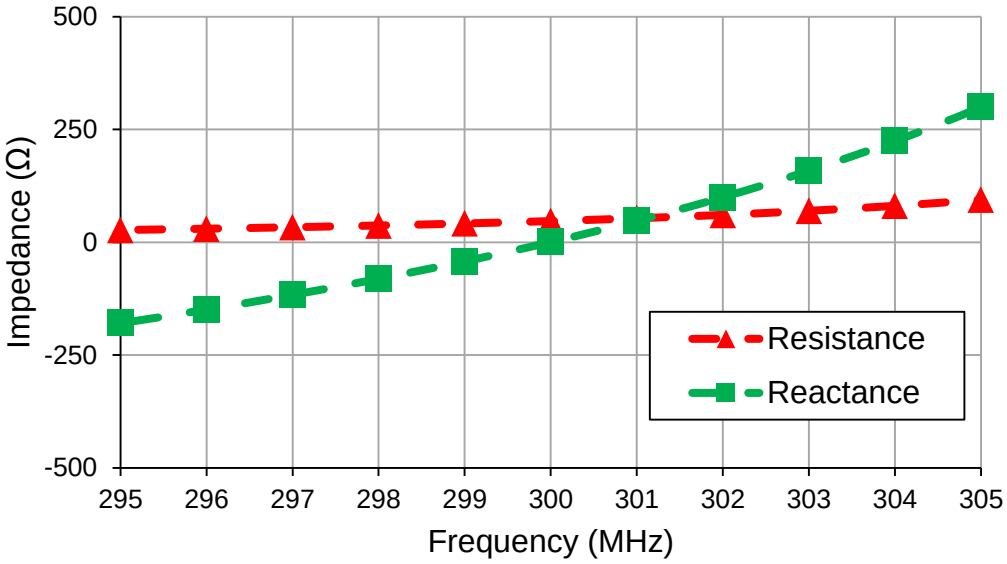

Figure 2-4: Resistance and reactance of the 2D EAD antenna when ka = 0.35.

While the 2D EAD antenna is shown to be well matched to its 50Ω source when ka = 0.35 (i.e., a = 56 mm ~ $\lambda_0/18$), we can determine its performance characteristics at other electrical sizes, particularly its bandwidth, radiation efficiency, and directivity. The designs for different ka values were obtained by modifying the dimensions of the NFRP and driven elements, as well as the value of the in-line inductor. Fixing the resonance frequency to be f_0 = 300 MHz, the design procedure that was followed is summarized here:

1. Specify a value of $ka = 2\pi a / \lambda_0 = 2\pi f_0 a / c$, where $c = 299{,}792{,}458$ m/s.
2. Select the substrate radius to match this value of a.
3. Modify the geometry of the NFRP and driven elements, along with the value of the inductor, until the antenna design produces a value of $|S_{11}| \leq$ -20 dB at f_0.
4. Repeat steps 1-3 for all desired values of ka.

The $|S_{11}|$ curves that were obtained from the simulations of the 2D EAD antenna designs at various values of *ka* are shown in Figure 2-5. The inductor values used to tune the designs and the resulting half power (3dB) bandwidths are summarized in Table 2-1. To be explicit, the 3dB bandwidths (BW_{3dB}) were found by determining the frequencies $f_{\pm}$ at which $|S_{11}|$ equaled -3dB, where $f_{\pm}$ is the nearest frequency value above (+) and below (–) the resonance frequency f_0, and then by calculating BW_{3dB} as $BW_{3dB} = f_+ - f_-$. The results show that the fractional 3dB bandwidth, $FBW_{3dB} = BW_{3dB} / f_0$, decreases with decreasing *ka*, as is discussed in Chapter 3 and is expected from the theoretical bounds [2], [3], [4], [5]: $Q_{lb,elec} \approx 1.5\ \eta\ (ka)^{-3}$ and $FBW_{3dB} = 2/\ Q_{lb,\ elec} \propto (ka)^3$ when $ka << 1$.

To clarify the performance characteristics of the 2D EAD antenna, an equivalent circuit model was derived and investigated. It was used to determine how certain physical parameters of the antenna design affect the input impedance of the antenna. The equivalent circuit model for the top-hat loaded dipole antenna derived in [26] can be slightly modified to replicate the 2D EAD antenna results by adding a series capacitor and a parallel resistor. These additional circuit elements are meant to model the effects of the driven element coupling to the NFRP element through the substrate. This 2D EAD antenna equivalent circuit is illustrated in Figure 2-6. It was found that this circuit model was also appropriate for the 3D EAD antenna.

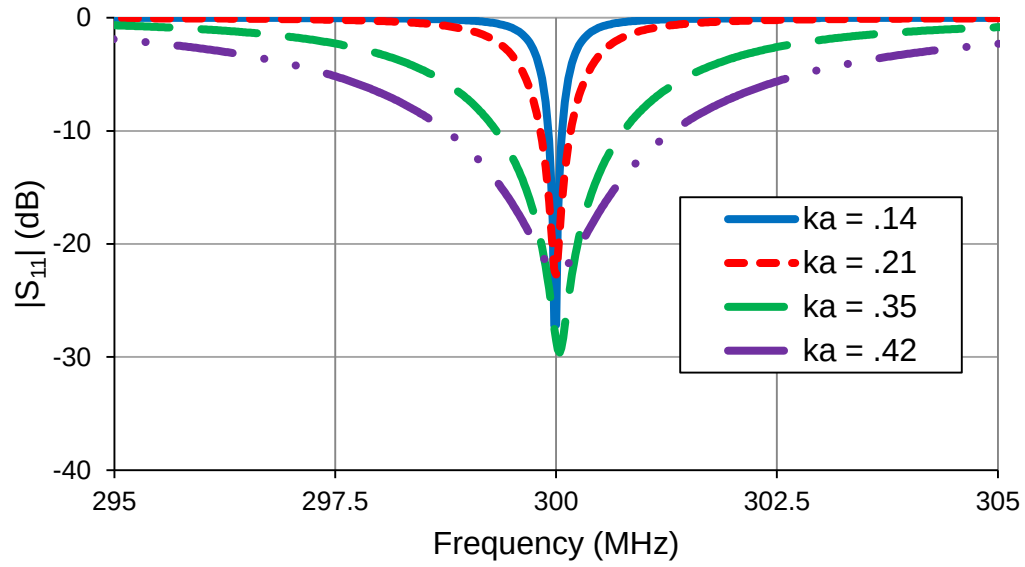

Figure 2-5: $|S_{11}|$ versus frequency for the 2D EAD antenna for several values of *ka*.

Table 2-1: Inductor and BW_{3dB} values for 2D EAD antennas with different *ka* values

ka	**Inductor Value**	**-3dB Bandwidth**
0.14	365.0 nH	0.17 %
0.21	225.9 nH	0.35 %
0.35	94.3 nH	1.44 %
0.42	53.0 nH	2.64 %

By comparing the predictions of the equivalent circuit model to the results given by the full wave HFSS simulations, values for C_{sub}, L_{eff}, C_{eff}, C_{higher}, R_{sub}, and l_{eff} were determined. The inductor value L is already known, since it is the value of the in-line inductor used to tune the 2D EAD antenna to 300 MHz. A plot comparing the input impedances for the *ka* = 0.35 2D EAD antenna simulated with HFSS and calculated with the equivalent circuit is shown in Figure 2-7. The agreement is very good.

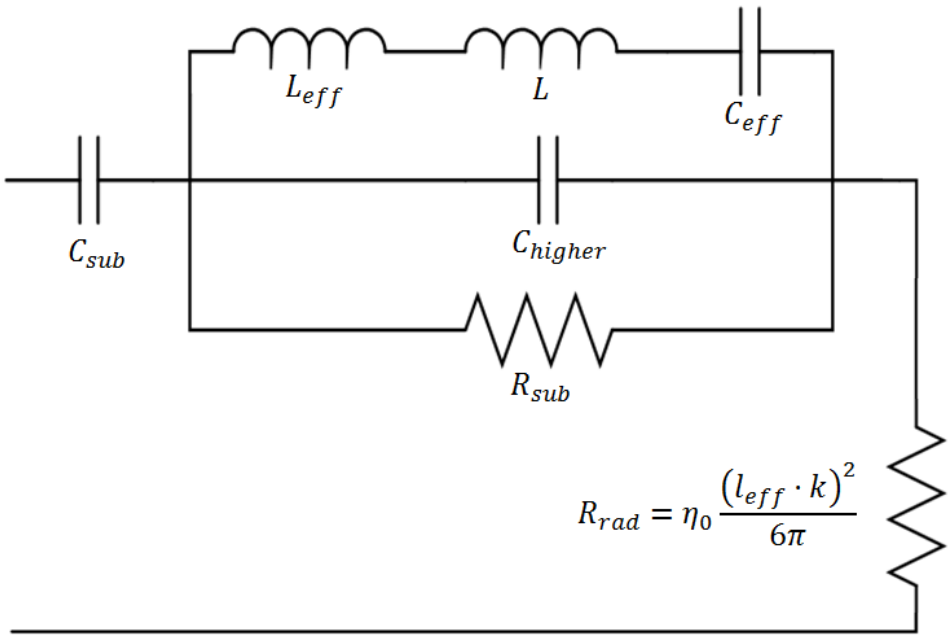

Figure 2-6: Equivalent circuit model for the 2D and 3D EAD antenna designs (note that η_0 in this diagram represents the impedance of free space, not the radiation efficiency).

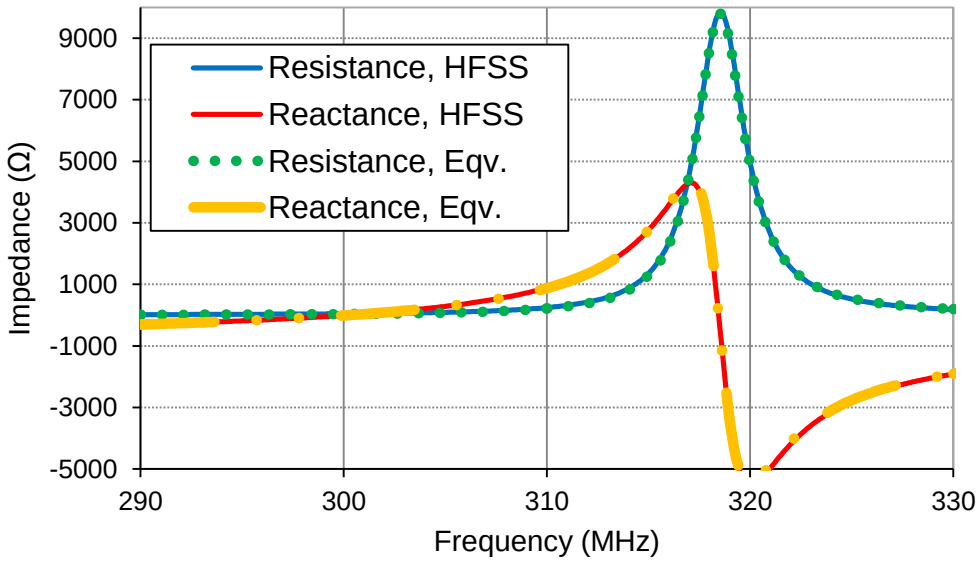

Figure 2-7: Resistance and reactance curves for the 2D EAD antenna with *ka* = 0.35, calculated with the full wave simulation (HFSS), and with the equivalent circuit shown in Figure 2-6 with C_{sub} = 0.92 pF, L_{eff} = 257.5 nH, C_{eff} = 1.1 pF, C_{higher} = 2.0 pF, R_{sub} = 9.8 kΩ, and l_{eff} = 70.0 mm.

2-2 Three-Dimensional (3D) Egyptian Axe Dipole

As shown in the previous section, the passive bandwidth of the 2D EAD antenna is quite narrow, especially since it is planar and does not effectively fill its radiansphere [5]. Consequently, it was desired to determine whether a 3D version, referred to here as the 3D EAD design, could lead to an even larger frequency agile bandwidth and, subsequently, a larger NIC-facilitated bandwidth.

The baseline 3D EAD design is shown in Figure 2-8. The same substrate was used for the 3D EAD as for the 2D EAD. The radius of the ground plane is 5.0mm larger than the radius of the substrate, and the ground plane is 0.2 mm thick. The traces of the NFRP element are all 1.0 mm wide, and the width of the monopole is 0.5 mm wide. The NFRP element includes an inductor across a gap in its vertical trace. The inductor gap is 1.0mm long. The gaps between the ends of the NFRP element and the ground plane are identical. These gaps, along with the trace widths, the monopole length, and the inductor value can be adjusted to achieve impedance matching once the value *ka* is selected.

The SMA-connector, as shown in Figure 2-8, was also included. While its presence has little impact on the results reported here, its presence would have a large impact on a version of the design without the ground plane. This was found in a related rectenna EAD application reported previously [27].

To demonstrate that the 3D EAD antenna is matched to a 50Ω source after it has been properly tuned, the resistance and reactance of its input impedance with $ka = 0.35$ are shown in Figure 2-9. Based on the simulated data, it has a complex input impedance $Z_{in} = 47.6 - j5.6\ \Omega$ at $f_0 = 300$ MHz. Therefore, by employing (2-1) and (2-2), we

calculate that at 300 MHz, $|S_{11}|$ = -24.1 dB. This indicates that when it is properly tuned, the 3D EAD antenna is very well matched to its 50Ω source.

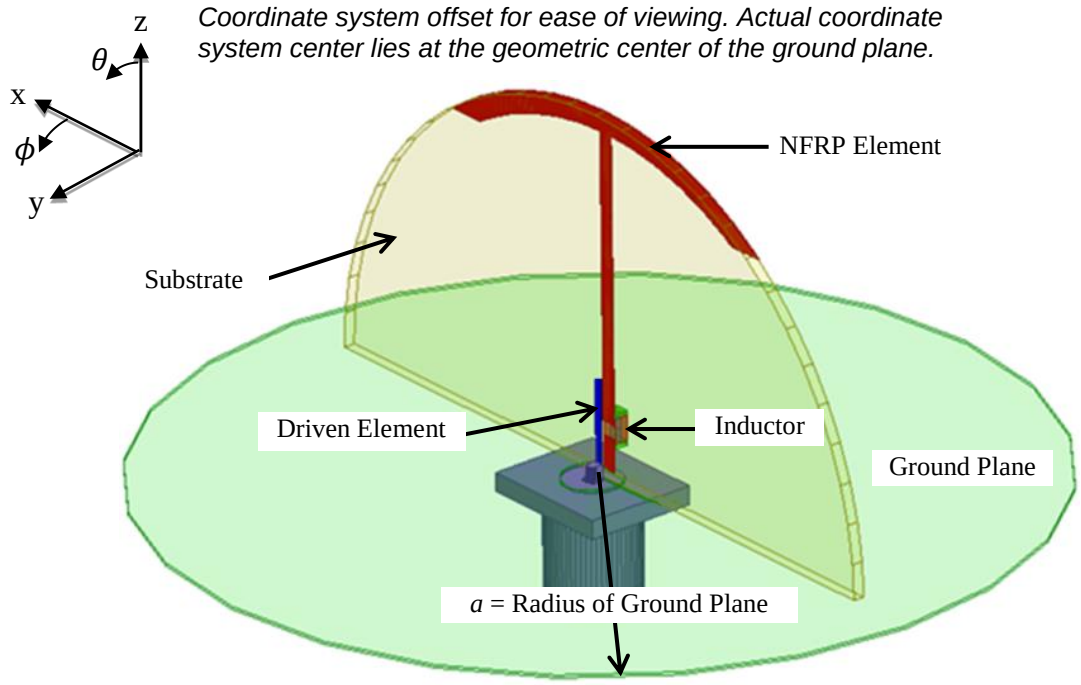

Figure 2-8: Isometric view of the three-dimensional Egyptian axe dipole (3D EAD) antenna. The substrate and the ground plane are semi-transparent for ease of viewing.

Since the NFRP element of the 3D EAD antenna, which is the main radiator, physically looks like an electrically small monopole over a finite ground plane, we would expect its directivity patterns to look like those of the small monopole antenna. As observed in Figure 2-10, this turns out to be exactly the case. The maximum directivity of the 3D EAD is 1.53 (1.85 dB) when *ka* equals 0.35. Similar to the case with the 2D EAD, the maximum directivity of the 3D EAD is greater than 1.5, which is the maximum directivity of an electrically small monopole over a finite circular ground plane. Thus, the 3D EAD antenna also must be radiating a mix of the lowest order TE and TM modes, but

primarily the TM mode and less of the TE mode than in the 2D design, to achieve this directivity value.

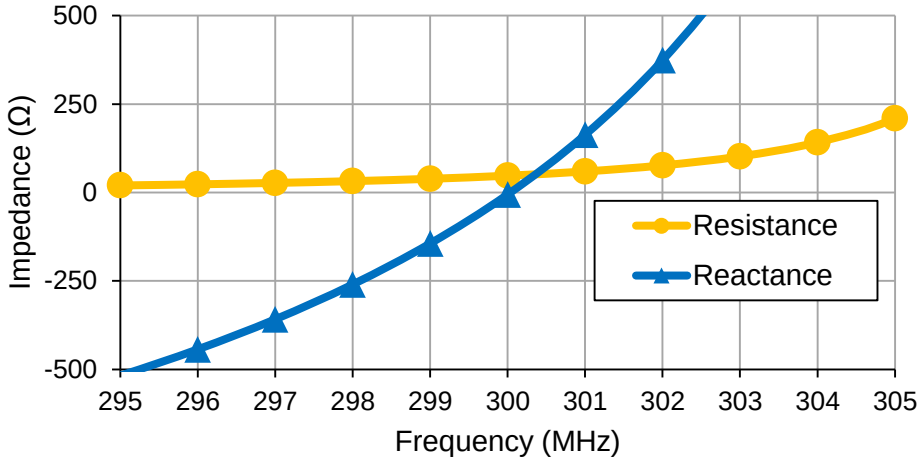

Figure 2-9: Resistance and reactance for the 3D EAD antenna when ka = 0.35.

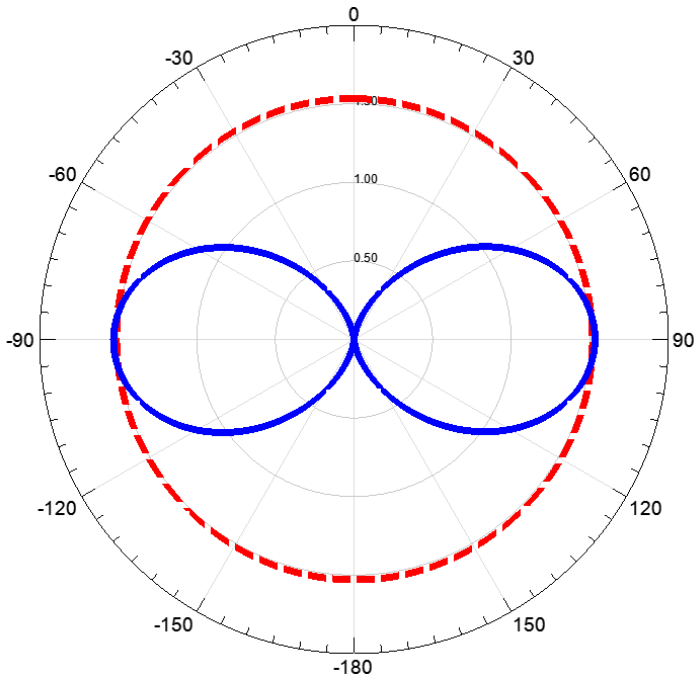

Figure 2-10: Directivity patterns of the 3D EAD antenna at f_0 = 300 MHz. The solid blue curve is the E-plane pattern plotted versus θ; the dashed red curve is the H-plane pattern plotted versus ϕ.

For further understanding of the far-field pattern of the 3D EAD antenna, a vector plot showing the magnitude and direction of the surface current on the NFRP element of the 3D EAD system at resonance is shown in Figure 2-11. The current at resonance is observed to be mainly along the vertical strip of the NFRP element. This confirms that the 3D EAD antenna acts as an electrically small, electric dipole antenna.

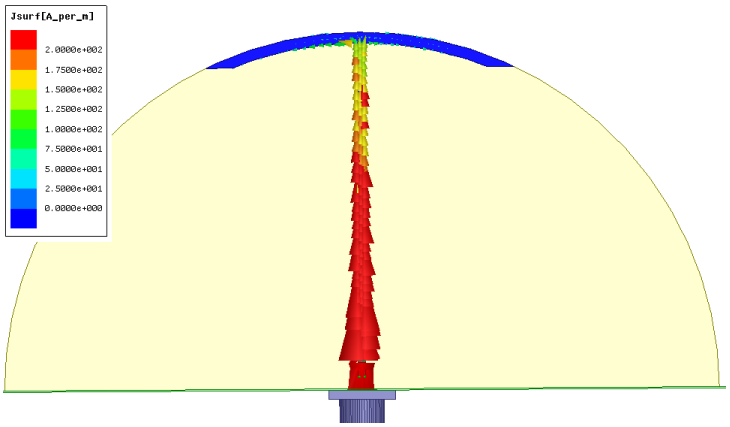

Figure 2-11: Plot showing the magnitude and direction of the surface current on the 3D EAD antenna's NFRP element at 300 MHz when *ka* = 0.35 and the phase is set at 0°.

By performing the same *ka* parameter study as with the 2D version, one obtains the $|S_{11}|$ curves shown in Figure 2-12. The inductor values and the corresponding FBW_{3dB} values are given in Table 2-2.

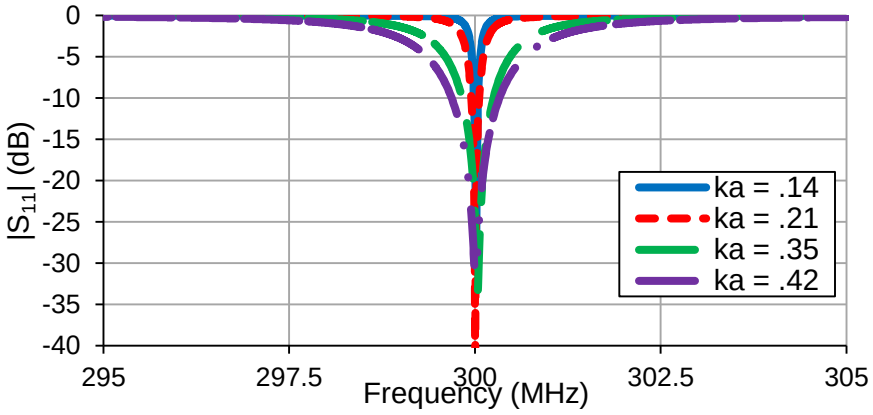

Figure 2-12: $|S_{11}|$ of the 3D EAD for varying values of *ka*.

Table 2-2: Inductor and BW_{3dB} values for 3D EAD antennas with different *ka* values

ka	**Inductor Value**	**-3dB Bandwidth**
0.14	460.2 nH	0.06 %
0.21	340.8 nH	0.11 %
0.35	199.0 nH	0.43 %
0.42	165.3 nH	0.65 %

One unexpected difference in these results, when compared to the corresponding 2D values, is the slope of the reactance through the resonance. As will be discussed in detail later, the quality factor can be calculated from the slopes of the resistance and reactance curves. Comparing Figure 2-12 with Figure 2-5, it is apparent that, for each value of *ka*, the 2D EAD antenna has a larger bandwidth than its 3D version. Moreover, one finds in comparing Table 2-2 with Table 2-1 that the inductor values in the 2D design are about half the 3D design values. With the circuit model, one can confirm that the smaller the inductor value, the broader the bandwidth. Consequently, despite the 3D nature of this EAD design, it has an instantaneous bandwidth disadvantage over the 2D version.

As was done with the 2D EAD antenna, the equivalent circuit for the 3D EAD was generated and used to give further insight into the physics behind the 3D EAD design. Not surprisingly, the equivalent circuit shown in Figure 2-6 can also be used for the 3D EAD antenna. The full wave HFSS simulation and the circuit model input impedance results are compared in Figure 2-13. The agreement is very good.

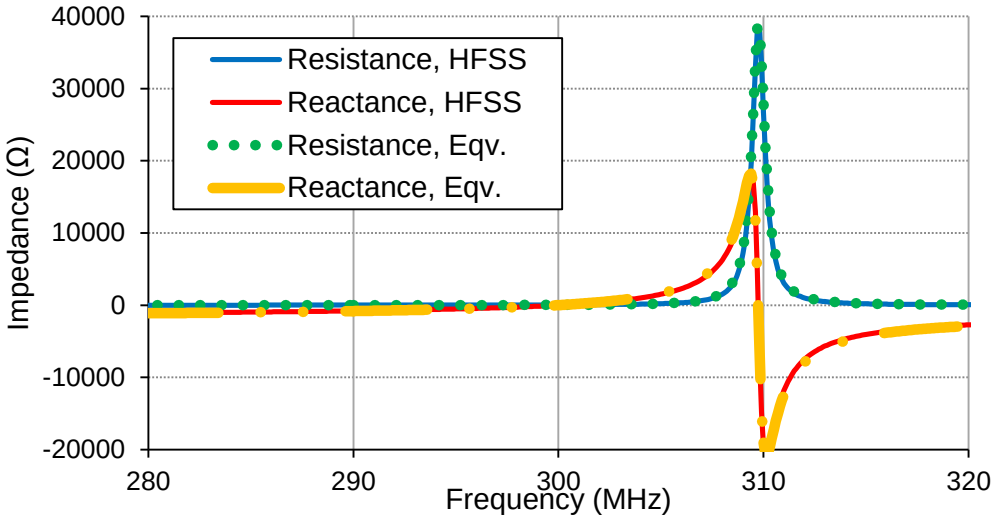

Figure 2-13: Resistance and reactance of the 3D EAD antenna, calculated with full wave simulations (HFSS), and the equivalent circuit in Figure 2-6 with C_{sub} = 0.4 pF, L_{eff} = 153 nH, C_{eff} = 1.2 pF, C_{higher} = 2.0 pF, R_{sub} = 39.1 kΩ, and l_{eff} = 50.0 mm.

As is apparent already, the 2D and 3D EAD antennas behave differently. In general, the impedance bandwidth of the 2D EAD antenna is larger than that of the 3D design. Although the slopes of the resistance curves are similar for both antenna designs at their resonance frequency, 300 MHz, the slopes of their reactance curves are quite a bit different there. These facts are important to keep in mind, mostly because they are critical clues that will help explain the bandwidth differences between these two antennas.

In addition, when comparing the circuit values for the 3D and 2D designs, one may notice immediately that the effective inductance L_{eff} and resistance R_{sub} values of the former are significantly larger than in the latter. On the other hand, the effective length l_{eff} and the capacitance C_{sub} are lower for the 3D case. These additional clues will again aid in understanding the corresponding variations in the radiation efficiency and bandwidth characteristics of these designs. These characteristics for each antenna design will be compared and contrasted with much more detail in the following chapter.

CHAPTER 3 | ANALYSIS OF THE INSTANTANEOUS PERFORMANCE OF THE EAD ANTENNAS

It was shown in the previous chapter that by including an inductor in the NFRP element, both the 2D and 3D EAD antennas can be simultaneously electrically small and matched with a 50Ω transmission line with no external matching network. Moreover, the results showed unexpected differences in their bandwidth properties. Here, we explore why these differences occur and how they impact the performance characteristics of these antennas as the value of *ka* is varied.

3-1 Analysis of the Bandwidth Values

As observed from the $|S_{11}|$ plots (Figure 2-5 and Figure 2-12), the bandwidth of each antenna design tends to decrease as *ka* decreases. This is in good agreement with the theoretical lower limits on the quality factor *Q* for passive antenna systems [2], [3], [4], [5]. In particular, one has the Chu limit [2] (as improved by McLean [3]), which accounts for the reactive energy exterior to the radian sphere,

$$Q_{Chu} = \frac{1}{(ka)^3} + \frac{1}{ka}, \tag{3-1}$$

and the more restrictive Thal limit which includes the reactive energy within the radian sphere [4]:

$$Q_{Thal} = \frac{1}{\sqrt{2}\,ka} + \frac{3}{2\,(ka)^3}. \tag{3-2}$$

Furthermore, accounting for the radiation efficiency of the antenna, these limits can be tightened further [5], [28] to give the lower bound on *Q*

$$Q_{sphere,lb} = \eta\left[\frac{1}{\sqrt{2}\,ka} + \frac{3}{2\,(ka)^3}\right] \tag{3-3}$$

which is tightened even further [5] for a planar antenna

$$Q_{planar,lb} = \frac{3\pi}{4} Q_{sphere,lb}\,. \tag{3-4}$$

The quality factor of an antenna is related to its fractional bandwidth as [29]

$$FBW = \frac{2\sqrt{\beta}}{Q}, \tag{3-5}$$

where

$$\beta = \frac{|S_{11}|^2}{1 - |S_{11}|^2}\,. \tag{3-6}$$

Consequently, for the -3dB points, we have $|S_{11}|^2$ = 0.5, and the half-power (3dB) fractional bandwidth can be calculated as

$$FBW_{3dB} = \frac{2}{Q}\,. \tag{3-7}$$

Furthermore, using the -10dB points where $|S_{11}|^2$ = 0.1 and $\sqrt{\beta} = 0.33$, one finds that $FBW_{3dB} = 3 \cdot FBW_{10dB}$. The lower bound on Q means that the upper bound on the fractional bandwidth is given by the expression:

$$FBW_{sphere,ub,3dB} = \frac{2}{Q_{sphere,lb}} = \frac{1}{\eta}\left[\frac{4(ka)^3}{3 + \sqrt{2}(ka)^2}\right]. \tag{3-8}$$

This limit requires that the FBW_{3dB} value decreases as *ka* decreases. It also explains why, in practice, the radiation efficiency is often sacrificed to obtain more bandwidth. For

small values of *ka*, the expressions (3-3) and (3-4) yield, respectively, $Q_{sphere,lb} \approx 1.5\,\eta\,(ka)^{-3}$ and $Q_{planar,lb} \approx 2.36\,\eta\,(ka)^{-3}$, which with (3-7) immediately implies that an electrically small antenna that utilizes the full spherical volume should exhibit more impedance bandwidth than a planar one. Because of their nature, the 3D EAD antenna should be governed by (3-3), while the 2D EAD antenna should be governed by (3-4).

The values of the 3dB fractional bandwidth values for both the 2D and 3D EAD antennas, along with the Chu/McLean, Thal, and Lund limits on the 3dB fractional bandwidth values, are shown in Figure 3-1. It is found that the 2D EAD design closely approaches the theoretical limit as *ka* decreases. On the other hand, since it is governed by the spherical bound but actually utilizes only a small portion of the spherical volume, the 3D EAD antenna results are much further away from their corresponding limits.

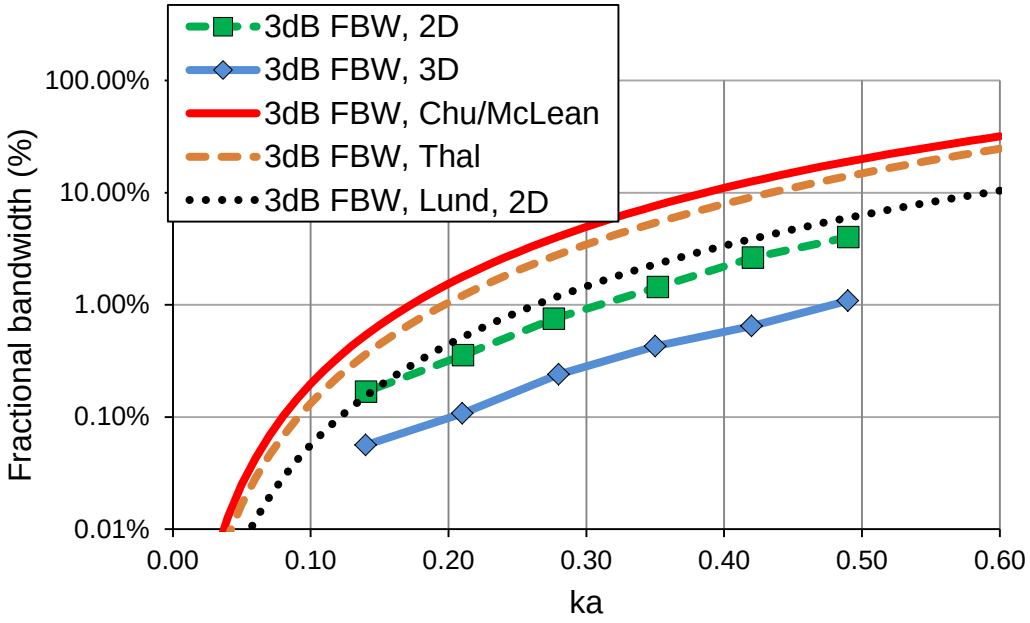

Figure 3-1: The 3dB fractional bandwidth values of the 2D and 3D EAD designs. Three theoretical limits for the 3dB fractional bandwidth are also shown.

Another observation that can be made from Figure 2-5 and Figure 2-12 is that the instantaneous bandwidths of the 2D EAD designs are always larger than their 3D counterparts for any given value of *ka*. To help explain this difference, we recall the alternative expression for the quality factor *Q* given in terms of the frequency variations of the resistance and reactance at the resonance frequency [30]:

$$Q(\omega_0) = \frac{\omega_0}{2R(\omega_0)}\sqrt{[R'(\omega_0)]^2 + \left[X'(\omega_0) + \frac{|X(\omega_0)|}{\omega_0}\right]^2}\ , \tag{3-9}$$

where $\omega_0 = 2\pi f_0$; $R(\omega_0)$ and $X(\omega_0)$ are, respectively, the input resistance and reactance at ω_0; and $R'(\omega_0)$ and $X'(\omega_0)$ are the corresponding angular frequency derivatives of the resistance and the reactance. Ideally, a perfectly matched antenna for the assumed 50 Ω source would have $R = 50\ \Omega$ and $X = 0\ \Omega$ at f_0. Under these conditions, (3-9) simplifies to

$$Q(\omega_0) = \frac{\omega_0}{100}\sqrt{[R'(\omega_0)]^2 + [X'(\omega_0)]^2}\ . \tag{3-10}$$

From this equation, it is apparent that the slopes of the input resistance and reactance at the resonance frequency dictate the quality factor *Q* and, hence, the half-power fractional bandwidth. Consequently, it becomes apparent that larger slopes yield higher *Q* values and, hence, lower bandwidths. By combining Figure 2-4 with Figure 2-9 into one plot, Figure 3-2 then shows that the 2D and 3D EAD designs have nearly identical resistance slopes near 300 MHz.

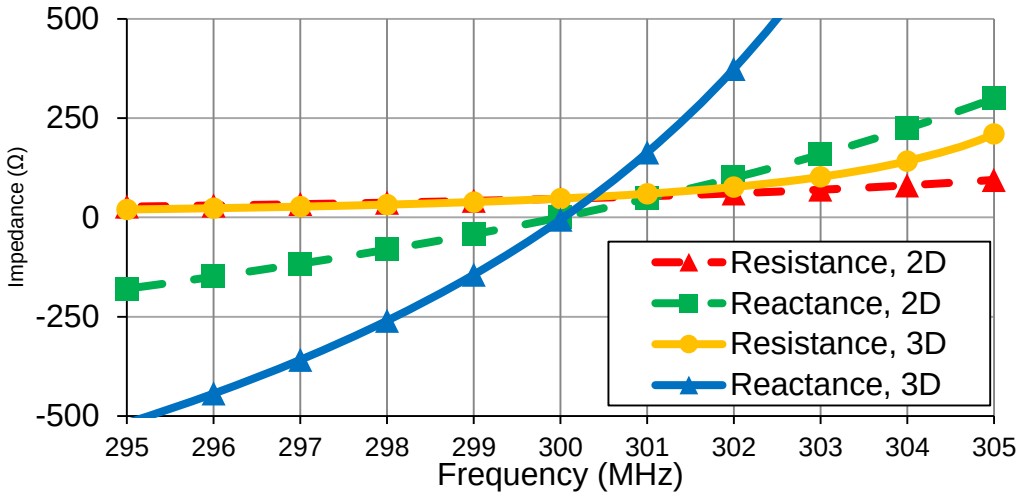

Figure 3-2: Real (resistance) and imaginary (reactance) parts of the input impedance for the 2D and 3D EAD designs when *ka* = 0.35.

Therefore, the difference in bandwidth between these two designs can be attributed to the fact that the 3D EAD designs have a much larger reactive slope than the 2D counterparts at the resonance frequency.

To investigate the physics behind why the reactance slope of the 3D EAD design with *ka* = 0.35 is larger than that of the 2D version, the equivalent circuit shown in Figure 2-6 can be utilized. The two circuit parameters that most affect the slope of the reactance curve at the resonant frequency are C_{sub}, which is meant to represent the capacitance through the substrate between the driven and NFRP elements, and R_{sub}, which is meant to represent the resistance between the driven and NFRP elements caused by the substrate. Higher (lower) values of C_{sub} and R_{sub} tend to increase (decrease) the reactance slope at the resonant frequency. Therefore, by comparing the values of C_{sub} and R_{sub} for the *ka* = 0.35 case (shown in Table 3-1), it would be expected that the 2D EAD antenna would have a larger bandwidth than its 3D counterpart.

Table 3-1: Comparison of Element Values of the Circuit Model for the 2D and 3D EAD Antennas

Design	C_{sub}	R_{sub}
2D EAD	0.92 pF	9.8 kΩ
3D EAD	4.00 pF	39.1 kΩ

Finally, the electric fields present within the substrate for both the 2D and 3D EAD designs should be compared to explain why the 3D EAD antenna has much higher values for both the C_{sub} and R_{sub} equivalent circuit parameters. The electric fields within the substrate on a plane at half the substrate thickness are shown for the 2D and 3D EAD antennas with ka = 0.35 in Figure 3-3 and Figure 3-4, respectively. From these figures, it is apparent that the electric fields, on average, are much more concentrated in the substrate for the 3D EAD antenna. This is the most likely reason why the R_{sub} and C_{sub} parameters are much larger for the 3D EAD design. It also explains the differences in their radiation efficiency values, which are given in the next subsection.

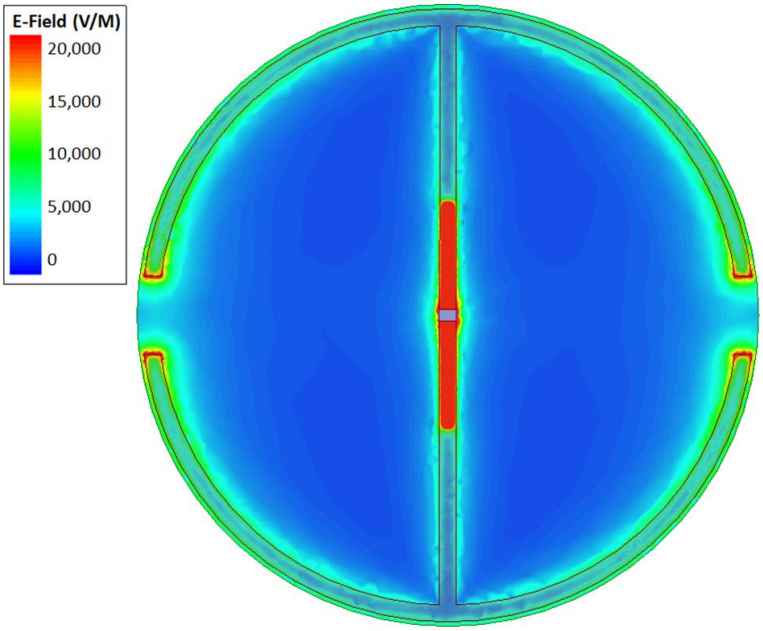

Figure 3-3: Electric fields within the substrate for the 2D EAD antenna when ka = 0.35.

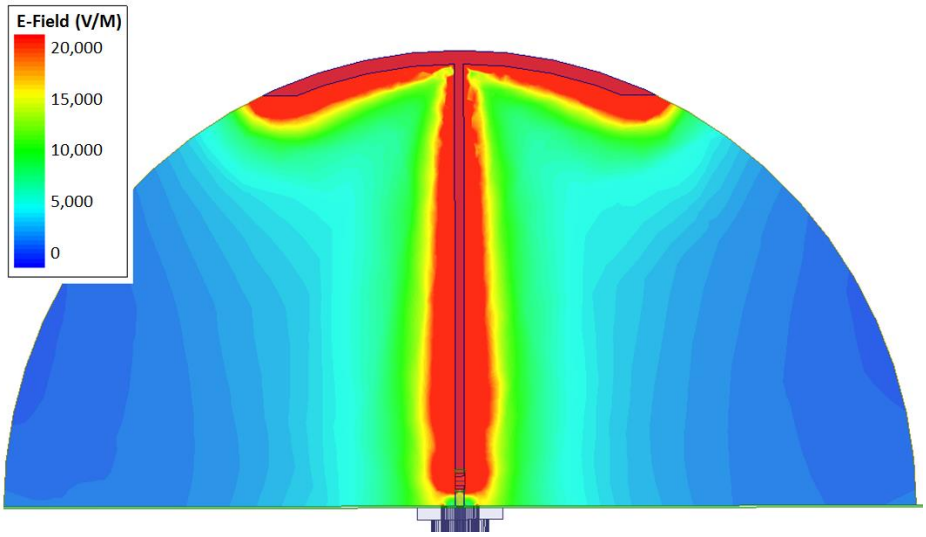

Figure 3-4: Electric fields within the substrate for the 3D EAD antenna when *ka* = 0.35.

3-2 Analysis of the Directivity and Radiation Efficiency Values

Comparisons of the directivities and radiation efficiencies of the 2D and 3D EAD designs for various values of *ka* were also made. Since the basis of each design is relatively consistent for all *ka* values and they all represent electrically small structures, one would expect the maximum directivity of both the 2D and 3D designs to remain relatively constant versus *ka*. As shown in Figure 3-5, this proves to be true. Moreover, despite the fact that both the 2D and 3D designs are, in reality, three-dimensional structures, they primarily radiate the fundamental TM mode. Consequently, one would expect their directivities to be near 1.5, which is verified by the results given in Figure 3-5.

On the other hand, both the 2D and 3D EAD antennas are lossy because of the presence of the dielectric substrate and the copper traces. At lower frequencies, there is more field penetration into the metal and more concentration of the field in the dielectric.

Consequently, one would expect their radiation efficiencies to decrease as *ka* decreases. This behavior is shown to be true in Figure 3-6.

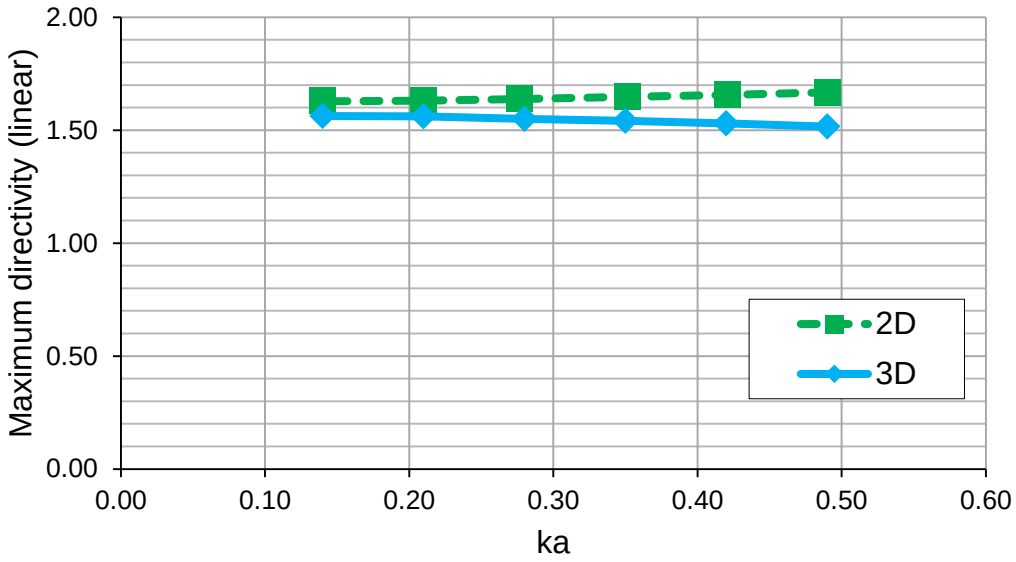

Figure 3-5: Maximum directivity of the 2D and 3D EAD antennas versus *ka*.

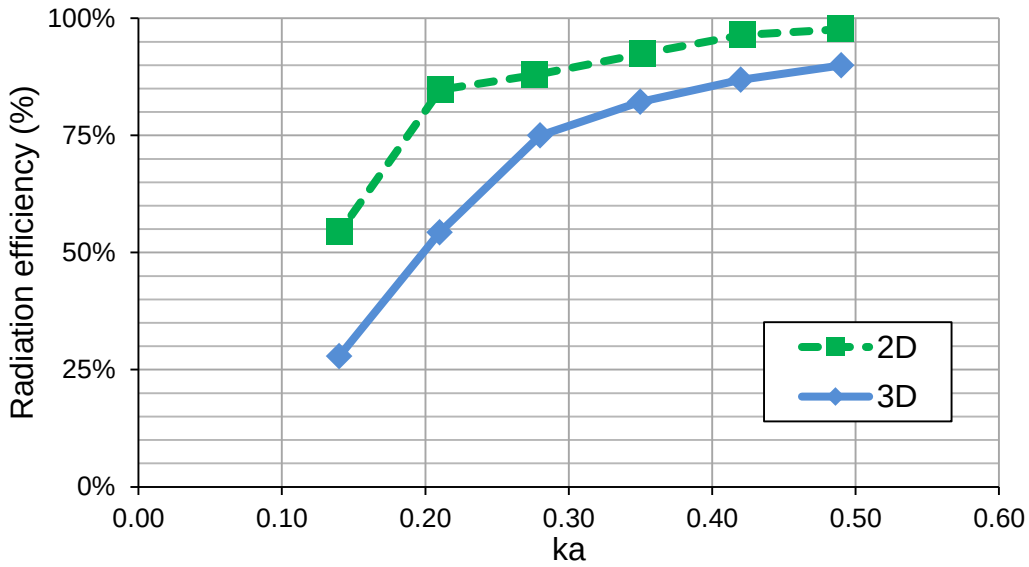

Figure 3-6: Radiation efficiency of the 2D and 3D EAD designs versus *ka*.

Moreover, since the radiation efficiency is related to the gain of an antenna as

$$G = \eta \cdot D, \tag{3-11}$$

and since the result in Figure 3-5 demonstrates that the directivity of each small antenna is nearly constant as *ka* decreases, and since Figure 3-6 shows that the radiation efficiency decreases as *ka* decreases, we can conclude that the gain of each antenna must decrease as *ka* decreases.

Figure 3-6 also shows another instance of unexpected behavior. Originally it was thought that the 3D design would exhibit higher radiation efficiencies than its 2D counterpart. Nonetheless, the radiation efficiencies of the 3D designs are clearly less than those of the 2D designs for every value of *ka*. This is a consequence of two issues. First, as noted previously, the 3D EAD antenna has larger field strengths in the substrate. As a result, it has lower radiation efficiencies and a faster roll-off with decreasing *ka* values. Second, it must be noted that the copper traces in the 2D design were in general wider than those in the 3D design. Since the metal resistance is proportional to the inverse of the cross-sectional area of a conducting volume ($R \propto 1/A$), then from (1-19) it follows that the radiation efficiencies of the 2D designs should indeed be larger than those of the 3D designs for all values of *ka*. When the width of the copper traces in the 3D EAD design are made wider and the antenna is re-tuned at each value of *ka*, then the radiation efficiencies of the 3D design approach those of the 2D design. This effect is illustrated in Figure 3-7 for the 3D EAD when *ka* = 0.35.

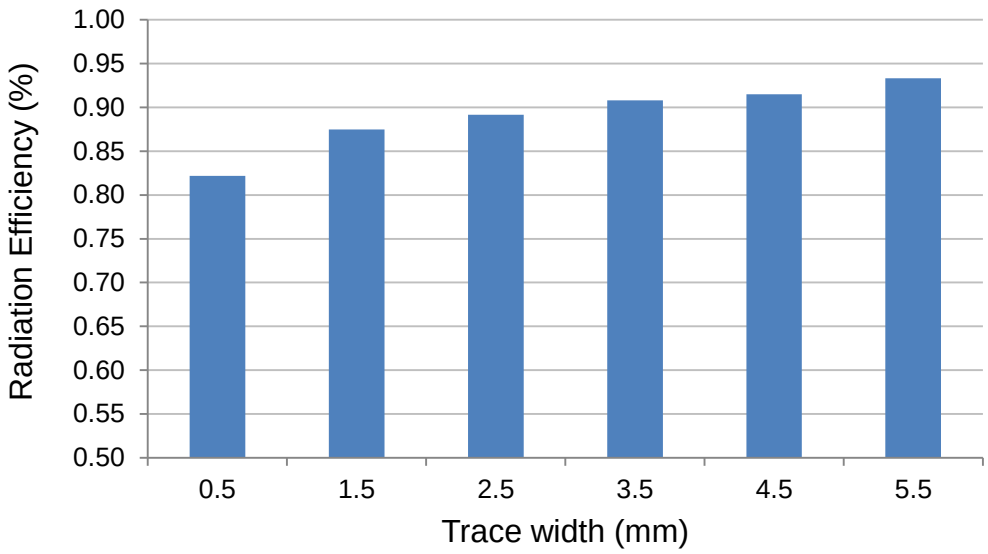

Figure 3-7: Radiation efficiency of the 3D EAD at *ka* = 0.35 for varying trace widths. The width of the NFRP element was increased at the same rate as the width of the monopole element.

CHAPTER 4 | FREQUENCY AGILE PERFORMANCE OF THE EAD ANTENNAS

As explained in Chapter 2, both the 2D and 3D EAD antennas contain an inductive element that is in-line with the NFRP. In the next few sections, it will be shown that by changing the value of this inductive element, the resonant frequency of the 2D and 3D EADs can be tuned. By choosing multiple values for the inductor, we can thus determine the frequency agile performance of each antenna design.

The first section of this chapter will compare the frequency agile performance of the 2D and 3D EAD designs. Then, for instructional purposes, procedures for obtaining and plotting frequency agile data will be detailed. Section 4-2 will detail the procedure using HFSS, and Section 4-3 will explain the procedure in ADS, with results compared to the data obtained using HFSS.

4-1 Comparisons between the 2D and 3D EAD Frequency Agile Results

As was explained in the introduction, the frequency agile performance of each antenna design can be determined by fixing the geometry and material properties, and then only varying the value of the inductive element; i.e., the physical geometry of the antennas remain the same while the value of the inductor is varied. This corresponds with manually or electronically changing the inductor value. The results of this process are demonstrated here with the 2D EAD design with $ka = 0.35$. For this particular geometry, an inductor value of 94.3 nH gave the antenna a center frequency of 300 MHz. As the inductor's value is varied, the center frequency, bandwidth, and complex input impedance at the center frequency also vary. This means that a wide range of $|S_{11}|$ curves

can be generated by varying only the inductor value. A few of these curves are shown in Figure 4-1.

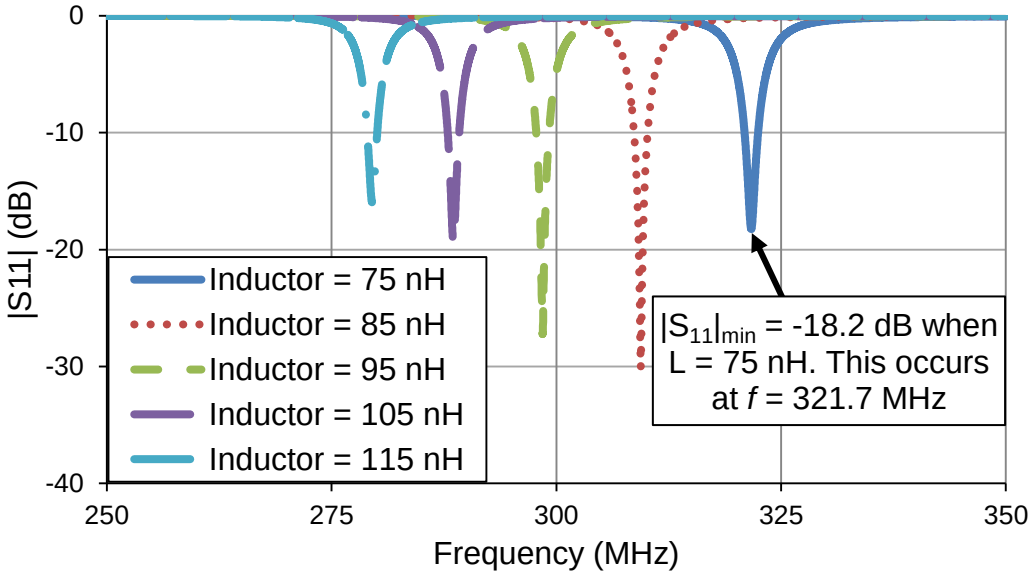

Figure 4-1: $|S_{11}|$ plots for the 2D EAD antenna with ka = 0.35 when its inductor value is varied (obtained using HFSS).

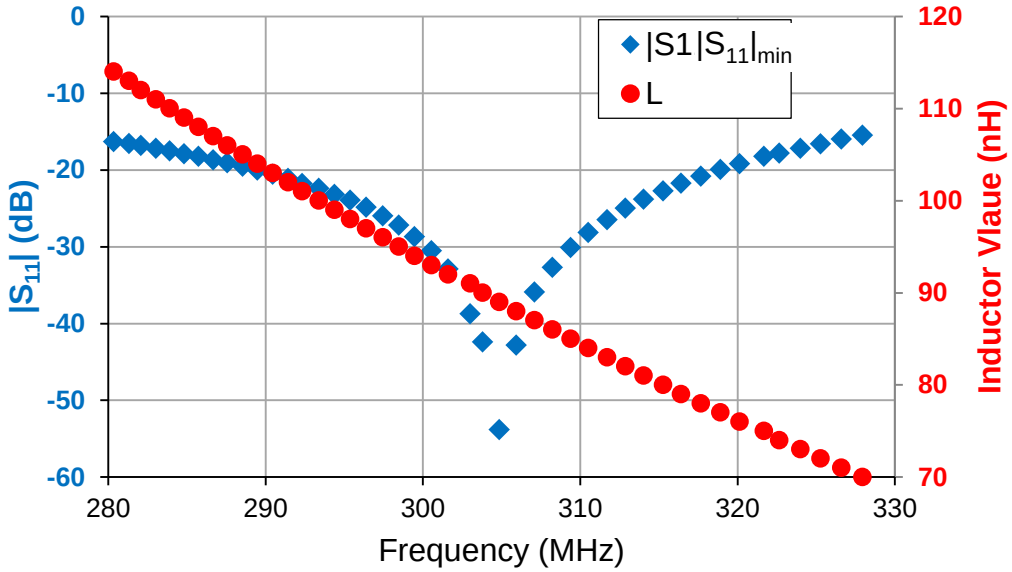

Figure 4-2: Inductor values and the corresponding $|S_{11}|_{min}$ values plotted against the resulting resonance frequencies for the 2D EAD antenna with ka = 0.35 (obtained using HFSS).

The inductor values (red dots) are plotted against the resulting resonance frequencies in Figure 4-2 and Figure 4-3 for the 2D and 3D cases, respectively, when *ka* = 0.35. The corresponding minimum $|S_{11}|$ values (blue triangles) are also plotted. For example, from Figure 4-2, it is observed that a 75 nH inductor within the 2D EAD yields a resonance frequency of 321.7 MHz with $|S_{11}|_{min}$ = -18.2 dB. One noticeable difference between Figure 4-2 and Figure 4-3 is the bandwidth of the frequency agile $|S_{11}|$ values. The 3D design has a much larger frequency agile bandwidth (2.85 times larger) than the 2D version. These bandwidths are so large that we report only the 20dB bandwidths in Table 4-1 for comparison. Not only do these results demonstrate that both the 2D and 3D EAD antennas provide large frequency agile bandwidths, they seem to contradict the instantaneous bandwidth results considered above.

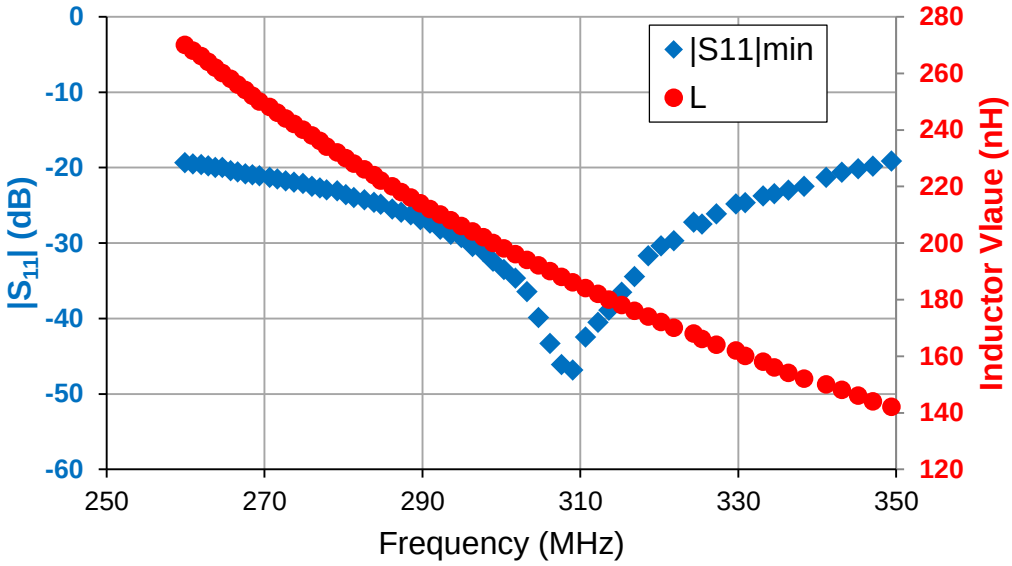

Figure 4-3: Inductor values and the corresponding $|S_{11}|_{min}$ values plotted against the resulting resonance frequencies for the 3D EAD antenna with *ka* = 0.35 (obtained using HFSS).

Table 4-1: -20 dB bandwidths for the 2D and 3D EAD frequency agile designs with $ka = 0.35$ (obtained using HFSS).

Design	-20 dB Bandwidth
Frequency Agile 2D EAD	28.2 MHz ≈ 9.2%
Frequency Agile 3D EAD	80.5 MHz ≈ 26.1%

To explain this bandwidth curiosity, the resistance and reactance were calculated for each frequency agile inductor value at the frequency for which $|S_{11}|$ (in dB) was at its minimum. These results are summarized in Figure 4-4. Since the inductor value can be set to any value, it essentially cancels out the reactance inherent in both the 2D and 3D EAD designs (i.e., it forces the derivative of the reactance to equal zero). Therefore, the fractional bandwidth only depends on the derivative of the resistance when dealing with frequency agile designs. This behavior is the opposite that of the instantaneous designs. In the instantaneous designs, the fractional bandwidth depended primarily upon the derivative of the reactance. Since the derivative of the reactance was much greater than that of the resistance, it dominated the outcome. In particular, note how Figure 3-2 shows the resistances and reactances of the antenna designs with a fixed inductor value over all frequencies, whereas Figure 4-4 shows the resistances and reactances of the antenna designs when the inductor value is allowed to vary over frequency.

As Figure 4-4 illustrates, the 2D EAD's resistance increases more rapidly with increasing frequency. Therefore, it has a larger resistance derivative than the 3D EAD. Since the bandwidth of the frequency agile design depends on this resistance derivative, it

follows from (3-10) that the 2D EAD has a smaller frequency agile bandwidth than the 3D EAD.

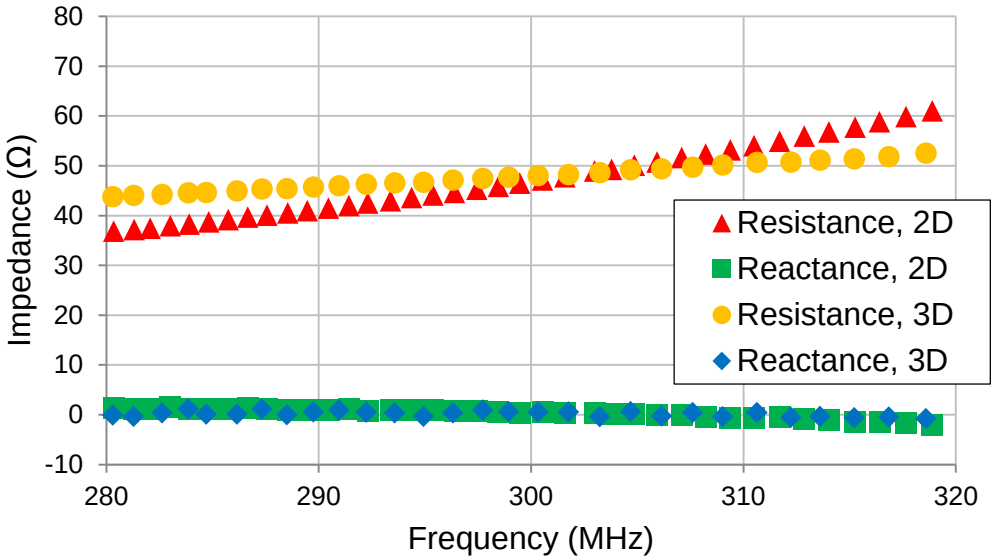

Figure 4-4: The real (resistive) and imaginary (reactive) parts of the input impedance for the frequency agile 2D and 3D EAD designs when $ka = 0.35$.

4-2 Frequency Agile Simulations in HFSS

While HFSS is a great tool for obtaining frequency agile data using the built-in "Parametric" feature, formatting the data for plotting within HFSS is a different matter. In fact, the author found it more convenient to export the data from HFSS as a Comma Separated Values (CSV) file and then to make the frequency agile plot in either Excel or MATLAB. Therefore, the first part of this section will demonstrate a procedure for obtaining the frequency agile data, while the second part of this section will show the method used by the author for plotting this data.

4-2-1 Obtaining the Frequency Agile Data in HFSS

As shown in Section 4-1, the first step in obtaining the frequency agile curve is to simulate the frequency response of an antenna with varying values of the inductor. Conveniently, HFSS has a built-in tool, called "Optimetrics", which makes running multiple simulations very easy. The first step in the set-up is to add a "Parametric" run. Within the model tree, right click on "Optimetrics", and then mouse-over "Add", and then click on "Parametric", as shown in Figure 4-5.

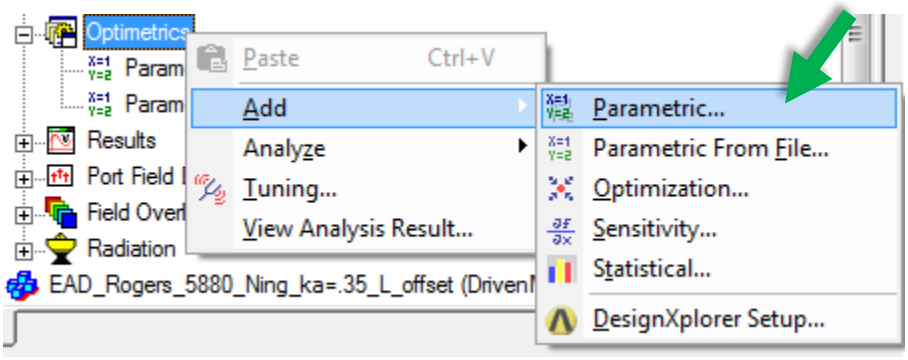

Figure 4-5: Creating a "Parametric" run within HFSS.

After making these selections, the "Setup Sweep Analysis" window will appear. To create a parametric sweep, click on the "Add" button, which will cause the "Add/Edit Sweep" window to appear. For this example, the inductor value was varied from 70 nH to 122 nH by 1 nH increments. Therefore, the "inductor" variable was selected from the drop-down menu in the "Add/Edit Sweep" window. The value 70 nH was entered into the "Start" box, 122 nH into the "Stop" box, and 1 nH into the "Step" box. To finalize these sweep values, one must then click the "Add" button. At this point, the "Add/Edit" sweep window should look identical to Figure 4-6. Once this has been verified, click the "OK" button.

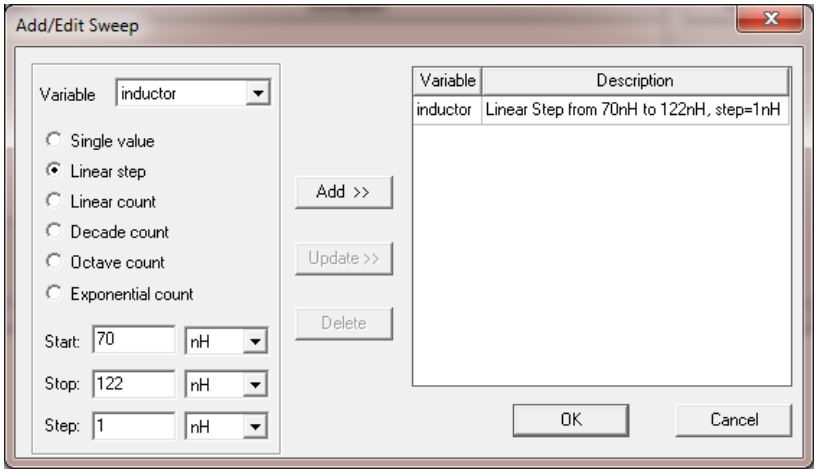

Figure 4-6: "Add/Edit Sweep" window after finalizing the sweep values.

At this point, HFSS returns to the "Setup Sweep Analysis" window. To choose which set-up will be run during the parametric sweep, click on the "General" tab. Then, in the "Sim. Setup" sub-window, ensure that the "Include" box is checked by the correct simulation set-up. Typically, only one of the set-ups should be checked. This is shown in Figure 4-7. For the example 2D EAD simulations, Setup 2 contained the correct simulation set-up and frequency sweep.

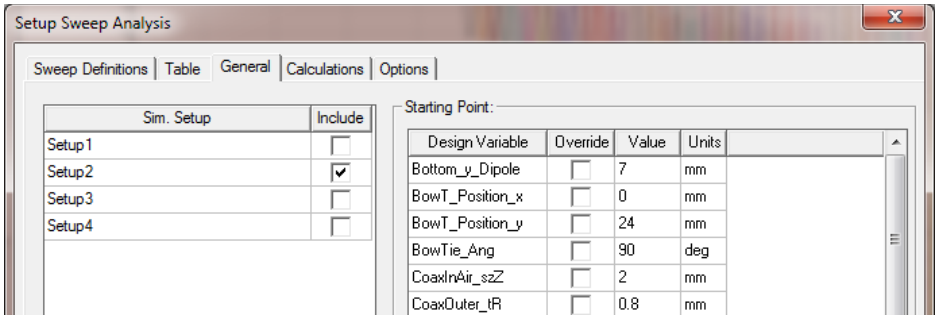

Figure 4-7: Selecting only one simulation set-up from the "General" tab of the "Setup Sweep Analysis" window.

Finally, to run the parametric sweep, right-click on the new Parametric Setup, and then click "Analyze", as demonstrated in Figure 4-8.

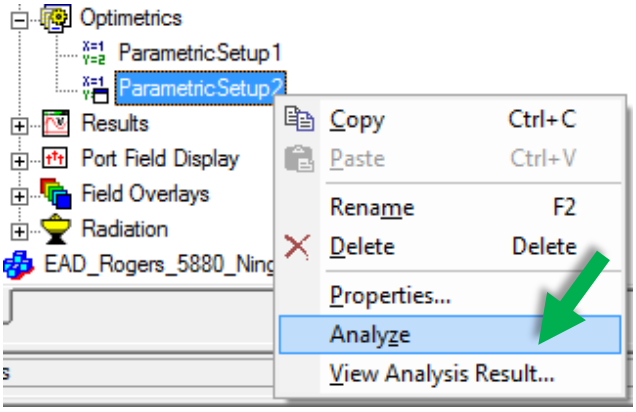

Figure 4-8: Running the frequency agile parametric setup within HFSS.

4-2-2 Exporting the Frequency Agile Data from HFSS

As shown in Section 4-2-1, creating and running the frequency agile simulations within HFSS is quite simple. However, the author found that plotting only the frequency agile results proved to be quite difficult. Therefore, this section will detail how to export the frequency agile results, such that they may be plotted in either Excel or MATLAB, or any plotting software that accepts CSV file types. This method involves creating a Data Table, and then exporting the Data Table as a CSV file.

To accomplish this task, first right-click on "Results" within the model tree, then mouse-over "Create Modal Solution Data Report", and then click on "Data Table", as demonstrated in Figure 4-9.

The first goal is to list the minimum value of each $|S_{11}|$ curve (in dB) versus inductor value. From the "Solution" drop-down menu, select the correct solution set-up. If the solution set-up has more than one sweep, select the correct sweep from the "Domain" drop-down menu. At this point, the "Report" window should look as shown in Figure 4-10.

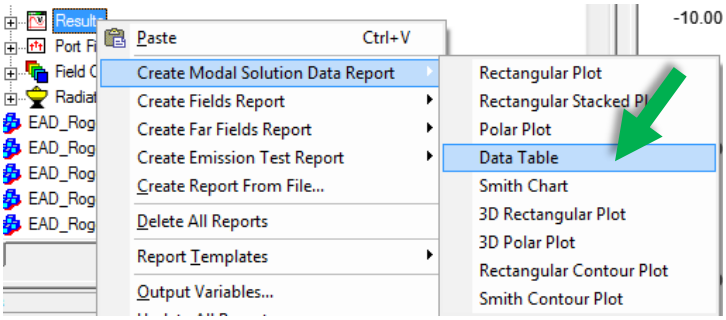

Figure 4-9: First step in creating the frequency agile data table in HFSS.

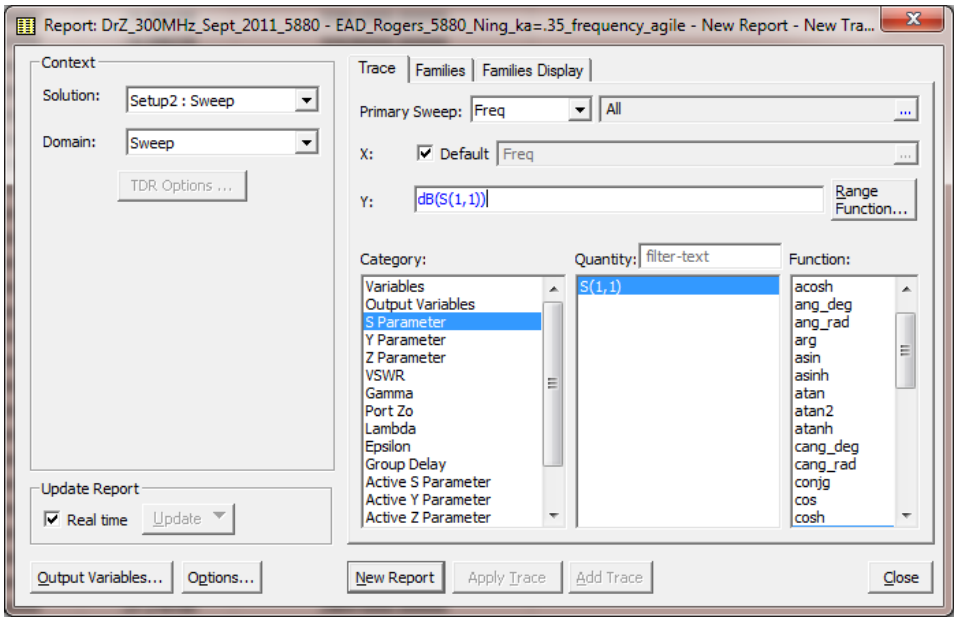

Figure 4-10: The "Report" window after selecting the applicable set-up and sweep.

To extract the minimum value of each $|S_{11}|$ curve versus inductor value, one needs to use the "Range Function" tool. By clicking on "Range Function", the "Set Range Function" window will appear. From the "Function" drop-down menu, select the "min" function. The "Set Range Function" window should now look exactly like Figure 4-11. Once this has been verified, click "OK".

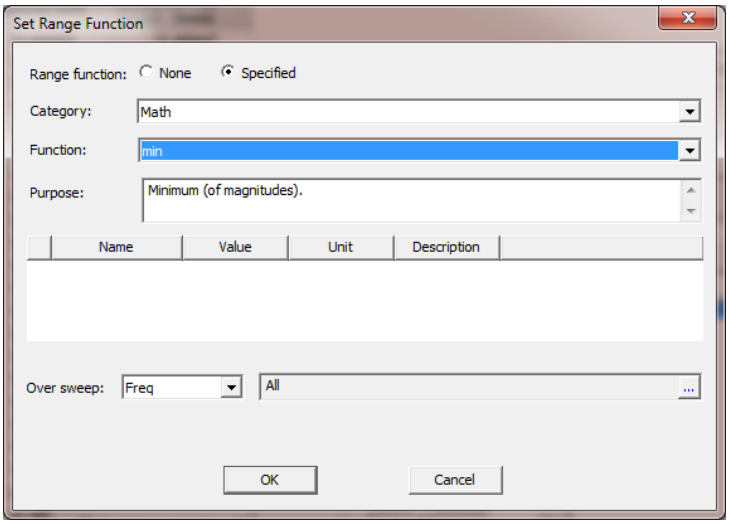

Figure 4-11: The "Set Range Function" window after selecting the "min" function.

After clicking "OK" in the "Set Range Function" window, HFSS will return to the "Report" window. At this point, check the "Primary Sweep" drop-down menu, and ensure that the inductor variable is selected. The "Report" window should then look as shown in Figure 4-12. Once this has been verified, click the "New Report" button to generate the first half of the frequency agile data table.

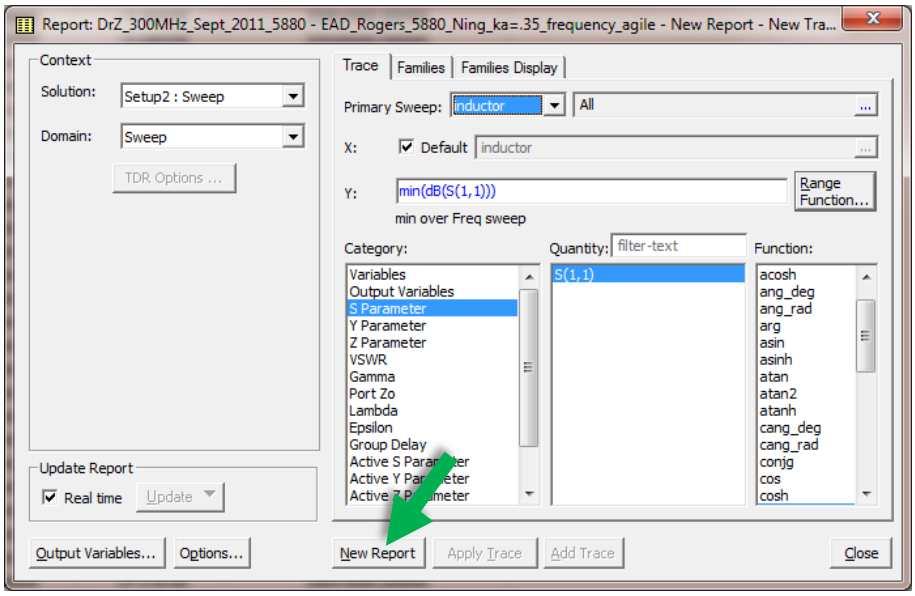

Figure 4-12: The "Report" window after setting the range function.

The frequency agile data table will display the inductor values used for the parametric sweep in the first column, and the minimum of each $|S_{11}|$ curve in the second column. The first five rows of the data table are shown in Figure 4-13.

	inductor [nH]	min(dB(S(1,1))) Setup2 : Sweep
1	70.000000	-15.469447
2	71.000000	-15.995098
3	72.000000	-16.595226
4	73.000000	-17.202449
5	74.000000	-17.827361

Figure 4-13: First two columns of the frequency agile data table.

Next, a column is added to the data table that shows the frequency at which the minimum of each $|S_{11}|$ curve occurs. To do this from the "Report" window, again click on the "Range Function" button. This will again bring up the "Set Range Function" window. This time, in the "Function" drop-down menu, click the "XAtYVal" function. The "Set Range Function" window should now look as shown in Figure 4-14. Leave everything else the same, and click the "OK" button.

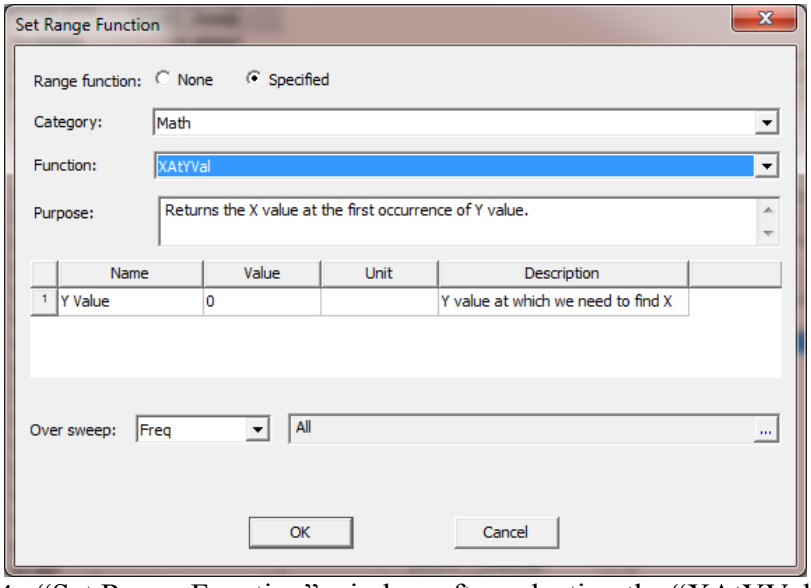

Figure 4-14: "Set Range Function" window after selecting the "XAtYVal" function.

At this point, HFSS will return to the "Report" window. In the "Y" edit box, it should say XAtYVal(dB(S(1,1)) , 0). However, we would like to obtain the frequency value when each $|S_{11}|$ curve is at its minimum value. To do so, we must modify the text in the "Y" edit box to read as follows: XAtYVal(dB(S(1,1)) , min(dB(S(1,1)))). If done correctly, the "Report" window should now appear as shown in Figure 4-15. To add this new column to the data table, click on the "Add Trace" button. Be careful, **do not** click on the "Apply Trace" button, since this will overwrite the second column of data instead of adding a third column with the new data.

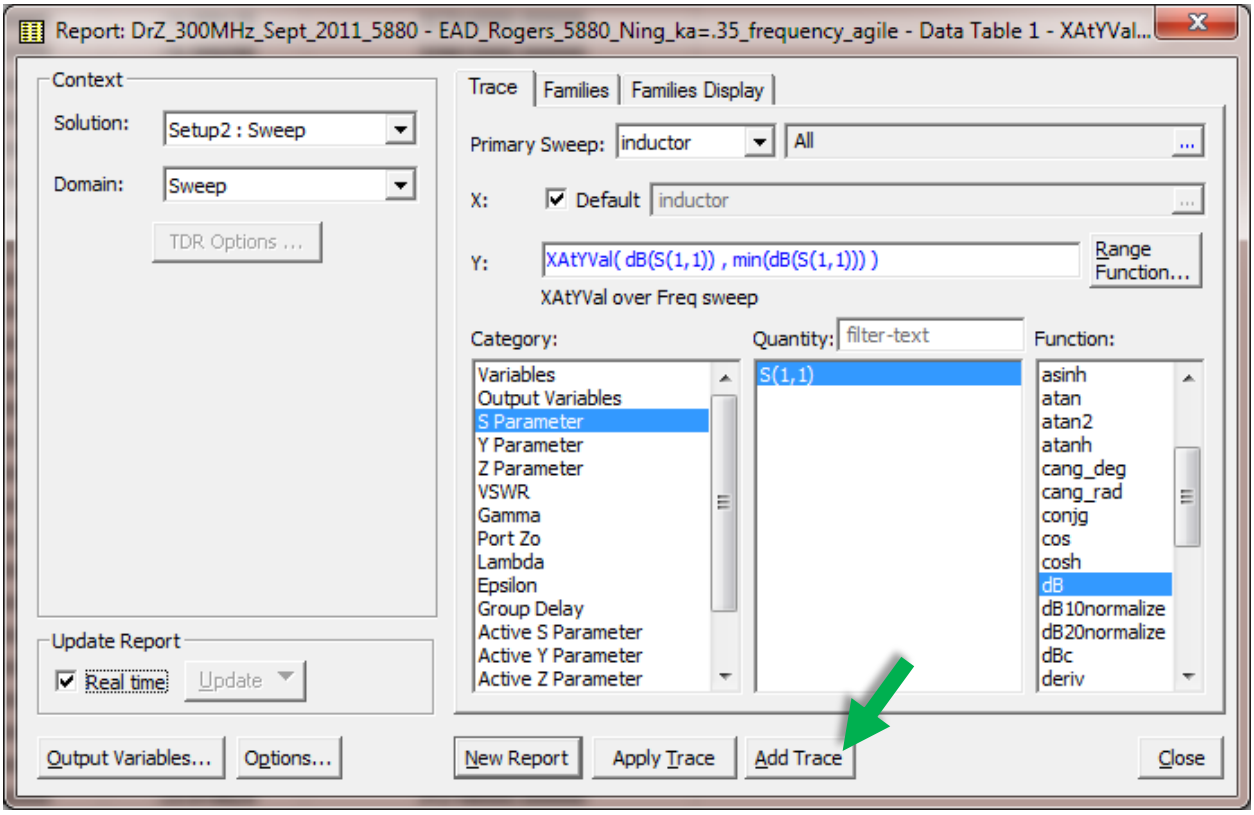

Figure 4-15: "Report" window before adding the third column to the frequency agile data table.

After clicking the "Add Trace" button, the data table will have a third column. This column shows the frequency (in Hz) at which the $|S_{11}|$ curve is minimized for a given inductor value. An example of the data table with the third column added is shown below in Figure 4-16.

	inductor [nH]	min(dB(S(1,1))) Setup2 : Sweep	XAtYVal(dB(S(1,1)) , min(dB(S(1,1)))) Setup2 : Sweep
1	70.000000	-15.469447	327950000.000000
2	71.000000	-15.995098	326610000.000000
3	72.000000	-16.595226	325280000.000000
4	73.000000	-17.202449	324000000.000000
5	74.000000	-17.827361	322670000.000000

Figure 4-16: Frequency agile data table with all three columns.

Finally, it is desired to export this data table such that the results can be plotted in either Excel or HFSS. To achieve this goal, right-click on the Data Table, and then click "Export", as shown in Figure 4-17. This allows the user to export the Data Table, and to save the results in a CSV file format.

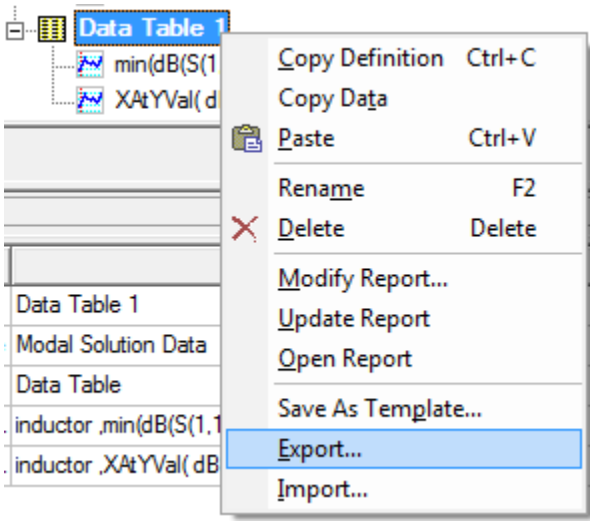

Figure 4-17: Demonstration on how to export the Data Table from HFSS.

Now the user may import the CSV file into Excel, MATLAB, or any other software that offers plotting utilities for CSV files. Thus, the frequency agile curve may be plotted. Examples of such frequency agile curves were shown in Figure 4-2 and Figure 4-3.

4-3 Frequency Agile Simulations in ADS

Similar to HFSS, Agilent's Advanced Design System (ADS) provides tools for easily calculating the $|S_{11}|$ curves of a frequency agile antenna. However, generating the single frequency agile curve is again a challenge, but can be done directly in ADS without the help of external software packages.

Since ADS is not a full wave solver, the process of obtaining the frequency agile curve begins with a simulation in HFSS. For this section, the 2D EAD design will again be used as the example antenna. With this antenna, the inductor sheet (otherwise known as the lumped RLC boundary) must be changed to a lumped port. After deleting the lumped RLC boundary from the model, and replacing that boundary with a lumped port excitation, the model tree will appear as shown in Figure 4-18.

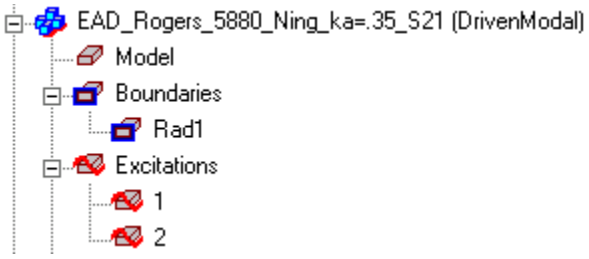

Figure 4-18: Model tree after deleting the lumped RLC boundary, and adding the second lumped port excitation.

Once this step has been accomplished, the model should be simulated using a valid set-up and frequency sweep. When the simulation has completed, the S2P file for the model must be exported. This can be accomplished by right-clicking on “Results”, and then clicking on the “Solution Data” button. Once the “Solutions” window appears, the proper set-up and sweep must be selected from the drop-down menus, and the check box next to “Display All Freqs” must be checked. Once the “Solutions” window looks similar to Figure 4-19, the S2P file may be exported by clicking on the “Export Matrix Data” button.

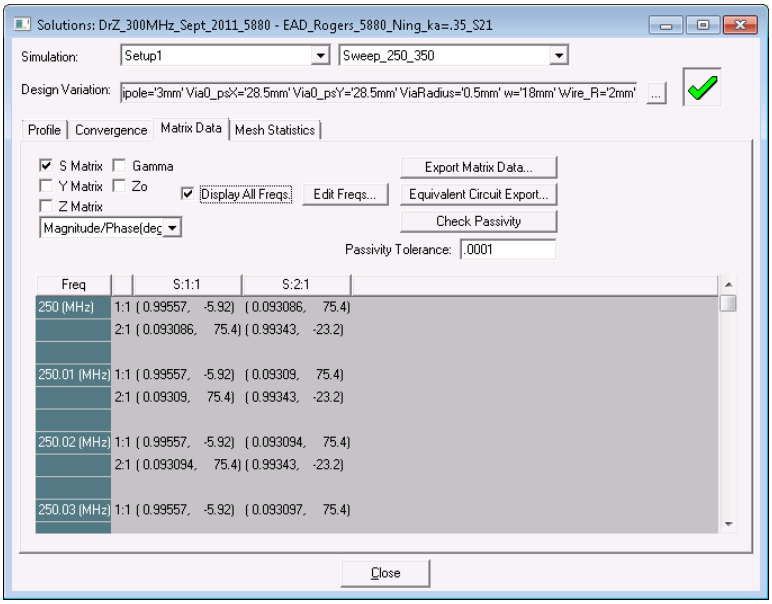

Figure 4-19: The “Solutions” window prior to exporting the S2P file.

At this point, HFSS will ask the user to specify the S2P file’s location, and will ask whether to renormalize the solution modes. Although it does not seem to make much of a difference, this author used the settings shown in Figure 4-19 when exporting the S2P files.

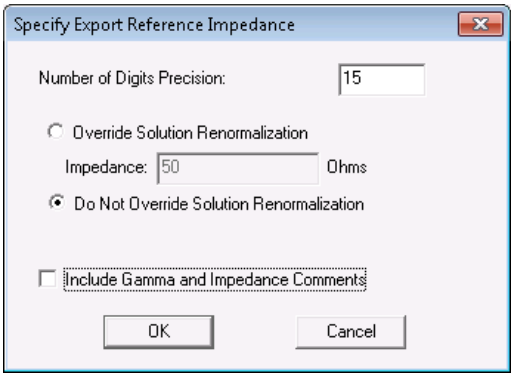

Figure 4-20: Settings used when exporting the S2P files.

Once one has obtained a valid S2P file for the antenna, this file may be used as a "S2P" block within ADS. Subsequently, for the 2D EAD antenna, the circuit model shown in Figure 4-21 was constructed.

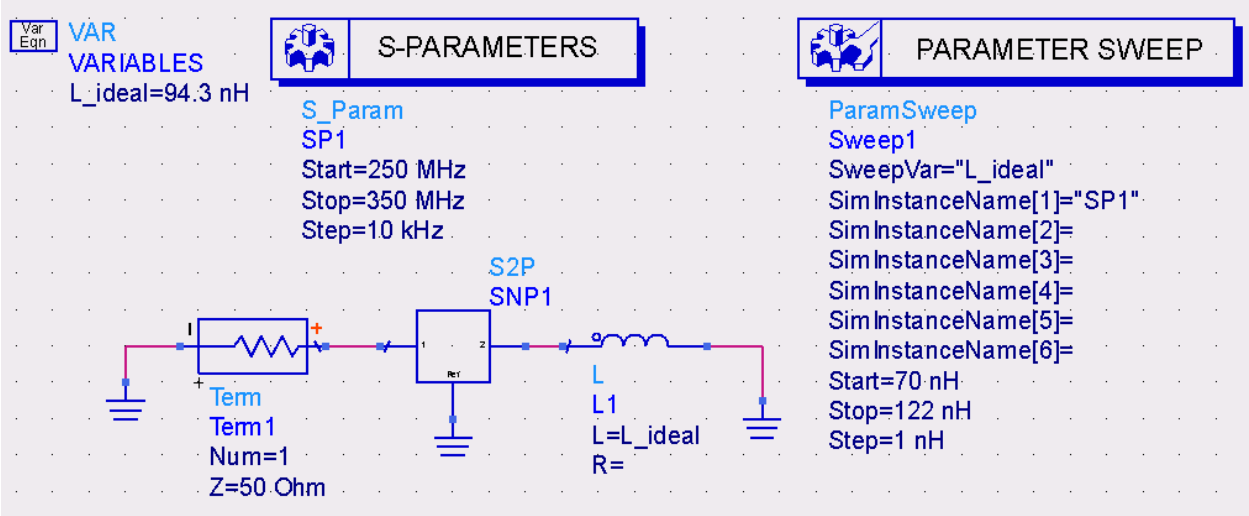

Figure 4-21: ADS circuit model and parameter sweep settings for the 2D EAD frequency agile simulation.

The "S2P" block requires a user to point to an S2P file. After double-clicking on the "S2P" block, the user can point the block to the S2P file created from HFSS. Then, for the frequency agile simulations, it was found that the "Parameter Sweep" simulation easily allows a user to sweep across variable values when the step size is constant. As

shown in Figure 4-21, for the 2D EAD model, the parameter sweep is performed on the *L_ideal* variable using the *SP1* simulation settings for each sweep value. When the circuit and the parameter sweep are correctly configured, the ADS simulation can be run by clicking on the "Simulate" button.

After ADS has successfully swept through each value of *L_ideal*, the ADS plotting tool will appear in a new window. To view each of the $|S_{11}|$ curves, a new rectangular plot can be created, and then the dB(S(1,1)) values can be added to the plot. Once completed, the new rectangular plot should appear as shown in Figure 4-22.

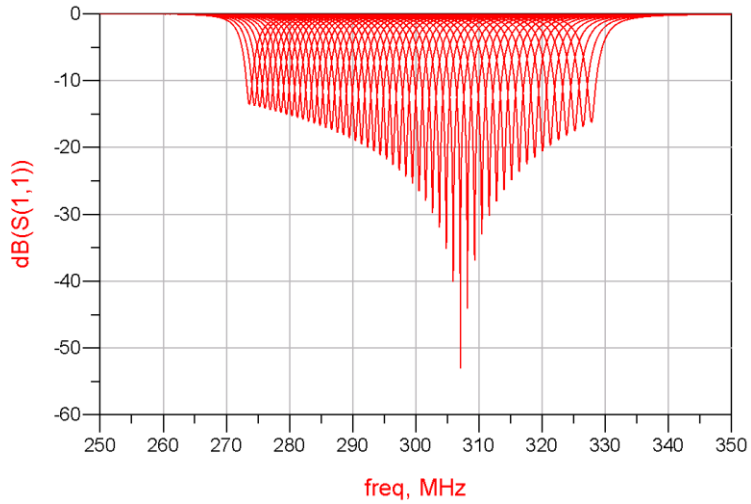

Figure 4-22: Individual $|S_{11}|$ curves from the ADS frequency agile simulation for the 2D EAD (ka = 0.35) as the inductor value was swept.

Next, the frequency agile curve is desired. This part is a bit trickier, but can be done completely within ADS. By inserting the four equations shown in Figure 4-23, the frequency agile information can be obtained directly within ADS. The formulation of these equations will not be described in detail herein, so the interested reader is referred

to the "Design Tools → Measurement Expressions" section of the ADS Help documentation.

```
Eqn minS11 = min(dB(S(1,1)))

Eqn indepValuesMatrix = get_indep_values(dB(S(1,1)),minS11)

Eqn indepValuesExpanded = expand(indepValuesMatrix)

Eqn minFreqs = indepValuesExpanded[0,::]
```

Figure 4-23: Equations used to generate the frequency agile curve within ADS.

After inserting these four equations, the frequency agile curve can be plotted by adding the following equation to a rectangular plot: plot_vs(minS11,minFreqs). The inductor values that cause the particular values of *minFreqs* may be added to the same plot by adding the following equation: plot_vs(L_ideal,minFreqs). It is also convenient to adjust the plot such that the inductor values are given on the Right Y-Axis. This can be accomplished by adjusting the plot properties. After doing so, the rectangular plot looks as shown in Figure 4-24.

At this point, the frequency agile data may be exported to a tab-delimited ASCII file for further use. This is important, because by having this tab-delimited file, a user is able later to obtain the non-Foster curve of the antenna. To do so, select the plot within ADS by left-clicking on the plot that contains the frequency agile curve, and then go through the steps "File → Export → Write selected item to tab-delimited ASCII", as shown in Figure 4-25.

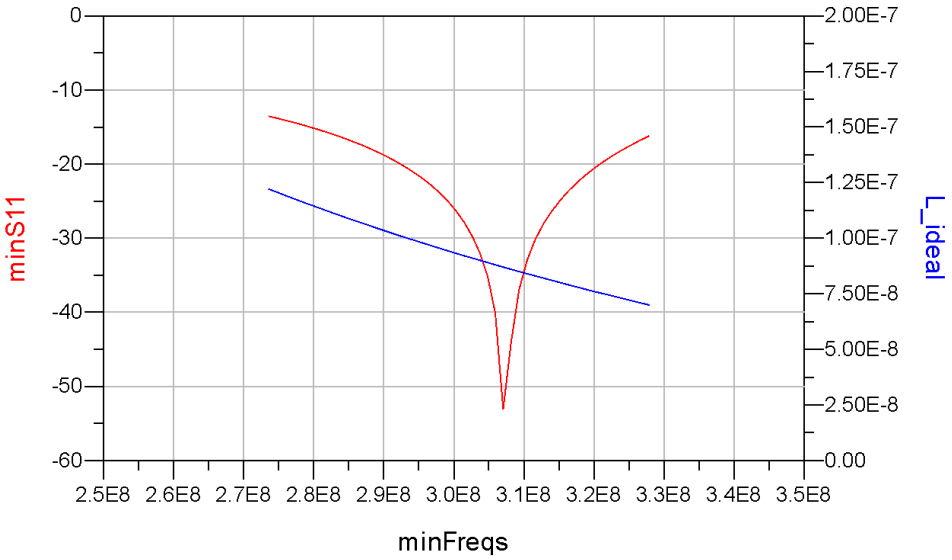

Figure 4-24: Frequency agile curve generated directly within ADS for the 2D EAD antenna (*ka* = 0.35).

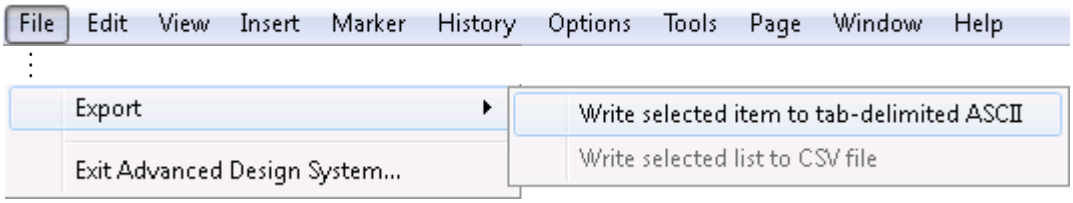

Figure 4-25: Exporting ADS data to a tab-delimited ASCII file.

At this time, a comparison between the frequency agile curve obtained using HFSS and the frequency agile curve obtained using ADS is warranted. These comparisons are shown in Figure 4-26 for the 2D EAD and in Figure 4-27 for the 3D EAD designs. The figures show that the frequency agile bandwidth performance predicted in each of the two simulation packages is nearly identical. However, a slight shift occurs between the null frequencies predicted in HFSS versus those predicted in ADS. Albeit small, this shift occurs for both the 2D EAD and the 3D EAD results. The root cause behind this frequency shift has not yet been adequately explained. It is present

in all such examples and is believed to be associated with the differences between the full-wave (HFSS) and the circuit (ADS) simulation approaches.

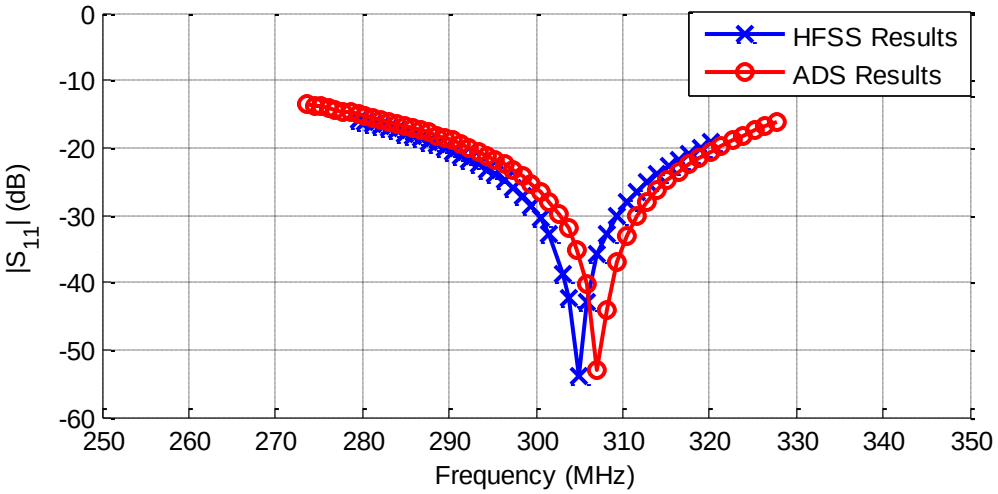

Figure 4-26: Comparison between the frequency agile curves obtained using HFSS and ADS for the 2D EAD antenna (*ka* = 0.35).

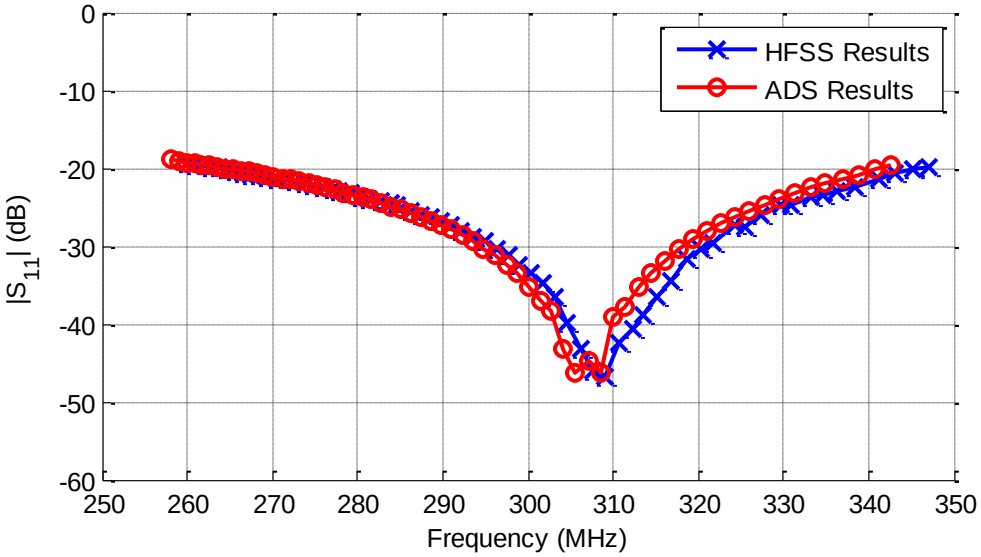

Figure 4-27: Comparison between the frequency agile curves obtained using HFSS and ADS for the 3D EAD antenna (*ka* = 0.35).

CHAPTER 5 | PERFORMANCE OF THE NON-FOSTER AUGMENTED EAD ANTENNAS

The previous chapter discussed the frequency agile performance of both the 2D and 3D EAD antennas. Because of their non-Foster behaviors, their frequency agile performances can only be obtained in theory from these passive designs. In reality, an active component, such as a frequency dependent NIC element, must be incorporated with the antenna, and then the reactance of the NIC can be adjusted to produce the requisite non-Foster behavior. When an element with frequency-dependent reactance is added to an antenna system, the antenna is said to be *augmented* with the new element. When this element produces a non-Foster behavior, the performance of this antenna is referred to as the *non-Foster augmented* performance.

This chapter first discusses the $|S_{11}|$ performance of the 2D and 3D EAD antennas when they have been augmented with an element that has a frequency-dependent reactance that decreases with increasing frequency. The second section of the chapter reveals the radiation efficiency of these non-Foster augmented designs. The third section then delves into the development of the reactance regression equation used to define the non-Foster element with more detail. Finally, Section 5-4 and 5-5 discuss how to obtain the non-Foster results from HFSS and ADS, respectively. Section 5-5 also compares the non-Foster $|S_{11}|$ curves obtained in HFSS and ADS.

5-1 Comparisons between the 2D and 3D EAD Non-Foster Results

A tunable inductor would be needed to achieve the frequency agile antennas described in the previous section. If, as suggested, an electronically tuned inductor was

employed, the only way one could achieve a real-time frequency agile design in a receiving antenna would be to include a sensor and feedback control loop to ensure that the antenna system was always using the optimal inductor value available. This would require more components and would cause more complexity coupled with a reduction in efficiency. Moreover, with a quick calculation based on the inductance curves shown in Figure 4-2 and Figure 4-3, one finds that those values require $X'(\omega_0) < 0$, i.e., a non-Foster behavior must be produced by the component.

If one could design a non-Foster element to reproduce the requisite inductance behavior, one could produce an antenna system with a large instantaneous bandwidth. Thus, one could avoid many of the issues associated with a frequency agile system design. Moreover, NIC realizations of the required non-Foster element have been reported, e.g., [17]. They require matching the response of the non-Foster element to the frequency agile values. A process has been developed for the 2D and 3D EAD designs. It is based on a curve-of-best-fit approach to the predicted inductance versus frequency values.

Step 1: Determine the Frequency Agile Inductor Values

Before manufacturing a wide-band electrically small antenna, simulations can show how well a given antenna design will perform when combined with a non-Foster element. The first step in creating the non-Foster element is to determine how the inductance must change with frequency. This step has already been performed by analyzing the frequency agile performance, and the results are shown in Figure 4-2 and Figure 4-3.

Step 2: Fit a Regression Equation to the Requisite Inductor Values

The next step is to develop a regression equation that describes the inductor values versus frequency. Regression analysis can be performed to develop this curve-of-best-fit. These types of analyses are built into many common software packages, such as Excel or MATLAB. The resulting regression equation should be a function of frequency and should output an inductor value. The form of the regression equation used for the 2D and 3D EAD designs was

$$L = \xi + \alpha \mathrm{e}^{-\beta \cdot f} \tag{5-1}$$

where f is the frequency in MHz, and L is the inductance value returned in nH. The reason behind choosing this form of regression equation is discussed in Section 5-3. The values of ξ, α, and β calculated from the frequency agile data are shown in Table 5-1.

Table 5-1. Regression parameter values for the 2D and 3D EAD with *ka* = 0.35

Parameter	2D EAD	3D EAD
ξ	-30.7043	42.0292
α	1236.4637	2493.7878
β	0.0076568273	0.0092273287

The inductor values calculated with the regression equation, along with the original data points used to generate the regression equation, are shown in Figure 5-1 and Figure 5-2 for the frequencies between 280 MHz and 320 MHz.

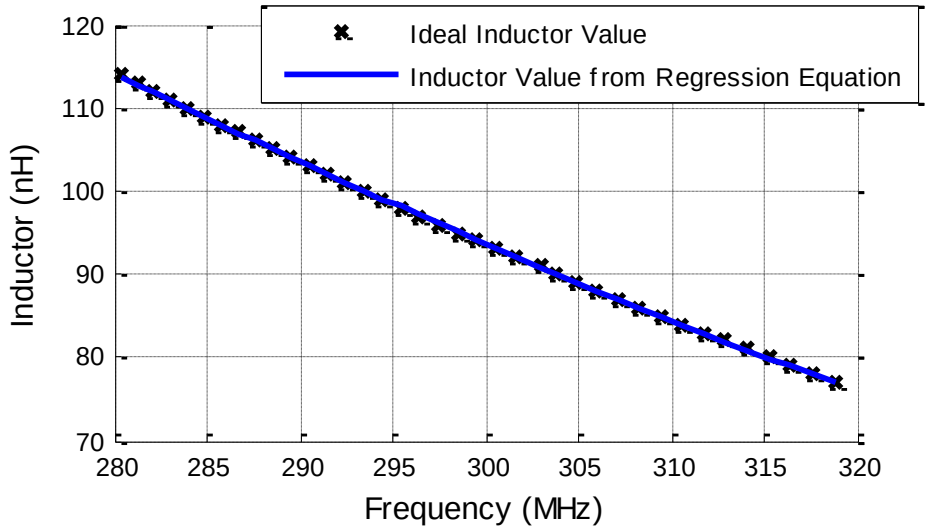

Figure 5-1: The inductor values of the frequency agile 2D EAD design (*ka* = 0.35) obtained with HFSS are compared to those calculated using (5-1).

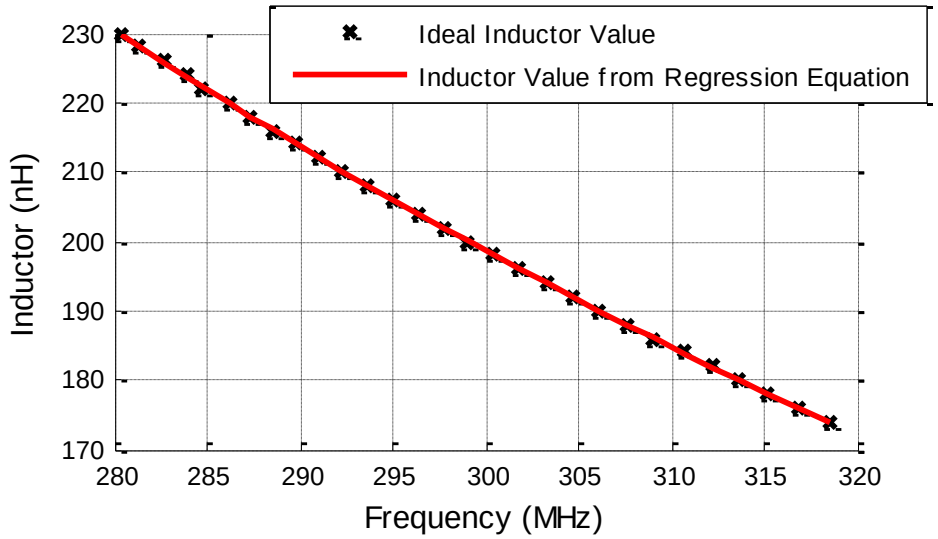

Figure 5-2: The inductor values of the frequency agile 3D EAD design (*ka* = 0.35) obtained with HFSS are compared to those calculated using (5-1).

The agreement is very good, which can be proven by calculating the percent error of the inductor values found with the regression equation. The percent error is given by

$$\% \, Error = \frac{|L_{ideal} - L_{regression}|}{|L_{ideal}|} \times 100 \qquad (5\text{-}2)$$

As shown in Figure 5-3, the percent error of the 2D EAD inductor values are all less than 0.25% between 280 MHz and 320 MHz. As shown in Figure 5-4, the percent error of the 3D EAD inductor values are all less than 0.15% in the same frequency range.

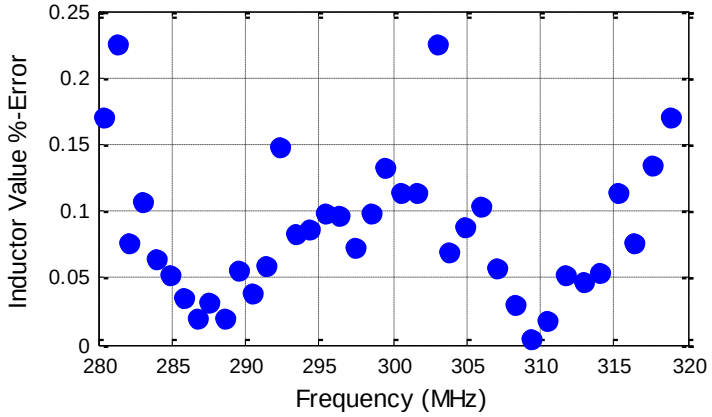

Figure 5-3: The percent error, calculated with (5-2), for the inductor values found using the regression equation for the 2D EAD when *ka* = 0.35.

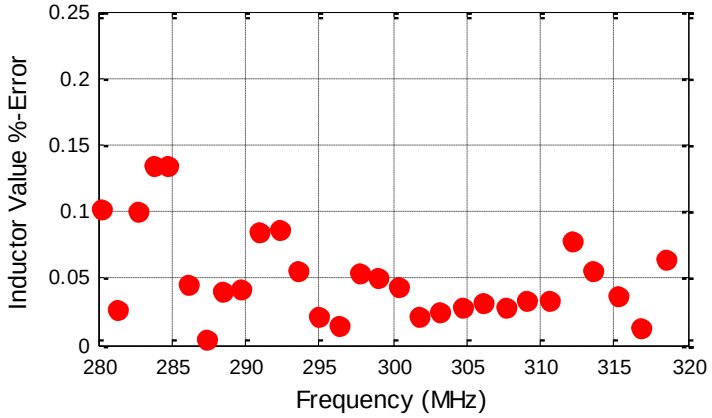

Figure 5-4: The percent error, calculated with (5-2), for the inductor values found using the regression equation for the 3D EAD when *ka* = 0.35.

Step 3: Analyze Non-Foster Performance

Finally, the performance of the 2D and 3D EAD designs when a non-Foster element is incorporated into the NFRP element can be obtained from another set of HFSS simulations. The method used to determine the non-Foster performance of the 2D and 3D EAD designs is as follows:

1. Using one of the fixed (ideal) inductor values specified during the frequency agile simulation, determine the corresponding frequency value where the value of $|S_{11}|$ is minimized. Call this value f_{null}.
2. Insert f_{null} into the regression equation to determine the non-Foster inductor value. Call this $L_{regression}$.
3. Run the antenna simulation using $L_{regression}$ as the inductor value.
4. Using the $|S_{11}|$ curve generated when the inductor value is set as $L_{regression}$, find the value of $|S_{11}|$ at f_{null}. This is the antenna's non-Foster $|S_{11}|$ performance at f_{null}.
5. Repeat steps 1 – 4 for all desired values of f_{null}.

The procedure for analyzing the non-Foster performance at a single value of f_{null} is illustrated in Figure 5-5. First, we choose a value of the inductor, in this case 89 nH. Then, the $|S_{11}|$ curve is generated with an HFSS simulation by using this inductor value. For the 89 nH inductor, it was found that the minimum $|S_{11}|$ value occurred at 304.87 MHz. Next, the value of 304.87 MHz is substituted for f in (5-1), and the regression equation specified value of L is found to be $L_{regression}$ = 89.08 nH. Then using $L_{regression}$ in a new HFSS simulation, a new $|S_{11}|$ curve was generated. The value of $|S_{11}|$ at 304.87 MHz specified by this result was found to be -25.2 dB. Note that despite the

small percent error in the inductor value, there is a small but non-trivial shift in the resonance value. If the null were not deep enough, the value of $|S_{11}|$ (in dB) at the original resonance frequency could be much larger than desired.

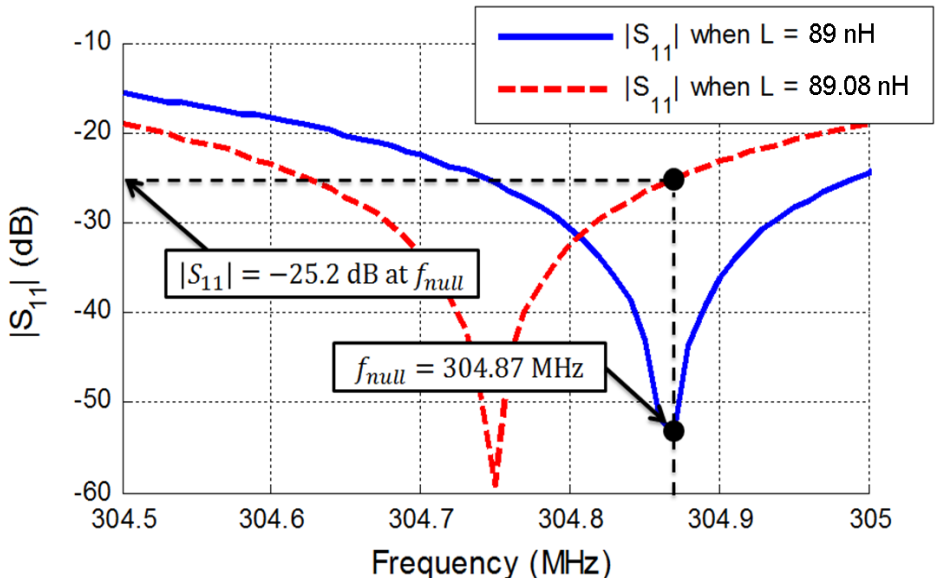

Figure 5-5: Illustration of the procedure for calculating the performance of the non-Foster 2D EAD antenna (*ka*=0.35) at a single frequency.

This procedure was repeated many times, thus generating the performance curve of the non-Foster 2D EAD antenna. The effectiveness of the non-Foster 2D EAD antenna, i.e., a comparison of the $|S_{11}|$ values calculated for each L (frequency agile inductor) and $L_{regression}$ (non-Foster – i.e., instantaneous – inductor), is shown in Figure 5-6. The corresponding comparison for the non-Foster 3D EAD antenna is given in Figure 5-7. A summary of the -20 dB bandwidth of each antenna is given in Table 5-2.

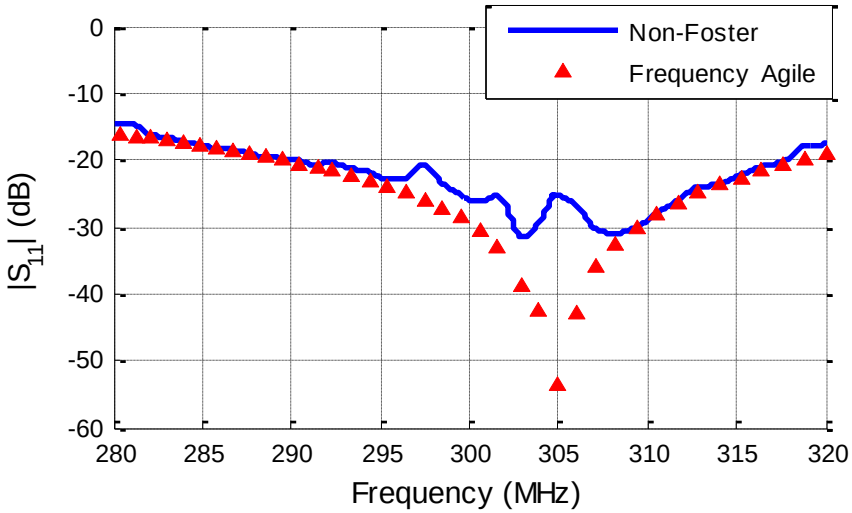

Figure 5-6: Comparison of the non-Foster 2D EAD antenna $|S_{11}|$ (dB) values with the original frequency agile values when ka = 0.35.

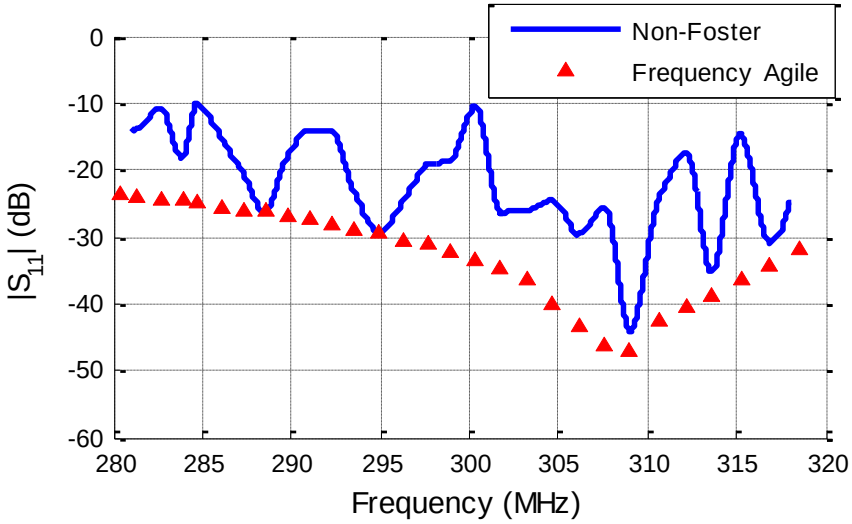

Figure 5-7: Comparison of the non-Foster 3D EAD antenna $|S_{11}|$ (dB) values with the original frequency agile values when ka = 0.35.

Table 5-2: Largest continuous -20 dB bandwidths for the non-Foster 2D and 3D EAD designs with ka = 0.35

Design	**Largest Continuous -20 dB Bandwidth**
Non-Foster 2D EAD	27.6 MHz ≈ 9.1%
Non-Foster 3D EAD	10.2 MHz ≈ 3.3%

As witnessed by the $|S_{11}|$ performance of the non-Foster 2D and 3D EAD designs given in Figure 5-6 and Figure 5-7, the former performs better than the latter when the non-Foster inductive element is included in the design. This is despite what was observed in the original frequency agile results. The authors offer an explanation as to why this occurs.

The first question that must be answered concerns the regression equations. Did the regression equation for the 2D EAD design do a better job predicting the inductor values than the regression equation for the 3D EAD version? In fact, upon re-examining Figure 5-3 and Figure 5-4, it is clear that the regression equation for the 3D EAD antenna generated smaller percent-error values than that of the 2D EAD design. Therefore, the differences between the non-Foster performances cannot be attributed to the regression equations.

This conclusion then leads to the next question: Why is the performance of the non-Foster 3D EAD antenna more sensitive to the small perturbations in the inductor values produced by the regression equation? It is found that the fractional bandwidth of the original design is responsible for this behavior. In particular, because the fractional bandwidth of the original 3D EAD antenna is much smaller than that of the 2D EAD design, it is more sensitive to those small perturbations in the inductor values. This is clearly illustrated when comparing Figure 5-6 and Figure 5-7. Consequently, since the instantaneous bandwidth of these antennas is primarily driven by the slope of the reactance curve at resonance (as discussed in Chapter 3), this leads to the conclusion that

the non-Foster performance is governed by the derivative of the reactance at the resonant frequency.

To prove this important point graphically, let us compare the performance of the non-Foster 2D and 3D EAD antennas around 300 MHz. For the original 2D EAD design, an inductor value of 93 nH is used to plot its $|S_{11}|$ curve, shown in blue in Figure 5-8. This gives a value of $f_{null} = 300.55$ MHz. The regression equation (5-1) for the 2D EAD then gives a value of 93.11 nH at this particular value of f_{null}. This second inductor value is then used in HFSS to calculate the corresponding $|S_{11}|$ curve. This result is plotted as the dashed red curve in Figure 5-8, from which the non-Foster performance value of $|S_{11}|$ can be derived. As observed, because the original 2D EAD antenna has a relatively wide instantaneous bandwidth around a deep null, the non-Foster performance is quite good at this frequency.

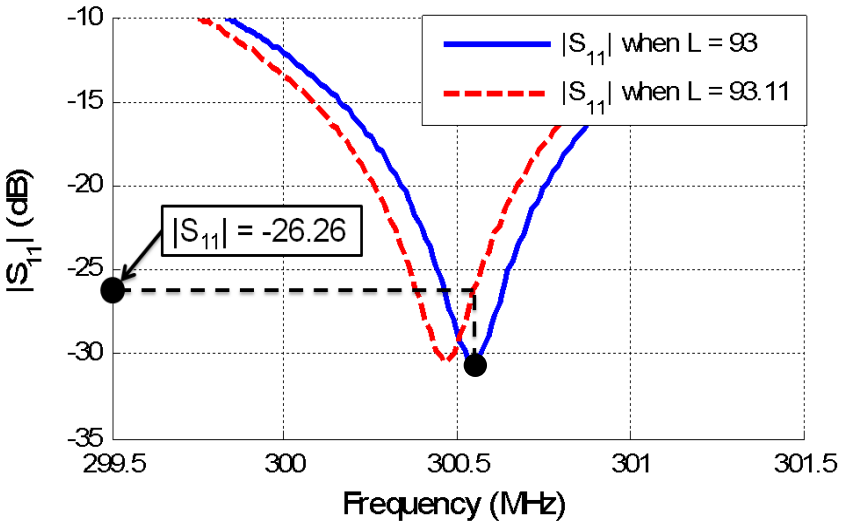

Figure 5-8: The relatively wide instantaneous bandwidth of the original 2D EAD antenna leads to a good non-Foster performance.

We can then contrast these results with the corresponding performance of the 3D EAD antennas. Using an inductor value of 198 nH for the original design, the blue curve in Figure 5-9 is generated. From this curve, a value of 300.34 MHz is found for f_{null}, which in turn leads to $L_{regression}$ = 198.09 nH, as calculated from the 3D EAD's regression equation (5-1). It should be noted that this inductor shift is smaller in magnitude than the inductor shift seen in the example for the 2D EAD antenna. This regression equation-specified value of the inductor is used to generate the dashed red curve in Figure 5-9. Now, as can be observed, the relatively narrow instantaneous bandwidth of the 3D EAD design causes a large degradation in the non-Foster performance, even though the inductor value was perturbed by only a very small amount. This sensitivity would make a practical realization of a non-Foster 3D EAD quite difficult.

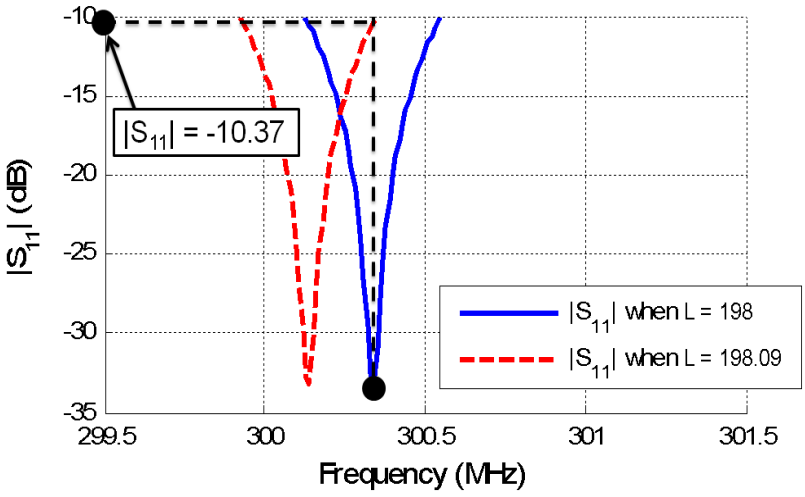

Figure 5-9: The relatively narrow instantaneous bandwidth of the original 3D EAD leads to a poor non-Foster performance.

These examples thus show that antennas with larger instantaneous bandwidths (i.e., smaller reactance slopes) would be less sensitive to small perturbations in the circuit

elements used to derive the non-Foster performance. Thus, they are better suited to realize the full benefits of placing a non-Foster circuit element within the NFRP element of an antenna design. This is in agreement with the original observations in [14].

As emphasized initially, the adaptive meshes for all of the previous HFSS simulations were generated at a frequency of 400 MHz. One might wonder: What impact does the choice of adaptive mesh frequency have on the predicted non-Foster performance? To help answer this question, the frequency agile simulations were re-run using an adaptive mesh frequency of 500 MHz, i.e., with a finer mesh. The results were then used to generate new regression equations, and the performance of both the non-Foster 2D and 3D EAD antennas were recalculated, again using an adaptive mesh frequency of 500 MHz. These results are shown in Figure 5-10 and Figure 5-11.

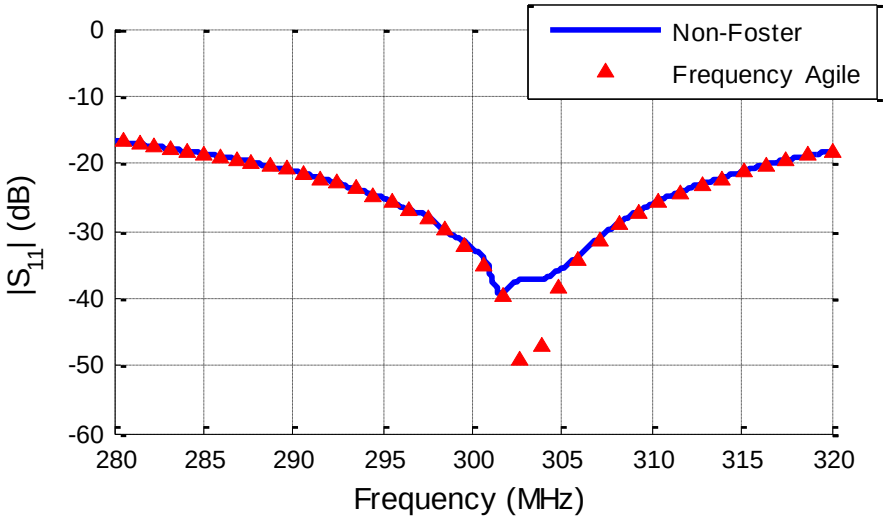

Figure 5-10: Non-Foster performance of the 2D EAD (*ka* = 0.35), calculated using an adaptive mesh frequency of 500 MHz.

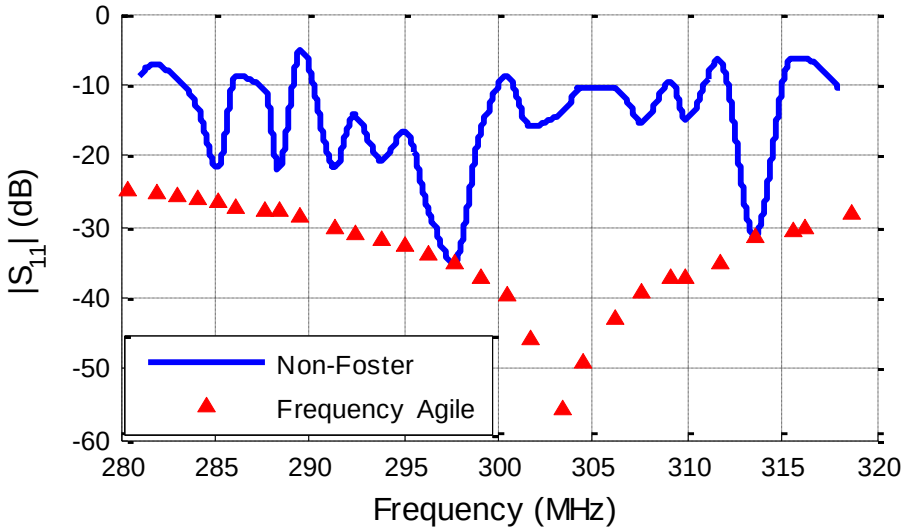

Figure 5-11: Non-Foster performance of the 3D EAD (*ka* = 0.35), calculated using an adaptive mesh frequency of 500 MHz.

By comparing Figure 5-6 and Figure 5-10, it is obvious that by allowing the adaptive mesh to be generated at 500 MHz, the predicted non-Foster performance has improved for the 2D EAD design. In contrast, by comparing Figure 5-7 with Figure 5-11, one can tell that the predicted non-Foster performance for the 3D EAD has degraded significantly. It was found that the 3D EAD design is even more sensitive to the small perturbations in the inductor values when a finer adaptive mesh is employed. Therefore, when simulating the non-Foster behavior of these antennas, it is recommended that multiple results be obtained using different adaptive mesh frequencies in order that they can be compared and contrasted.

5-2 Radiation Efficiencies of the Non-Foster Augmented EAD Antennas

Finally, one very important antenna characteristic that should be considered when examining the performance of a non-Foster electrically small antenna design is its

radiation efficiency over all frequencies of interest. Our simulations have shown that the radiation efficiencies of the non-Foster 2D EAD design over all frequencies are higher than those of the corresponding 3D design. Since the original designs showed the same behavior for varying values of *ka*, this outcome was expected. Both the non-Foster 2D and 3D EAD designs also show decreasing radiation efficiency as the frequency decreases, i.e., as *ka* decreases. Again, this behavior was also expected from the results of the original designs. Nevertheless, as shown in Figure 5-12, the radiation efficiencies of both the non-Foster 2D and 3D EAD designs remain quite stable over more than a 10% fractional bandwidth. In fact, the non-Foster 2D EAD design maintains a radiation efficiency greater than 90% over this bandwidth. Moreover, it shows much less variation over the same frequency interval than was expected from the original results shown in Figure 3-6, as well as less variation than the corresponding 3D design.

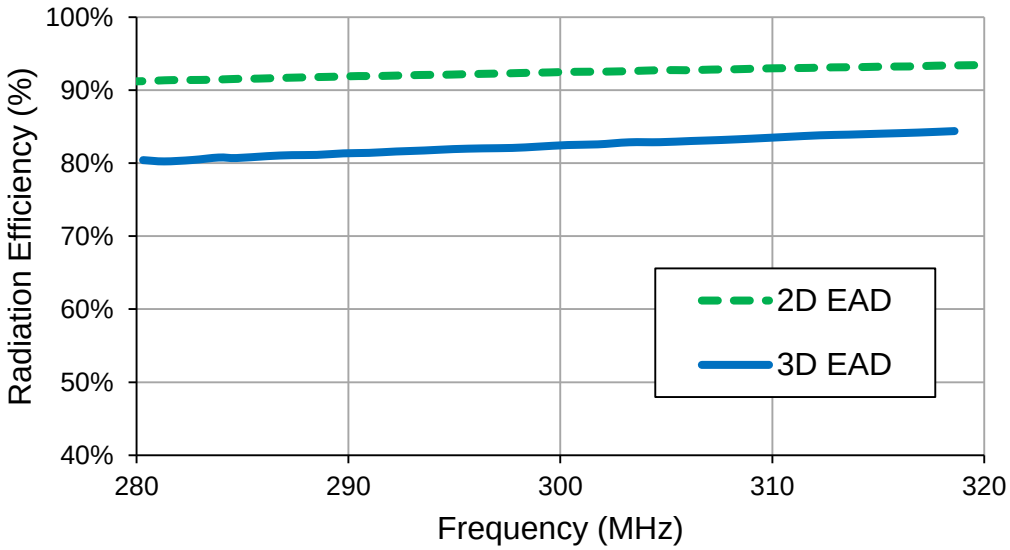

Figure 5-12: Radiation efficiencies of the 2D and 3D non-Foster designs when *ka* = 0.35.

5-3 Details on How to Calculate the Exponential Regression Coefficients

In Section 5-1, it was mentioned that the frequency agile data was used to generate an exponential regression equation of the form given in (5-1). However, the procedure for calculating the coefficients for this type of a regression equation was omitted. In this section, a procedure for calculating the regression coefficients ξ, α, and β shall be detailed.

Before proceeding, the reasoning behind choosing this particular form of the regression equation should be explained. During the simulations, it was often convenient to calculate the regression coefficients with subsets of the L_{ideal} and frequency values. However, this regression equation still needed to predict the inductor values accurately outside of this subset (i.e., accurate extrapolation was desired). It was found that polynomial-based regression equations did a relatively good job of predicting the inductor values within the sub-range, but they did not perform well when their results were extrapolated outside of the sub-range. On the other hand, the exponential regression equation performed well both in the sub-range and in the extrapolation regions. Therefore, the exponential form of the regression equation was selected for all of the curve-fit applications.

From the frequency agile simulations, we have obtained the ideal inductor values versus frequency for certain discrete frequency samples. Ideally, it would be nice to calculate the values of ξ, α, and β by performing a matrix inversion. However, due to the form of (5-1), it is impossible to directly perform the matrix inversion. Therefore, the equation must be converted to a form that allows one to perform a pseudo matrix

inversion for a given value of ξ. Once one understands how to perform the pseudo matrix inversion, then the resulting nonlinear equation can be solved to get the optimum values of ξ, α, and β, i.e., the values that minimize the differences between L_{ideal} and $L_{regression}$.

To begin forming the equation that allows a pseudo matrix inversion, start with (5-1), move ξ to the left-hand side of the equation, and then take the natural logarithm of both sides to obtain

$$\ln(L-\xi) = \ln\left(\alpha \mathrm{e}^{-\beta \cdot f}\right). \tag{5-3}$$

From this equation, we can use the properties of the logarithm to write

$$\ln(L-\xi) = \ln(\alpha) - \beta f \tag{5-4}$$

or

$$\mathrm{X} = A + Bf \tag{5-5}$$

where $\mathrm{X} = \ln(L-\xi)$, $A = \ln(\alpha)$, and $B = -\beta$. If we first guess a value for ξ, then, from the frequency agile data, we have multiple values for X and for f. Thus, we can write (5-5) in matrix form as

$$\begin{bmatrix} \mathrm{X}_1 \\ \vdots \\ \mathrm{X}_n \end{bmatrix} = \begin{bmatrix} 1 & f_1 \\ \vdots & \vdots \\ 1 & f_n \end{bmatrix} \begin{bmatrix} A \\ B \end{bmatrix} \tag{5-6}$$

or

$$\mathrm{X} = FD\,. \tag{5-7}$$

Thus, we can solve for D using a pseudo matrix inversion, so that

$$D = F^{\dagger}\mathrm{X}\,. \tag{5-8}$$

where $F^{\dagger} = (F^{\mathrm{T}}F)^{-1}F^{\mathrm{T}}$ represents the pseudo-inverse of the matrix F. Then, D is a column vector with exactly two entries, and thus we can determine α from $\alpha = \exp(D_1)$, and we can determine β from $\beta = -D_2$.

Now, as explained originally, this formulation works after we have guessed a value of ξ. We would like to have a software package, such as MATLAB, solve for the value of ξ that minimizes the difference between the ideal inductor values and the inductor values calculated using (5-1). Conveniently, MATLAB has a function called *fsolve* (used for solving non-linear equations) that does just this. By constructing a function (referred to as *myfun* in Appendix B) that accepts ξ as an input and then performs the pseudo matrix inversion based on that given value of ξ, we can have MATLAB solve for the value of ξ that minimizes the difference between L_{ideal} and $L_{regression}$. Once we find the minimizing value of ξ, we need to perform one final pseudo matrix inversion to find the α and β values associated with that particular value of ξ.

A MATLAB script that solves for ξ, α, and β based on an input frequency agile data set is shown in Appendix B. This script requires the auxiliary function *myfun* to be saved as a separate M-file; also, *myfun.m* must be located in the MATLAB path in order for the script to work properly.

5-4 Non-Foster Simulations in HFSS

Similar to the frequency agile simulations, it is easy to obtain the necessary data from HFSS to create the non-Foster plot. However, actually creating the non-Foster plot in HFSS proves to be difficult. Thus, the first part of this section explains how to obtain the necessary data within HFSS, and the second part explains how to export that data and then process the data to obtain the desired non-Foster plot. The last part of this section explains how to obtain the corresponding non-Foster radiation efficiency of an antenna structure.

5-4-1 Obtaining the Necessary Data from HFSS for the Non-Foster Plot

Once we have obtained the regression coefficients (i.e., ξ, α, and β), we can obtain the inductor values predicted by the regression equation, referred to as $L_{regression}$. For example, say that during the ideal frequency agile simulation of the 2D EAD, an L_{ideal} value of 70 nH was found to produce a minimum $|S_{11}|$ value that occurs at 327.95 MHz. Then, by using the regression equation given by (5-1) and the corresponding regression coefficients shown in Table 5-1, we find that an f value of 327.95 MHz produces a $L_{regression}$ of 69.6748 nH. By repeating this process, we can obtain an $L_{regression}$ value for each value of f. For the next steps to work, the same number of $L_{regression}$ values must be calculated as the original number of L_{ideal} values used during the frequency agile simulations.

Once each $L_{regression}$ value has been determined, these values can be stored in a CSV file. The MATLAB script in Appendix B shows how to save the $L_{regression}$ values

directly to a CSV file from MATLAB (lines 87–91). Then, in HFSS, a new Parametric Sweep can be created by loading this CSV file. This is accomplished by right-clicking on "Optimetrics", mousing-over "Add", and then clicking on "Parametric from File", as shown in Figure 5-13. Then one must navigate to the CSV file that contains the $L_{regression}$ values, and click "OK". If the CSV file is formatted correctly, HFSS will automatically create a new parametric analysis with those $L_{regression}$ values.

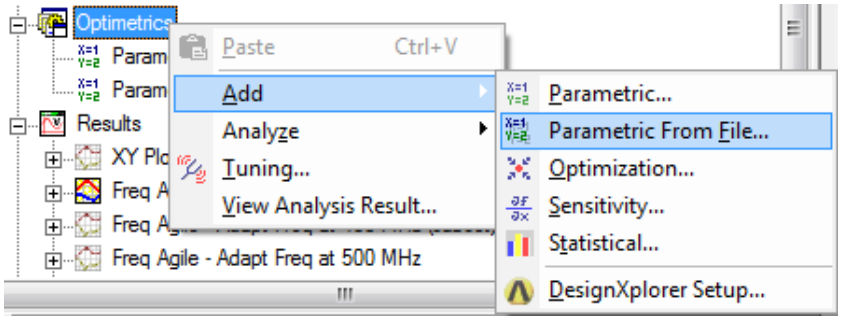

Figure 5-13: Screenshot of creating a parametric sweep from a CSV file.

However, HFSS defaults to using all of the simulation set-ups for this new parametric analysis. Thus, the user should check to make sure that only the desired set-up is being used for this parametric sweep. This can be done by right-clicking on the parametric sweep, clicking "Properties", and then clicking on the "General" tab. It is very important that the exact same simulation set-up and frequency sweep used for the frequency agile simulations is again used for these regression simulations.

Once the parametric sweep is properly configured, right-click on the newly created parametric sweep, and click "Analyze" to begin the simulations.

5-4-2 Creating the Non-Foster $|S_{11}|$ Curve

After the new parametric sweep is completed, the data needs to be exported to a CSV file to obtain the desired non-Foster curve. First, each $|S_{11}|$ curve that was simulated using the $L_{regression}$ values must be plotted within HFSS. In order to perform this task, right-click on "Results", mouse-over "Create Modal Solution Data Report", and then click on "Rectangular Plot", as shown in Figure 5-14.

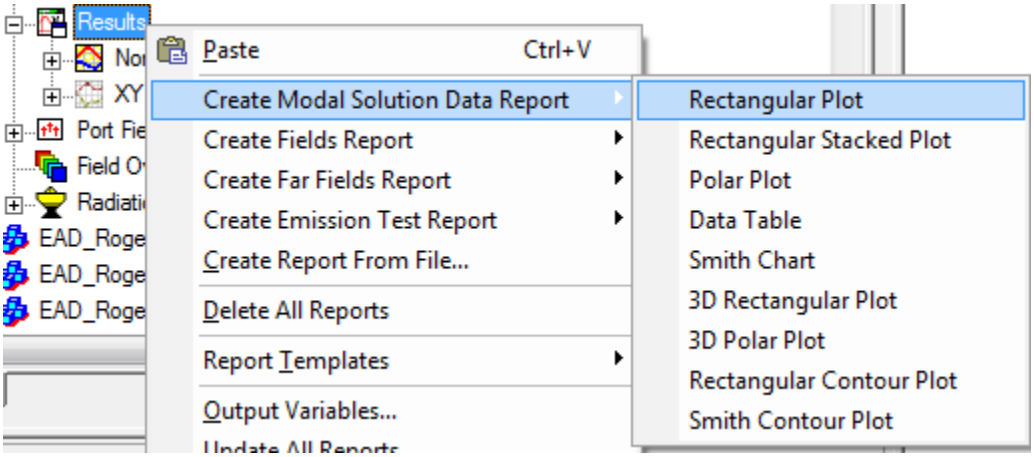

Figure 5-14: First step in creating the plot of the $L_{regression}$ simulation results.

After the "Report" window appears, ensure that the proper set-up is selected in the "Solution" drop-down menu. Also, click on the "Families" tab, and ensure that **only** the $L_{regression}$ inductor values are selected, as demonstrated in Figure 5-15. If more inductor values than required are selected, this will cause issues when attempting to generate the non-Foster plot.

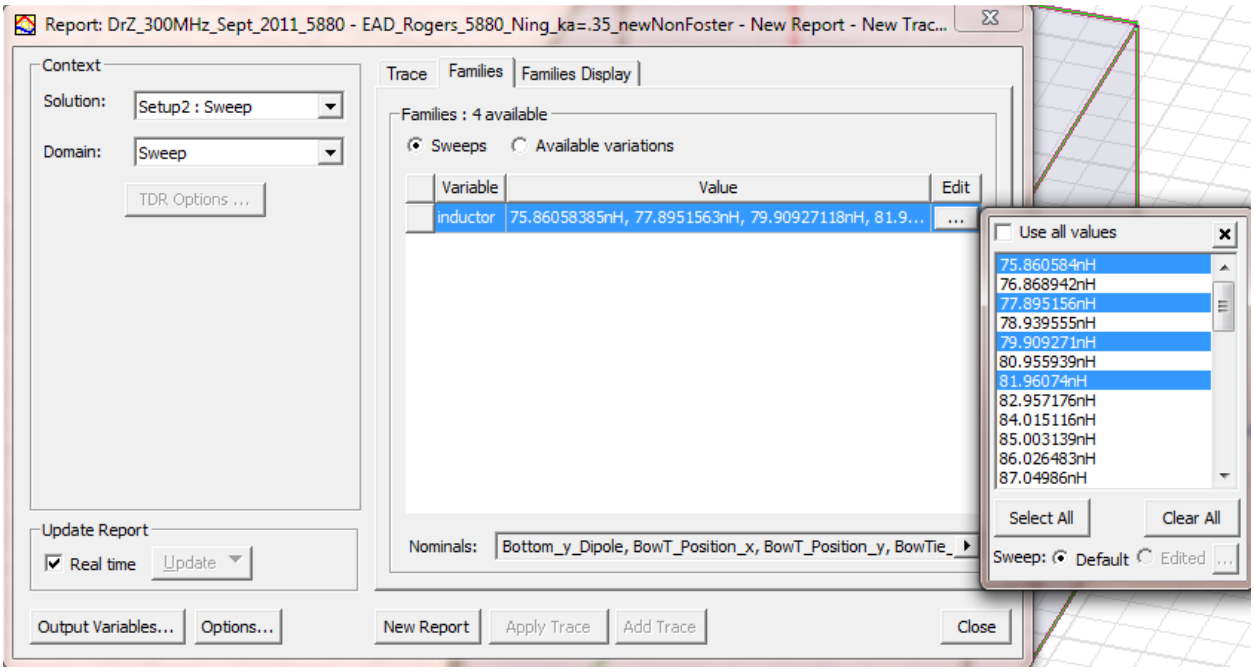

Figure 5-15: Selecting only the $L_{regression}$ inductor values.

Once the proper inductor values have been selected, click on the "New Report" button. This will generate a new plot with all of the $|S_{11}|$ curves, each one corresponding to a unique $L_{regression}$ value.

The next step is to export the data contained in the HFSS plot. To accomplish this task, right click on the new plot's icon in the model tree, and then click on "Export". This allows the user to save all of the data into a CSV file.

To calculate the non-Foster plot, the $|S_{11}|$ data obtained during the frequency agile simulations, which were created using the L_{ideal} values, must be used along with the $|S_{11}|$ data obtained during the regression simulations, which were created using the $L_{regression}$ values. For example, say that one first chooses the L_{ideal} value of 76 nH. From the frequency agile simulations of the 2D EAD antenna, the frequency at which $|S_{11}|$ is minimized is determined for this particular inductor value to be 320.14 MHz. Then, by

plugging this value of f into the regression equation, an $L_{regression}$ value of 75.8606 nH is obtained. Thus, to determine the non-Foster performance of the antenna at 320.14 MHz, the $|S_{11}|$ value of the antenna when the antenna system uses an inductor value of 75.8606 nH must be determined. From the regression simulations, it is found that the 2D EAD design has an $|S_{11}|$ of -17.66 dB at 320.14 MHz when the inductor value is set at 75.8606 nH. Thus, the (x,y) coordinate for the non-Foster plot from this result would be (320.14 MHz, -17.66 dB).

As might be surmised, the procedure for calculating each (x,y) coordinate of the non-Foster plot would be very tedious if done manually. Therefore, it is recommended that a software tool, such as MATLAB, is used to compute the non-Foster curve. As long as the frequency agile results are stored to a CSV file as detailed in Section 4-2-1 and Section 4-2-2, and the regression results are stored to a CSV file as shown in Section 5-4-1 and this section, then the MATLAB script shown in Appendix C (or a similar script) may be used to automatically generate the non-Foster curve. By using a script such as the one in Appendix C, researchers will have more time to focus on other interesting aspects of their research.

5-4-3 Creating the Non-Foster Radiation Efficiency Curve

Yet again, HFSS does not have an easy way of creating the non-Foster radiation efficiency curve. To generate this curve, the radiation efficiency of the antenna must be known at a specific frequency for a given specific inductor value. For example, if the frequency agile results for an ideal inductor value (L_{ideal}) of 76 nH gives a minimum

$|S_{11}|$ that occurs at 320.14 MHz, and if the regression equation gives a regression inductor value ($L_{regression}$) of 75.8606 nH, then the radiation efficiency of the antenna must be determined at a frequency of 320.14 MHz when the inductor is set to 75.8606 MHz.

As reported in the previous sections, methods have been developed for calculating all of the required input information to obtain the radiation efficiency curves. From the frequency agile results, all of the frequency values at which the minimum values of $|S_{11}|$ occur are known. From the regression equation, the associated $L_{regression}$ values for each of these frequency values also are known. Therefore, it would be nice to have HFSS automatically generate the radiation efficiency curve based on all of this input information.

With some scripting knowledge, this automatic generation of the radiation efficiency curve is indeed possible within HFSS. The HFSS software includes tools for recording and running macros, which execute certain operations automatically. An example macro script for generating and running the necessary radiation efficiency simulations is shown in Appendix D in the *Run_2DEAD_NF_RadEff.vbs* script. To summarize the actions of the script, it first sets the active design within HFSS. Then, it reads the necessary frequency and associated inductor values from a CSV file. The script then creates a new discrete sweep at a particular frequency, sets the inductor value of the model to the associated inductor value, and runs the simulation. It repeats these operations for each frequency/inductor value combination within the CSV file. To run this script, a user simply clicks on the "Tools → Run script" menu item within HFSS. At

the end of the script, a full wave simulation has been completed for each of the various frequency/inductor value combinations.

Next, the results must be plotted in order to visualize the radiation efficiency curve. Again, this can be facilitated by a macro. The script *Plot_2DEAD_NF_RadEff.vbs* in Appendix D is an example of a macro that can be used to generate the non-Foster radiation efficiency plot. This script again uses the same CSV file as mentioned previously to keep track of the number of frequency/inductor value combinations. By using the CSV file and the results of each radiation efficiency simulation, the macro automatically generates the radiation efficiency curve for the antenna within an HFSS rectangular plot. This process can be completed manually; but again, the automation achieved with the macro tool is quite beneficial.

5-5 Non-Foster Simulations in ADS

The ADS software package, comparable to HFSS, has simulation capabilities that make running the non-Foster simulations (i.e., the simulation runs using the $L_{regression}$ values) a relatively easy endeavor. However, also like HFSS, there is no easy way to plot the desired non-Foster $|S_{11}|$ performance curve. Therefore, a quick tutorial on how to perform these simulations and how to obtain the non-Foster performance curve shall be given. Also, at the end of this section, the non-Foster curves obtained with HFSS and ADS shall be compared, both for the 2D and 3D EAD antennas.

At this point, it is assumed that the frequency agile simulations have been completed and the appropriate CSV file that lists the applicable $L_{regression}$ values

calculated from the appropriate regression equation has been generated. One must next add a header row to the CSV file. This header row must contain the inductor variable name that will be used in the ADS circuit simulation. Also, this CSV file must list the inductor values in henries (H), not in nH. An example of one such CSV file is given in Figure 5-16.

```
L_regression
7.00537E-08
7.10426E-08
7.20286E-08
7.30189E-08
7.40055E-08
7.50038E-08
7.59901E-08
7.69878E-08
⋮
```

Figure 5-16: Snippet of an example CSV file used for the non-Foster simulations in ADS.

After modifying the CSV file appropriately, the circuit and applicable simulation blocks must be added to the ADS schematic. A screenshot of the circuit and simulation set-up for the non-Foster simulation is shown in Figure 5-17.

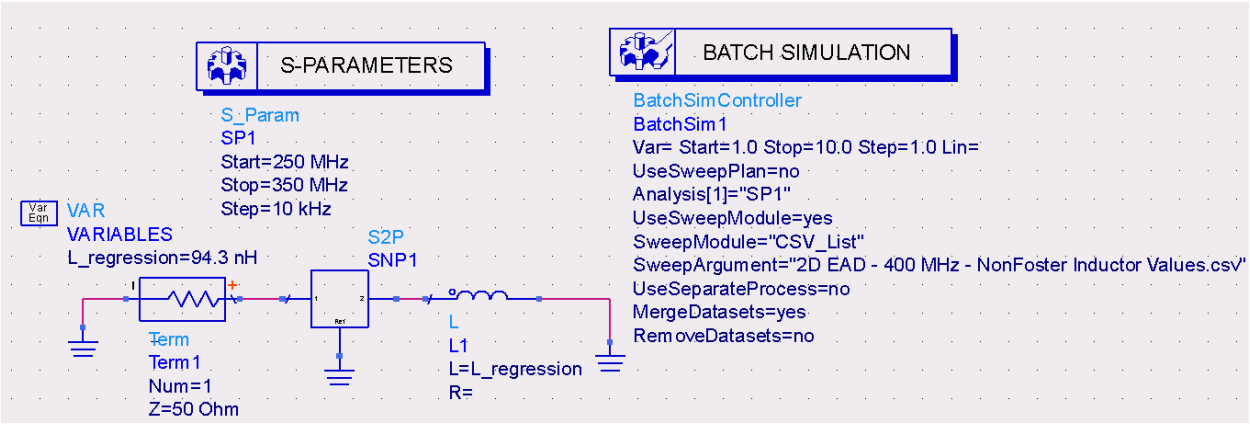

Figure 5-17: Screen shot of the ADS schematic for the non-Foster simulations.

For the non-Foster simulations, the same S2P file in the "S2P" block as was employed during the frequency agile simulations must be used. The main difference between the frequency agile set-up and the non-Foster set-up is the use of the "Batch Simulation" block instead of the "Parameter Sweep" block. A batch simulation allows the user to dictate the values of any combination of variables for each simulation run. Therefore, in the CSV file, each column represents a different variable, and each row represents a different simulation run. The "S-Parameters" block is also used, because the "Batch Simulation" block needs to know what kind of simulation to run for each variable combination specified in the CSV file.

Once the schematic has been constructed as shown in Figure 5-17, the simulation may be started by pressing the "Simulate" button. After performing the S-parameter analysis for each value of $L_{regression}$, ADS will open a new plotting tool window. To view all of $|S_{11}|$ curves, the user may insert a rectangular plot and add the dB(S(1,1)) equation to the plot. An example of one such plot is shown in Figure 5-18.

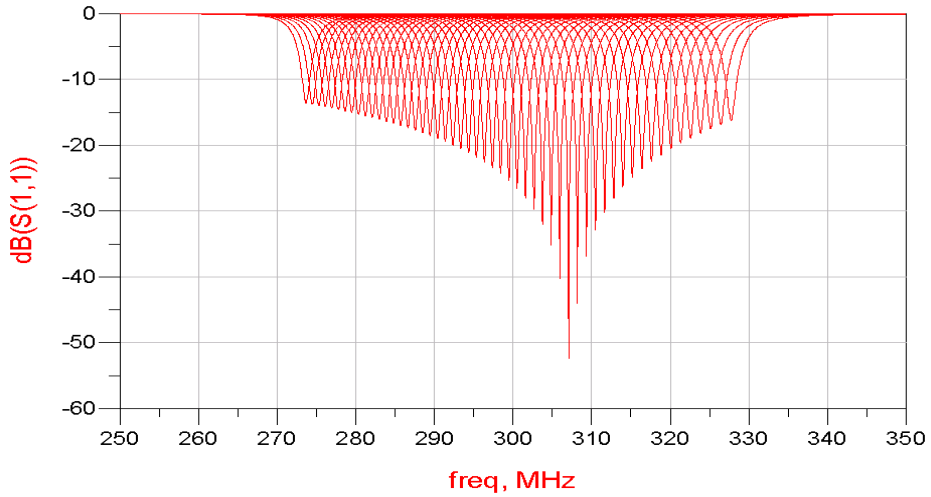

Figure 5-18: $|S_{11}|$ curves generated using the $L_{regression}$ values in ADS for the 2D EAD when ka = 0.35.

One may note that the $|S_{11}|$ curves generated using the $L_{regression}$ values (Figure 5-18) look very similar to the curves generated using the L_{ideal} values (Figure 4-22). This is highly desirable for comparison purposes because it is desired to have each $|S_{11}|$ curve lie on top of its associated $|S_{11}|$ curve generated from the ideal case.

Finally, we would like to generate the non-Foster curve for this antenna. However, like HFSS, this is very difficult to obtain within ADS itself. Therefore, the author recommends exporting the $|S_{11}|$ curves in a tab-delimited ASCII file, as described in Section 4-3, and then employing a MATLAB script similar as the one shown in Appendix C to create the non-Foster curve.

Once the non-Foster curve has been generated using ADS, the non-Foster $|S_{11}|$ curves obtained using HFSS and ADS may be compared. These curves are shown in Figure 5-19 for the 2D EAD antenna and in Figure 5-20 for the corresponding 3D EAD design.

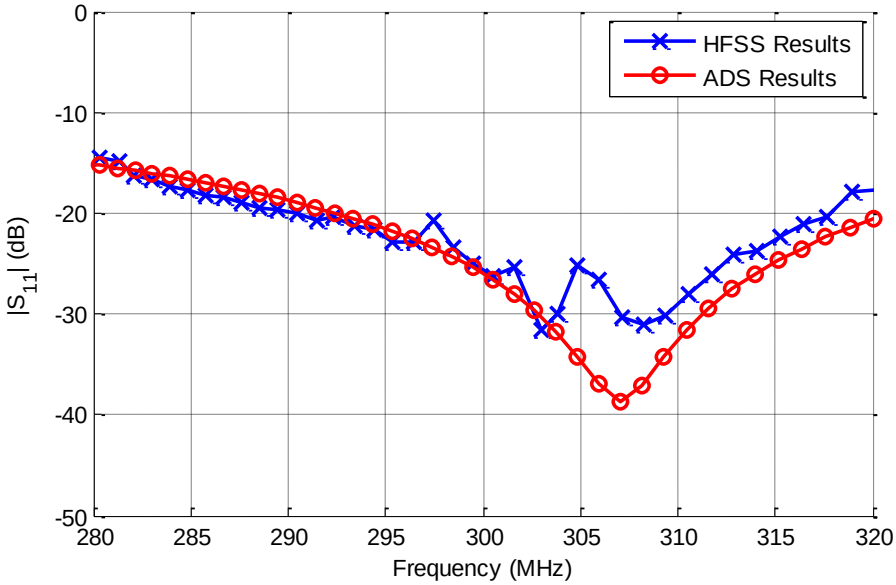

Figure 5-19: Non-Foster curves obtained using HFSS and ADS for the 2D EAD antenna (ka = 0.35).

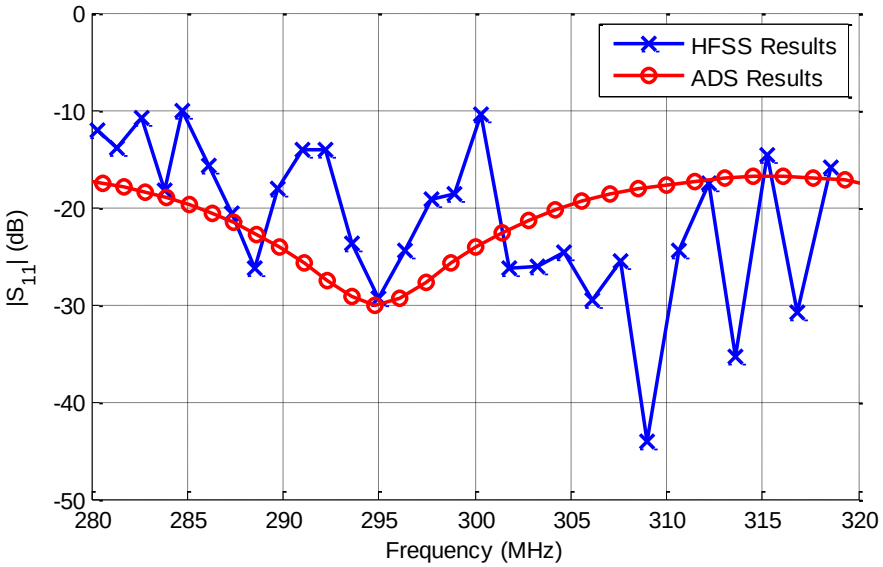

Figure 5-20: Non-Foster curves obtained using HFSS and ADS for the 3D EAD antenna (*ka* = 0.35).

The comparison between the non-Foster simulation curves for the 2D EAD antenna shows that the two are quite similar. In fact, if one was interested in obtaining a quick analysis of the non-Foster bandwidth of the 2D EAD antenna, the use of the ADS simulation tool would be a valid method. This would provide the estimate much quicker because only one full-wave simulation would need to be run within HFSS to generate the S2P file. The remainder of the simulations would be performed within ADS. This approach is beneficial because each individual ADS simulation run is much quicker than each individual HFSS simulation run.

However, the comparisons also show that the ADS non-Foster curve is much smoother than the HFSS generated non-Foster curve. The first explanation for these variations is based again on the inherent differences in the simulation packages. ADS is a circuit simulation tool, whereas HFSS is a full-wave solver. In this process, HFSS is

assumed to be predicting the correct results because it is solving the full-wave model for each value of L_{ideal} and $L_{regression}$, whereas ADS uses a single full-wave solution (the S2P file) and then performs circuit-like simulations based on that HFSS single solution. The other explanation is based on the fact that HFSS generates a new mesh for each simulated $|S_{11}|$ curve. Perhaps the models with certain meshes are obtaining better convergence than others. This behavior would lead to the jagged results when comparing the $|S_{11}|$ results between the L_{ideal} and $L_{regression}$ cases (which is how the non-Foster curve is formed). ADS does not use a new mesh for each inductor value; in fact, it uses the same S2P file for each unique simulation. Therefore, one could argue that it uses the same "mesh" for each simulation.

Since the actual root cause of the differences between the simulation results remains unclear at this time, it could be worth looking further into the cause or causes of these differences in the future.

CHAPTER 6 | CONCLUSIONS AND FUTURE WORK

6-1 Conclusions

By comparing the planar and 3D Egyptian axe dipole antenna designs, we have provided more insight into the physics which governs their behaviors. Although the planar (2D) EAD performed better than the 3D EAD in both the original and non-Foster designs, the frequency agile fractional bandwidth of the 3D EAD design was superior. Consequently, one cannot make gross *á priori* assumptions about such 2D versus 3D designs when considering what their potential performance characteristics may be. This observation is true whether one is considering simply a narrow-band NFRP antenna or its augmentation with frequency agile components to achieve large tunable bandwidths or with non-Foster elements to achieve large instantaneous bandwidths.

The results of this study indicate that initial antenna designs which have wider instantaneous bandwidths will perform better when augmented with non-Foster elements due to their decreased sensitivities to errors in the actual values produced by the non-Foster circuits. This is a very useful conclusion for any practical realization of a non-Foster augmented electrically small antenna. In general, either a frequency agile or a non-Foster design can greatly improve the bandwidth of an electrically small NFRP antenna. Nonetheless, one remains faced with the fact that the radiation efficiency of either design type is dictated by its value for the original non-augmented antenna design. Moreover, any additional losses introduced by augmentation with either the frequency agile or non-Foster elements will degrade the radiation efficiency values.

6-2 Future Work

While initial experimental studies discussed in the references support these conclusions, it would be very interesting to manufacture and test both the 2D and 3D EAD designs as both frequency agile and non-Foster augmented systems to validate the simulation results reported here. It would also be interesting to design, construct, and test other antenna designs with non-Foster augmentation.

Another possible future research topic deals with the instantaneous bandwidths of the 2D and 3D EAD versus the theoretical passive limits. In Figure 3-1, both the 2D EAD and the 3D EAD approach the theoretical bandwidth limit as *ka* decreases. With some more time, it would have been interesting to see how closely these antennas follow the theoretical limit as *ka* decreases even more.

Additionally, it is mentioned in Chapters 4 and 5 that there exist differences in the simulated frequency agile and non-Foster performances predicted by HFSS and ADS. This is somewhat troubling since it would be nice if both simulation packages provided the same predictions for both the frequency agile and the non-Foster $|S_{11}|$ curves. As presented in Section 5-5, there are a few theories as to why the results are different, but the root cause should be uncovered and validated at some point.

Any or all of these topics could provide another student with interesting research. In that vein, the author hopes that the knowledge imparted by this thesis will help future students understand the relationship between instantaneous, frequency agile, and non-Foster antenna performance, and hopefully the next student can grow the engineering community's knowledge of these topics even further.

APPENDIX A | ABBREVIATIONS, ACRONYMS, AND SYMBOLS LIST

Abbreviations and Acronyms

2D – Two dimensional

3D – Three dimensional

ADS – Agilent's Advanced Design System

CST – Computer Simulation Technology

dB – Decibels

EAD – Egyptian Axe Dipole

EM – Electromagnetic or Electromagnetics

ESA – Electrically Small Antenna

HFSS – ANSYS/Ansoft High Frequency Structure Simulator

NFRP – Near-Field Resonant Parasitic

NIC – Negative Impedance Converter

SMA – Sub Miniature version A (type of microwave connector)

TE – Transverse Electric

TM – Transverse Magnetic

Commonly Used Symbols with Typical Units

a – Typically referred to as the radius of the minimum sphere that will enclose the entire antenna structure, [m]

A – Cross-sectional area, [m^2]

b – Radius of the dipole or monopole wire, [m]

$\vec{\mathbf{B}}$ – Magnetic flux density, [Wb/m^2]

BW – Impedance bandwidth, [Hz] or [MHz]

c – Speed of light in a vacuum, [m/s]

D – Antenna directivity, [unitless]

$\vec{\mathbf{D}}$ – Electric flux density, [C/m^2]

$\vec{\mathbf{E}}$ – Electric field intensity, [V/m]

f_0 – Resonant frequency, center frequency, or frequency of interest, [Hz] or [MHz]

FBW – Fractional impedance bandwidth, [unitless]

f_{null} – Frequency at which the minimum $|S_{11}|$ (dB) value occurs, [Hz] or [MHz]

G – Antenna gain, [unitless]

h – Length of the monopole antenna wire, [m]

$\vec{\mathbf{H}}$ – Magnetic field intensity, [A/m]

$\vec{\mathbf{I}}_e$ – Vector electric current, [A]

I_0 – Scalar electric current, [A]

j – Imaginary unit $= \sqrt{-1}$, [unitless]

$\vec{\mathbf{J}}_c$ – Conduction electric current density, [A/m^2]

$\vec{\mathbf{J}}_i$ – Impressed electric current density, [A/m^2]

k – Free space wave number, [m^{-1}]

ka – Free space wave number times the radius of the antenna's minimum sphere, [unitless]

l – Length, [m]

l_{eff} – Effective length, [m]

L_{ideal} – Inductor value related to the frequency agile simulation results, [H] or [nH]

$L_{regression}$ – Inductor value calculated from the regression equation developed with the frequency agile results, [H] or [nH]

$\overrightarrow{\mathbf{M}}_i$ – Impressed magnetic current density, [V/m^2]

P_{rad} – Total power radiated, [W]

Q – Quality factor, [unitless]

q_{ev} – Electric charge density, [C/m^3]

q_{mv} – Magnetic charge density, [Wb/m^3]

R – Distance from any point in the source to the observation point, [m]

r – Spherical coordinate specifying the radial distance from the origin, [m]

$R(\omega)$ – Load resistance as a function of angular frequency, [Ω]

$R'(\omega)$ – Derivative of load resistance with respect to angular frequency, [Ω ·s/rad]

R_L – Loss resistance of the antenna structure, [Ω]

R_r or R_{rad} – Radiation resistance of the antenna structure, [Ω]

S_{11} – Scattering parameter equivalent to the complex reflected voltage value divided by the complex incident voltage value, [unitless]

$U(\theta, \phi)$ – Radiation intensity, [W/unit solid angle]

$X(\omega)$ – Load reactance as a function of angular frequency, [Ω]

$X'(\omega)$ – Derivative of load reactance with respect to angular frequency, [Ω ·s/rad]

Z_0 – Characteristic impedance, [Ω]

Z_{in} – Input impedance, [Ω]

α – Regression equation coefficient, [H] or [nH]

β – Regression equation coefficient, [Hz^{-1}] or [MHz^{-1}]

Γ – Complex reflection coefficient, [unitless]

ε – Permittivity of free space, [F/m]

η – Radiation efficiency, [unitless]

η_0 – Impedance of free space, [Ω]

θ – Spherical coordinate specifying the polar angle, [degrees] or [radians]

λ_0 – Wavelength in free space, [m]

μ – Permeability of free space, [H/m]

ξ – Regression equation coefficient, [H] or [nH]

ϕ – Spherical coordinate specifying the azimuth angle, [degrees] or [radians]

ω – Angular frequency, [radians/second]

ω_0 – Resonant angular frequency, center angular frequency, or angular frequency of interest, [radians/second]

APPENDIX B | MATLAB CODE FOR GENERATING THE REGRESSION-BASED INDUCTOR VALUES

calculateRegression.m

```
% Compute an exponential regression equation of the form
%
% L = xi + alpha*exp(-beta*f)
%
% from ideal frequency agile data.
%
% This function will also output two CSV files. The first can be read back
% into a "Parameteric from File" setup within HFSS for the non-Foster
% simulations. The second can be used along with an HFSS macro to compute
% the non-Foster radiation efficiency of the antenna.

%%%%%%%%%%%%%%%%%%%%%%%%%% USER PROVIDED INPUTS %%%%%%%%%%%%%%%%%%%%%%%%%%

% Set the filename for the ideal frequency agile results. This should be a
% CSV file with three columns: inductor value, min(dB(S(1,1))), and
% XAtYVal( dB(S(1,1)), min(dB(S(1,1))) ), in that specific order.
filename_IdealFrequencyAgileResults ...
    = '..\XLS and CSV Files\2D EAD - 400 MHz - Frequency Agile Results.csv';

% Set the lower and upper frequency limits. By doing this, the regression
% equation will only be constructed using inductor values that cause f_o
% values to fall between freq_low and freq_high.
freq_low = 280; % MHz
freq_high = 320; % MHz

% Set the inductor variable name, and the units. The inductor variable name
% is case sensitive in HFSS.
inductorVariableName = 'inductor';
inductorVariableUnits = 'nH';

% Set the first output file name. This CSV file will be used for the
% non-Foster |S11| simulations.
filename_nonFosterInductorValues ...
    = '..\XLS and CSV Files\2D EAD - 400 MHz - NonFoster Inductor Values.csv';

% Set the second output file name. This CSV file will be used for the
% non-Foster radiation efficiency simulations.
filename_nonFosterInductorValuesAndFrequencies ...
    = '..\XLS and CSV Files\2D EAD - 400 MHz - NonFoster L and f.csv';

%%%%%%%%%%%%%%%%%%%%%%%%%%%%%%%%%%%%%%%%%%%%%%%%%%%%%%%%%%%%%%%%%%%%%%%%%%%

% Define some important variables as globals (this is needed for the
% non-linear equation solver)
global L freq_MHz

% Import ideal frequency agile data and header
idealFrqAgile = importdata(filename_IdealFrequencyAgileResults);
L = idealFrqAgile.data(:,1);
S11 = idealFrqAgile.data(:,2);
freq = idealFrqAgile.data(:,3);
```

```
% Sort data so that frequency goes from low to high
data = [L,S11,freq];
data = sortrows(data,3);
L = data(:,1);
S11 = data(:,2);
freq = data(:,3);
freq_MHz = freq/1e6;

% Use only the inductor values that cause f_o to fall between freq_low and
% freq_high
indices_to_keep = (freq_MHz >= freq_low) & (freq_MHz <= freq_high);
freq_MHz = freq_MHz(indices_to_keep);
L = L(indices_to_keep);

% Solve a non-linear equation for xi
xi_in = 10; % initial guess for xi
options = optimset('Display','iter','TolFun',1e-12,'TolX',1e-12);
xi = fsolve(@myfun,xi_in,options);

% Compute alpha and beta
A = [ones(size(freq_MHz)),freq_MHz(:)];
b = log(L-xi);
% x = A\b;
x = inv(A'*A)*A'*b;
alpha = exp(x(1));
beta = -x(2);

% Make a plot comparing L with L_reg
L_reg = xi+alpha.*exp(-beta.*freq_MHz);
hold on
grid on
plot(freq_MHz,L_reg,'r','LineWidth',2)
plot(freq_MHz,L,'kx','LineWidth',2)
legend('Ideal Inductor Values','Inductor Values from Regression Equation')
xlabel('Frequency (MHz)','FontSize',8)
ylabel('Inductor (nH)','FontSize',8)
set(gca,'FontSize',7);

% Output the non-Foster inductor values to the first CSV file
fid = fopen(filename_nonFosterInductorValues,'w');
fprintf(fid,'%s[%s]\n',inductorVariableName,inductorVariableUnits);
fclose(fid);
dlmwrite(filename_nonFosterInductorValues,L_reg,...
         'delimiter',',','precision','%.6f','-append');

% Output the non-Foster inductor values and frequencies to the second CSV
% file
dlmwrite(filename_nonFosterInductorValuesAndFrequencies,[L_reg,freq_MHz],...
         'delimiter',',','precision','%.6f');
```

myfun.m

```
function out = myfun(xi_in)
global L freq_MHz
A = [ones(size(freq_MHz)),freq_MHz(:)];
b = log(L-xi_in);
x = A\b;
alpha = exp(x(1));
beta = -x(2);
L_reg = xi_in + alpha*exp(-beta*freq_MHz);
out = L - L_reg;
```

APPENDIX C | MATLAB CODE FOR PLOTTING THE NON-FOSTER $|S_{11}|$ CURVE

```
% Plot non-Foster results from ideal frequency agile and regression
% frequency agile data.

%%%%%%%%%%%%%%%%%%%%%%%%%% USER PROVIDED INPUTS %%%%%%%%%%%%%%%%%%%%%%%%%%

% Set the filename for the ideal frequency agile results. This should be a
% CSV file with three columns: inductor value, min(dB(S(1,1))), and
% XAtYVal( dB(S(1,1)), min(dB(S(1,1))) ), in that specific order.
filename_IdealFrequencyAgileResults ...
   = ['..\XLS and CSV Files\2D EAD - 400 MHz - Frequency Agile '...
      'Results (subset).csv'];

% Set the filename for the regression frequency agile results. This should
% be a CSV file with the first column specifying the frequencies, and the
% next n columns containing the dB(S(1,1)) results, each column containing
% the dB(S(1,1)) results for a unique inductor value vs. frequency.
filename_RegressionFrequencyAgileResults ...
   = ['..\XLS and Files\2D EAD - 400 MHz - Regression Frequency '...
     'Agile Results.csv'];

%%%%%%%%%%%%%%%%%%%%%%%%%%%%%%%%%%%%%%%%%%%%%%%%%%%%%%%%%%%%%%%%%%%%%%%%%%%

% Import ideal frequency agile data and header
idealFrqAgile = importdata(filename_IdealFrequencyAgileResults);
L_ideal = idealFrqAgile.data(:,1);
S11_ideal = idealFrqAgile.data(:,2);
freqs_ideal = idealFrqAgile.data(:,3);

% Import regression frequency agile data and header
regFrqAgile = importdata(filename_RegressionFrequencyAgileResults);

% parse header string into cell array
regFrqAgileHeader = regFrqAgile.textdata{1};
regFrqAgileHeader = strrep(regFrqAgileHeader,'dB(S(1,1))','');
[junk,regFrqAgileHeader] = regexp(regFrqAgileHeader,',','match','split');
regFrqUnit = sscanf(regFrqAgileHeader{1},'"Freq [%cHz]"'); % get frequency
units
regFrqAgileHeader(1) = []; % Delete frequency header

% determine number of sims two ways. throw error if there is a difference
numSims = length(regFrqAgileHeader);
numSims2 = length(L_ideal);
if numSims ~= numSims2
    error(['Number of inductor values used in ideal frequency agile '...
        'case does not match the number of sims used in the regression '...
        'frequency agile case.']);
end

% loop through cell array, getting inductor values along the way
L_reg = zeros(numSims,1);
for ii = 1:numSims
    digitLocs = isstrprop(regFrqAgileHeader{ii},'digit');
    startInd = find(digitLocs,1,'first');
```

```
    endInd = find(digitLocs,1,'last');
    L_reg(ii) = str2double(regFrqAgileHeader{ii}(startInd:endInd));
end

% Check that nothing went terribly wrong
if max(abs(L_ideal - L_reg))>0.35
    error('Difference between L_ideal and L_reg is too large.');
end

% Get frequency values used during regression frequency agile sims, convert
% to Hz if necessary
freqs_reg = regFrqAgile.data(:,1);
switch regFrqUnit
    case 'k'
        freqs_reg = 1e3*freqs_reg;
    case 'M'
        freqs_reg = 1e6*freqs_reg;
    case 'G'
        freqs_reg = 1e9*freqs_reg;
    otherwise
        % Do nothing
end

% Get S11 values from regression frequency agile sims
S11_reg = regFrqAgile.data(:,2:end);

% Determine the non-Foster performance
freq_nf = zeros(numSims,1);
S11_nf = zeros(numSims,1);
for ii = 1:numSims
    % Find closest regression frequency to ideal frequency for this
    % particular inductor value
    [val,pos] = min(abs(freqs_reg - freqs_ideal(ii)));
    % Store nf freq and performance
    freq_nf(ii) = freqs_ideal(ii);
    S11_nf(ii) = S11_reg(pos,ii);
end

% Sort the data so that frequencies are ordered from low to high
data = [freq_nf,S11_nf];
data = sortrows(data,1);
freq_nf = data(:,1);
S11_nf = data(:,2);

% Plot non-Foster data
figure
plot(freq_nf,S11_nf,'b-o','MarkerFaceColor','b')
xlabel('Frequency (Hz)')
ylabel('|S_1_1| (dB)')
grid on
axis([0.99*min(freq_nf) 1.01*max(freq_nf) 1.1*min(S11_nf) 0])
```

APPENDIX D | HFSS MACROS FOR GENERATING A NON-FOSTER RADIATION EFFICIENCY CURVE

Run_2DEAD_NF_RadEff.vbs

```
Dim oAnsoftApp
Dim oDesktop
Dim oProject
Dim oDesign
Dim oModule

Set oAnsoftApp = CreateObject("AnsoftHfss.HfssScriptInterface")
Set oDesktop = oAnsoftApp.GetAppDesktop()
Set oProject = oDesktop.SetActiveProject("DrZ_300MHz_Sept_2011_5880")
Set oDesign = oProject.SetActiveDesign("EAD_Rogers_5880_Ning_ka=.35_newNonFoster_RadEff")
Set oModule = oDesign.GetModule("AnalysisSetup")

Dim fs,objTextFile
Set fs=CreateObject("Scripting.FileSystemObject")
Dim arrStr
Set objTextFile =_fs.OpenTextFile("F:\Dr Z Projects\Non-Foster\XLS and CSV Files\2D EAD - 400 MHz - NonFoster L and f.csv")

Dim SweepNum
SweepNum = 1

Do while NOT objTextFile.AtEndOfStream
	arrStr = split(objTextFile.ReadLine,",")

	oModule.InsertFrequencySweep "Setup1", Array("NAME:Sweep"&SweepNum, "IsEnabled:=", true, "SetupType:=", _
		"SinglePoints", "ValueList:=", Array(arrstr(1)&"MHz"), "Type:=", "Discrete", "SaveFieldsList:=", Array( _
		true), "ExtrapToDC:=", false)

	oDesign.ChangeProperty Array("NAME:AllTabs", Array("NAME:LocalVariableTab", Array("NAME:PropServers", _
		"LocalVariables"), Array("NAME:ChangedProps", Array("NAME:inductor", "Value:=", _
		arrstr(0)&"nH"))))

	oDesign.Analyze("Setup1 : Sweep"&SweepNum)

	SweepNum = SweepNum + 1

	oProject.Save
Loop

objTextFile.Close
Set objTextFile = Nothing
Set fs = Nothing
```

Plot_2DEAD_NF_RadEff.vbs

```
Dim oAnsoftApp
Dim oDesktop
Dim oProject
Dim oDesign
Dim oModule

Set oAnsoftApp = CreateObject("AnsoftHfss.HfssScriptInterface")
Set oDesktop = oAnsoftApp.GetAppDesktop()
Set oProject = oDesktop.SetActiveProject("DrZ_300MHz_Sept_2011_5880")
Set oDesign = oProject.SetActiveDesign("EAD_Rogers_5880_Ning_ka=.35_newNonFoster_RadEff")
Set oModule = oDesign.GetModule("ReportSetup")

Dim PlotName
PlotName = "NF Rad Eff"

oModule.CreateReport PlotName, _
"Far Fields", _
"Rectangular Plot",  _
"Setup1 : Sweep1", _
Array("Context:=", "Infinite Sphere1"), _
Array("Freq:=", Array("All"), _
Array("NAME:VariableValues", "inductor:=","114.7372609nH", "Phi:=", "0deg", "Theta:=", "0deg")), _
Array("X Component:=",  "Freq", "Y Component:=", Array("RadiationEfficiency")), _
Array()

Dim fs,objTextFile
Set fs=CreateObject("Scripting.FileSystemObject")
Dim arrStr
Set objTextFile = _
fs.OpenTextFile("F:\Dr Z Projects\Non-Foster\XLS and CSV Files\D EAD - 400 MHz - NonFoster L and f.csv.csv")

Dim SweepNum
SweepNum = 1

Do while NOT objTextFile.AtEndOfStream
	arrStr = split(objTextFile.ReadLine,",")

	If SweepNum > 1 Then
		oModule.AddTraces PlotName, _
		"Setup1 : Sweep"&SweepNum, _
		Array("Context:=", "Infinite Sphere1"), _
		Array("Freq:=", Array("All"), _
		Array("NAME:VariableValues", "inductor:=", arrstr(0)&"nH", "Phi:=", "0deg", "Theta:=", "0deg")), _
		Array("X Component:=", "Freq", "Y Component:=", Array("RadiationEfficiency")), _
		Array()
	End If

	SweepNum = SweepNum + 1
Loop

oModule.ChangeProperty Array("NAME:AllTabs", Array("NAME:Scaling", Array("NAME:PropServers",  _
  PlotName&":AxisY1"), Array("NAME:ChangedProps", Array("NAME:Specify Min", "Value:=",  _
  true), Array("NAME:Min", "MustBeInt:=", false, "Value:=", "0"), Array("NAME:Specify Max", "Value:=",  _
  true), Array("NAME:Max", "MustBeInt:=", false, "Value:=", "1"))))
oModule.ChangeProperty Array("NAME:AllTabs", Array("NAME:Legend", Array("NAME:PropServers",  _
  PlotName&":Legend"), Array("NAME:ChangedProps", Array("NAME:DockMode", "Value:=",  _
  "Dock Right"))))
```

REFERENCES

[1] R. Hansen, "Fundamental limitations in antennas," *Proc. IEEE,* vol. 69, no. 2, pp. 170-182, Feb. 1981.

[2] L. J. Chu, "Physical limitations of omni-directional antennas," *J. Appl. Phys.*, vol. 19, no. 12, pp. 1163-1175, Dec. 1948.

[3] J. S. McLean, "A re-examination of the fundamental limits on the radiation Q of electrically amall antennas," *IEEE Trans. Antennas Propagat.,* Vols. AP-44, no. 5, pp. 672-676, May 1996.

[4] H. L. Thal, "Polarization, gain, and Q for small antennas," *IEEE Trans. Antennas Propag.*, vol. 59, no. 12, pp. 4844-4848, Dec. 2011.

[5] M. Gustafsson, C. Sohl and G. Kristensson, "Physical limitations on antennas of arbitrary shape," *Proc. Royal Soc. A,* vol. 463, pp. 2589-2607, Oct. 2007.

[6] C. E. Cooper, "Antenna with P.I.N. diode switched tuning inductors". United States of America Patent 4564843, 14 January 1986.

[7] R. Ziolkowski, P. Jin and C. Lin, "Metamaterial-inspired engineering of antennas," *Proc. IEEE,* vol. 99, no. 10, pp. 1720-1731, Oct. 2011.

[8] R. M. Foster, "A Reactance Theorem," *Bell Systems Tech. J.*, vol. 3, pp. 259-267, 1924.

[9] S. E. Sussman-Fort and R. M. Rudish, "Non-Foster impedance matching of electrically-small antennas," *IEEE Trans. Antennas Propag.*, Vols. AP-57, no. 8, pp. 2230-2241, Aug. 2009.

[10] J. T. Aberle, "Two-port representation of an antenna with application to non-Foster matching networks," *IEEE Trans. Antennas Propag.*, vol. 56, pp. 1218-1222, May 2008.

[11] C. Di Nallo, G. Bit-Babik and A. Faraone, "Wideband antenna using non-Foster loading elements," in *Proc. IEEE International Symposium on Antennas and Propagation*, Honolulu, HI, 10-15 June, 2007.

[12] H. Mirzaei and G. V. Eleftheriades, "A wideband metamaterial-inspired compact antenna using embedded non-Foster matching," in *Proc. IEEE International Symposium on Antennas and Propagation*, Spokane, WA, 3-8 July, 2011.

[13] R. W. Ziolkowski and P. Jin, "Introduction of internal matching circuit to increase the bandwidth of a metamaterial-inspired efficient electrically small antenna," in *Proc. IEEE International Symposium on Antennas and Propagation*, San Diego, CA, 5-11 July, 2008.

[14] P. Jin and R. W. Ziolkowski, "Broadband, efficient, electrically small metamaterial-inspired antennas facilitated by active near-field resonant parasitic elements," *IEEE Trans. Antennas Propag.,* vol. 58, no. 2, pp. 318-327, Feb. 2010.

[15] N. Zhu and R. W. Ziolkowski, "Active metamaterial-inspired broad bandwidth, efficient, electrically small antennas," *IEEE Antennas Wireless Propag. Lett.,* vol. 10, pp. 1582-1585, 2011.

[16] N. Zhu and R. W. Ziolkowski, "Design and measurements of an electrically small, broad bandwidth, non-Foster circuit-augmented protractor antenna," *Appl. Phys. Lett.,* vol. 101, 024107, Jul. 2012.

[17] N. Zhu and R. W. Ziolkowski, "Broad bandwidth, electrically small antenna augmented with an internal non-Foster element," *IEEE Antennas Wireless Propag. Lett.,* vol. 11, pp. 1116-1120, 2012.

[18] J. G. Linvill, "Transistor negative-impedance converters," *Proc. IRE,* vol. 41, no. 6, pp. 725-729, Jun. 1953.

[19] C. R. White, J. W. May and J. S. Colburn, "A variable negative-inductance integrated circuit at UHF frequencies," *IEEE Microw. Wireless Compon. Lett.*, vol. 22, pp. 35-37, 2012.

[20] D. L. Sengupta and T. K. Sarkar, "Maxwell, Hertz, the Maxwellians, and the early history of electromagnetic waves," *IEEE Antennas Propag. Mag.*, vol. 45, no. 2, pp. 13-19, Apr. 2003.

[21] C. A. Balanis, Advanced Engineering Electromagnetics, New York: John Wiley & Sons, 1989.

[22] C. A. Balanis, Antenna Theory, Hoboken: John Wiley & Sons, Inc., 2005.

[23] M. M. Weiner, "Monopole element at the center of a circular ground plane whose radius is small or comparable to a wavelength," *IEEE Trans. Antennas Propag.*, vol. 35, no. 5, pp. 488-495, May 1987.

[24] Z. Yan-jun, C. Ai-xin, S. Dong-lin and T.-J. Jiang, "Optimal design of a broadband matching network for an electrically small antenna," in *8th International Symposium on Antennas, Propagation and EM Theory, ISAPE 2008*, Kunming, China, 2-5 Nov. 2008.

[25] P. Jin and R. W. Ziolkowski, "High-directivity, electrically small, low-profile near-field resonant parasitic antennas," *IEEE Antennas Wireless Propag. Lett.*, vol. 11, pp. 305-309, 2012.

[26] C. Pfeiffer and A. Grbic, "A Circuit Model for Electrically Small Antennas," *IEEE Trans. Antennas Propag.*, vol. 60, no. 4, pp. 1671-1683, Apr. 2012.

[27] N. Zhu, P. Jin, R. W. Ziolkowski and H. Xin, "Design of a GPS L1 rectenna by using a metamaterial-inspired electrically small antenna," in *Proc. IEEE Antennas and Propagation Society International Symposium*, Spokane, WA, 3-8 July, 2011.

[28] S. R. Best, "Low Q electrically small linear and elliptical polarized spherical dipole antennas," *IEEE Trans. Antennas Propag.*, vol. 53, no. 3, pp. 1047-1053, Mar. 2005.

[29] A. K. Rashid and Z. Shen, "On the inverse relationship between quality factor and bandwidth of small antennas," *Proc. Asia Pacific Microwave Conference, 2009. APMC 2009,* pp. 44-47, 7-10 December 2009.

[30] A. D. Yaghjian and S. R. Best, "Impedance, bandwidth, and Q of antennas," *IEEE Trans. Antennas Propag.*, vol. 53, no. 4, pp. 1298-1324, Apr. 2005.